

# **Not All Chromosomes Are Created Equal**

Following individual chromosomes in mitosis and beyond

Sjoerd J. Klaasen

**ISBN:** 978-90-393-7532-7

**Copyright:** © S.J. Klaasen

**Cover design:** S.J. Klaasen

**Printed by:** Gildeprint | [www.gildeprint.nl](http://www.gildeprint.nl)

# **Not All Chromosomes Are Created Equal**

Following individual chromosomes in mitosis and beyond

Niet alle chromosomen zijn gelijk. Het volgen van  
individuele chromosomen in mitose en daarbuiten

(met een samenvatting in het Nederland)

## **Proefschrift**

Ter verkrijging van de graad van doctor aan de Universiteit Utrecht  
op gezag van de rector magnificus, prof.dr. H.R.B.M. Kummeling,  
ingevolge het besluit van het college voor promoties in het openbaar  
te verdedigen op

donderdag 23 februari 2023 des middags te 2.15 uur

door

**Sjoerd Jurian Klaasen**

Geboren op 5 januari 1993  
te Oegstgeest, Nederland

**Promotor:** Prof. dr. G.J.P.L. Kops

**Beoordelingscommissie:**

Prof. dr. ir. A. van Oudenaarden

Prof. dr. ir. J.P.W.M. Bakkers (voorzitter)

Prof. dr. S.M.A. Lens

Prof. dr. B. van Steensel

Dr. M. de Ruijter-Villani PhD



# Table of contents

<b>Chapter 1</b>	<b>7-30</b>
General introduction	8
Thesis outline	22
<b>Chapter 2</b>	<b>31-54</b>
Chromosome inequality: causes and consequences of non-random segregation errors in mitosis and meiosis	
<b>Chapter 3</b>	<b>57-96</b>
Nuclear chromosome locations dictate segregation error frequencies	
<b>Chapter 4</b>	<b>97-116</b>
LossTag: an aneuploidy selection tool to study the consequences of whole chromosome losses	
<b>Chapter 5</b>	<b>117-144</b>
High incidence of numerical and segmental chromosome mosaicism in inner cell mass and trophectoderm	
<b>Chapter 6</b>	<b>145-160</b>
Thesis summary	146
Discussion	147
<b>Addendum</b>	<b>161-171</b>
Nederlandse samenvatting	161
Curriculum Vitae	164
List of publications	165
Acknowledgements	166



# Chapter 1

## Introduction

Sjoerd J. Klaasen<sup>1,2</sup>

<sup>1</sup> Hubrecht Institute – KNAW (Royal Netherlands Academy of Arts and Sciences) and University Medical Centre Utrecht, Utrecht, the Netherlands.

<sup>2</sup> Oncode Institute, Utrecht, the Netherlands

## Cell division

It is vital for the survival of humans and many other multi-cellular organisms to sustain tissue homeostasis and create progeny using cell division. During cell division, cells are supposed to accurately segregate their genetic material into two new daughter cells. Somatic cells can create exact genetic copies during the process of mitosis, while germ cells use meiosis to generate cells with half the amount of DNA. To aid in this tightly regulated endeavor, cells require the help of many different proteins. These proteins are active during all parts of the cell cycle: cells in the G1 phase prepare for duplication of all of their genetic material in S phase. This is followed by the G2 phase, which is a period in which cells get ready for cell division.

Right before the onset of cell division, the genetic material is contained in the cell's interior nucleus as loosely intertwined chromosomes. At this point, each chromosome consists of two sister chromatids, which are stitched together by the cohesin complex<sup>1</sup>. Condensation of chromosomes gives them their characteristic X shape and also marks the onset of cell division (prophase) (Fig. 1). The purpose of the next few steps is for chromosomes to become bi-oriented, meaning the two kinetochores of one chromosome are attached to opposite poles. The nuclear envelope is broken down and microtubules randomly emanate from the once cytosolic centrosomes to search and capture chromosomes (prometaphase)<sup>2</sup>. Microtubules consist of tubulin subunits, which can polymerize and depolymerize, causing rapid growth and shrinkage<sup>3</sup>. The direct interaction of microtubules and chromosomes is facilitated by the kinetochore, which is a large multiprotein structure located on a small specialized area on the chromosome called the centromere<sup>4</sup>. Kinetochores make different types of interactions depending on their location in the nucleus. Kinetochores of chromosomes behind the centrosomes, also known as polar chromosomes, often first touch the walls of microtubules to make a lateral attachment before they make end-on attachments with the tips of microtubules (Fig. 2)<sup>2</sup>. However, chromosomes favorably positioned in between the two centrosomes have been suggested to immediately make end-on attachments (direct congression pathway).

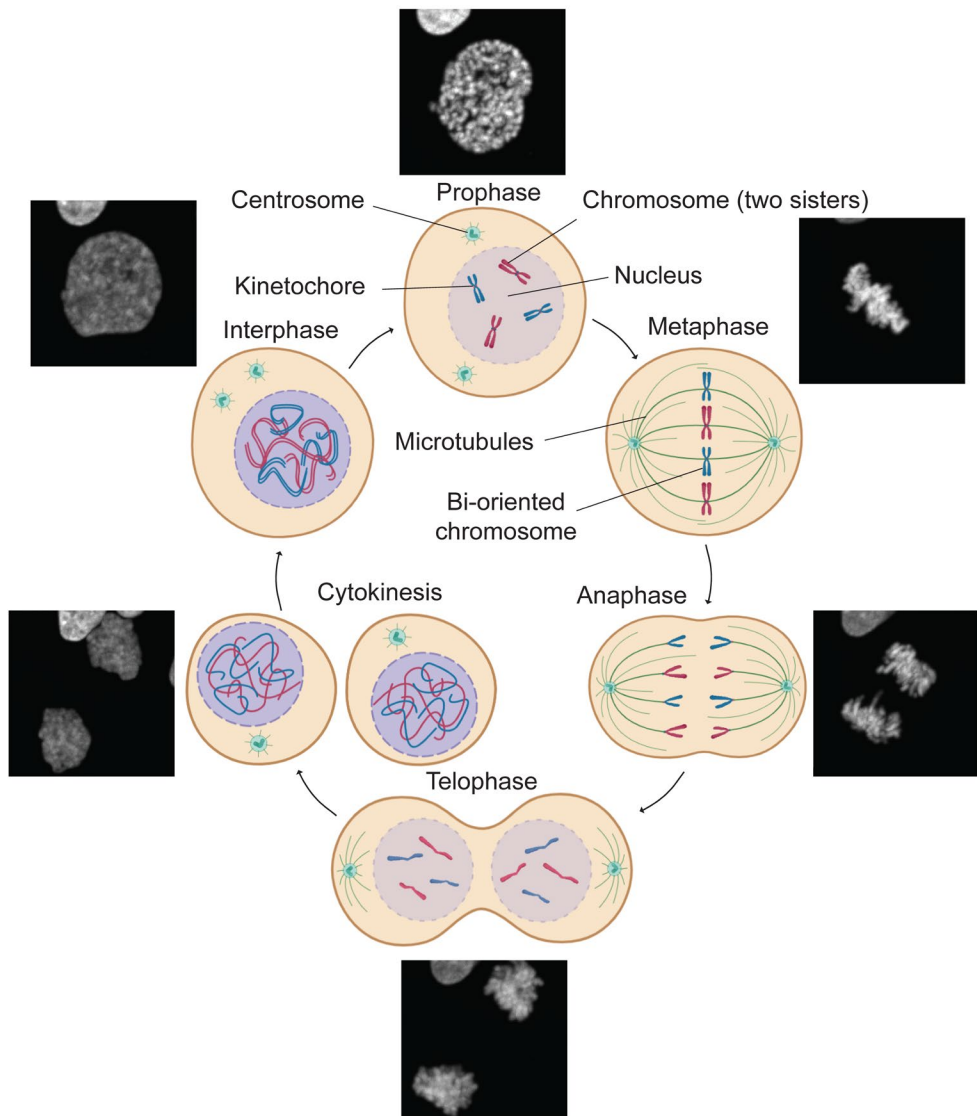


**Figure 1: Graphical representation of the cell cycle.** Cells in different phases of the cell cycle with corresponding live-cell images on the side. Created with BioRender.com.

Laterally attached kinetochores depend on the activity of motor proteins to become bi-oriented: polar chromosomes first travel to one of the centrosomes through the activity of the kinetochore-located motor protein dynein (peripheral congression

pathway)<sup>5,6</sup>. A second kinetochore-associated motor protein called CENP-E will then transport the centrosome-located chromosome to the metaphase plate with the help of polar ejection forces. Polar ejection forces are brought upon by chromosome arm-associated motor proteins. Here, the chromosomes change from lateral to an end-on attachments and are also favorably positioned to be captured by the opposite pole. Only when all chromosomes have made end-on attachments, cells initiate the removal of cohesin, which has been keeping the sisters together, and pull the sister chromatids to opposite sides (anaphase)<sup>1</sup>.

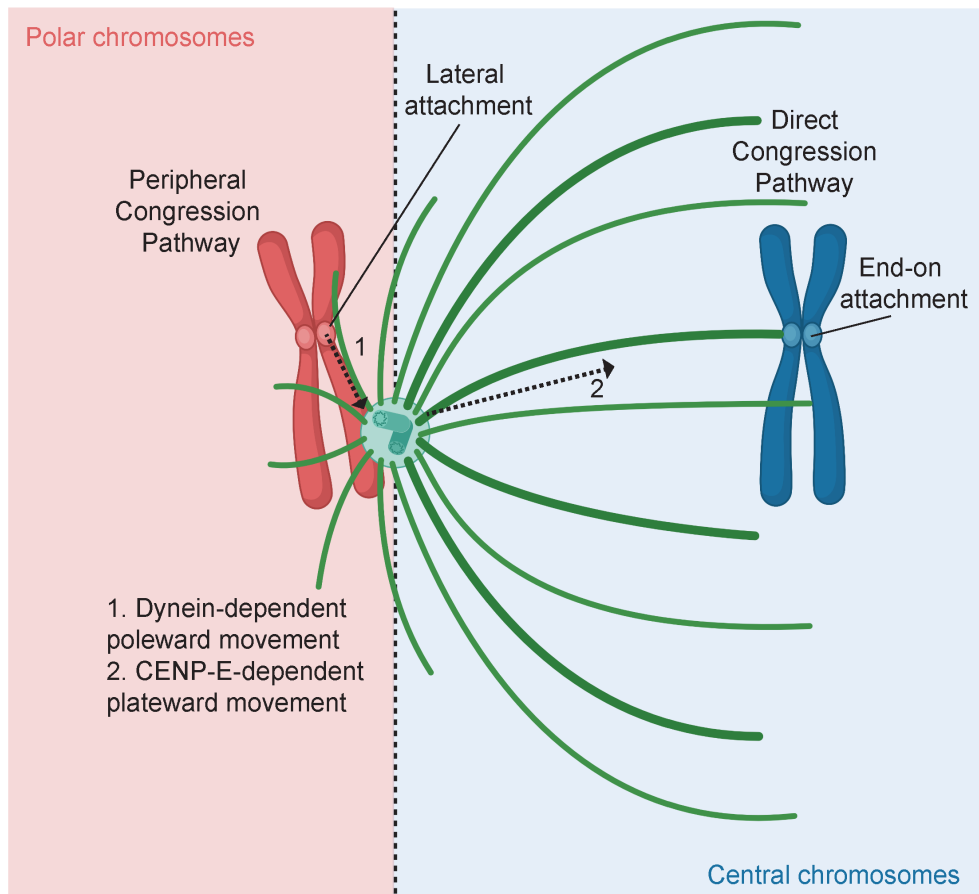


**Figure 2: Chromosomes can use one of two pathways to congress chromosomes.** Chromosomes within the blue area are favorably located between the two centrosomes at mitosis onset. Kinetochores of these chromosomes frequently first make end-on attachments and relatively quickly bi-orient (direct congression pathway). On the other hand, chromosomes located in the red area are behind the centrosomes and kinetochores of these chromosomes are often laterally attached (peripheral

congression pathway). They also require the assistance of motor proteins, such as dynein and CENP-E, to become bi-oriented. Created with BioRender.com.

Multiple surveillance pathways are active during cell division to check if chromosomes are behaving properly. The spindle assembly checkpoint (SAC) keeps cells in metaphase until all chromosomes bi-oriented<sup>4</sup>. The kinase Mps1 is the master regulator of the SAC, as its binding to the kinetochore triggers a phosphorylation cascade activating the checkpoint<sup>7</sup>. Mps1 physically competes with microtubules for kinetochores so that when microtubules have made end-on attachments Mps1 is not able to activate the checkpoint anymore<sup>8,9</sup>. End-on attachments can however still be erroneous, for example when both sisters are attached to one pole (syntely) or one kinetochore is attached to both poles (merotely)<sup>10</sup>. Due to the nature of the SAC it cannot recognize such attachments. This is where a second pathway comes into play; the error correction pathway<sup>11</sup>. This pathway employs the chromosomal passenger complex, which, among others, consists of the kinase Aurora B. Its localization to the inner centromere allows destabilization of attachments when tension between sisters (from unproductive attachments) is low. If the sister kinetochores are pulled far apart, which is what happens when they are properly attached to opposite poles, Aurora B cannot reach and phosphorylate the microtubule-interacting outer kinetochore proteins to destabilize microtubule-kinetochore interactions<sup>12</sup>. In the case of erroneous attachments, there is less tension on the sister kinetochores. This means the sister kinetochores are not pulled apart as much, allowing Aurora B to break the bond between microtubules and kinetochores. It must be noted that this model is likely an oversimplification, as there are studies showing erroneous attachments are corrected independent of tension<sup>13,14</sup>.

The process described above applies both to mitosis and meiosis, although meiosis differs in some aspects<sup>15</sup>. For example, cells in meiosis must undergo an extra step before sister chromatid separation: first the homologous chromosomes separate and then the sister chromatids<sup>16</sup>. In order for the homologous chromosomes to properly segregate they need to be cohesed together just like the sister chromatids. Not only

does the localization of the cohesin complex on the arms of homologous chromosomes facilitate this, but also the specialized structures resulting from genetic recombination called chiasmata help<sup>17</sup>. Furthermore, human oocytes primarily nucleate microtubules from chromosomes, because they do not contain centrosomes<sup>18</sup>.

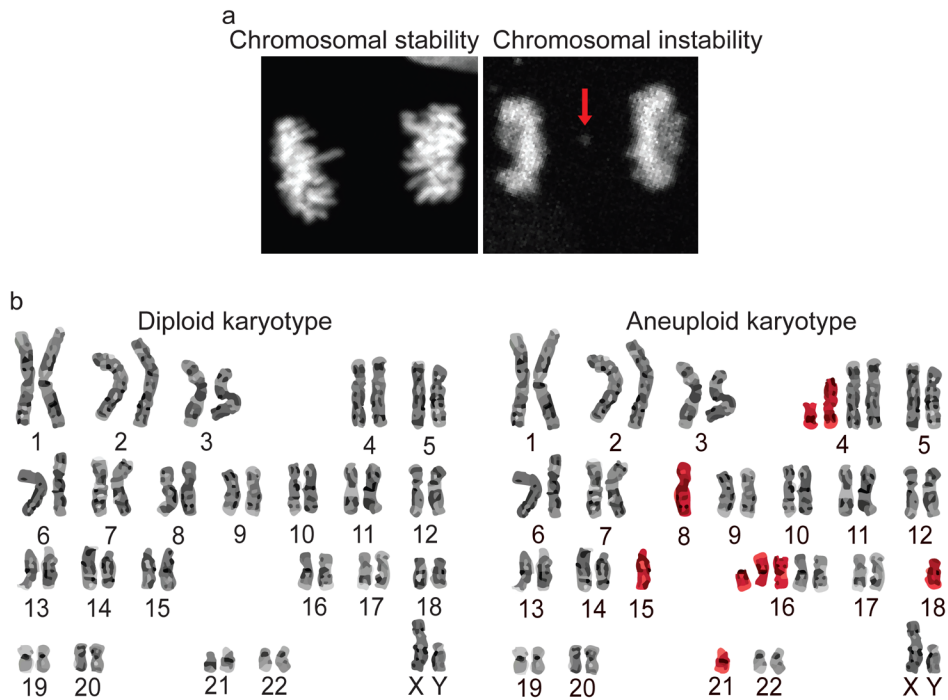


**Figure 3: Chromosomal instability leads to aneuploidy. a.** Two images depicting an error-free (left) and an erroneous cell division (right). Arrow in red depicts a mis-segregating chromosome. **b.** Graphic representation of a diploid karyotype (left) and an aneuploid one (right). Red chromosomes are either gained or show of which pair one is lost. Image was adapted from Uttamatinin *et al.*, (2013)<sup>19</sup>.

### Chromosomal instability, aneuploidy and micronuclei

Errors during any of the above described steps can lead to the unequal distribution of chromosomes. This process is also referred to as chromosomal instability (Fig. 3a) and leads to cells becoming aneuploid, which is defined as having an abnormal number of chromosomes (Fig. 3b). Chromosomes have an uneven chance to mis-segregate. For example, chromosome 1 more frequently undergoes segregation errors compared to chromosome 22. This depends on the causes and



characteristics of chromosomes and is discussed in more detail in **chapter 2**. When chromosomes mis-segregate there is a chance they become physically separated from the anaphase packs and form their own micronucleus. The membranes of micronuclei are prone to rupture, triggering the shattering and massive rearrangement of the chromosome that was in it<sup>20–22</sup>. Aneuploidy is relatively rare or common in normal healthy adult human cells depending on the report and tissue examined. For example, the liver, brain and skin only contained 3% of aneuploid cells in one report<sup>23</sup>, but neuronal brain cells contain up to 40% of such cells in another<sup>24</sup>. Aneuploidy is much more common in certain diseases or syndromes, such as Down's or mosaic variegated aneuploidy syndrome<sup>25,26</sup>. In cancer, around 68% of tumors have clonal aneuploidies<sup>27</sup>. Surprisingly, one other striking source of aneuploidy is found during human embryonic development. Errors during meiosis lead to a female age-dependent increase of aneuploidy from around 20% to 80% in early stage embryos<sup>28</sup>. Few days old human embryos also often display mosaic aneuploidies<sup>29,30</sup>, suggesting that mitosis in the first few divisions of the human embryo is error-prone.

### **Causes of aneuploidy**

Since aneuploidy is the result of mis-segregations during cell divisions, the majority of causes for aneuploidy found to date are related to improper functioning of chromosome segregation mechanisms (Fig. 4).

#### *Weakened spindle assembly checkpoint*

The SAC monitors the attachment state of chromosomes during cell division and arrests cells in mitosis until all kinetochores are attached<sup>4</sup>. Improper functioning of the SAC, for example when it is inhibited causes a premature anaphase onset, leading to massive mis-segregations and early onset of cancer in different mouse models<sup>31–33</sup>. Weakening of the SAC is sometimes, but not always observed in cancer cell lines<sup>34,35</sup> and it is unclear if it is actually the cause of the chromosomal instability in these lines. Mutations in SAC-related proteins in tumors are rare, so it is unclear what causes SAC weakening<sup>36</sup>. Defects of the SAC have also been suggested to cause mosaic aneuploidy in the developing embryo as in the roundworm

*Caenorhabditis elegans* and mice unattached kinetochores generated only a relatively short arrest<sup>37,38</sup>. Furthermore, mutations in the gene *TRIP13* were found in a limited number of mosaic variegated aneuploidy patients<sup>39</sup>. TRIP13 has a function in the SAC, so these mutations led to a severely weakened SAC.

#### *Changes in microtubule stability*

Another vital part of the segregation machinery are microtubules. Microtubules continuously polymerize and depolymerize in order to capture and move around chromosomes. Abnormal changes in the dynamics of these microtubules lead to chromosomal instability. Firstly, in normal healthy cells erroneous microtubule-kinetochore attachments are efficiently corrected by the error correction machinery. In certain cancer cells however, kinetochore-microtubule attachments are much more stable, leading to an increase in mis-segregations<sup>40</sup>. In turn, mis-segregations could partly be rescued in U2OS cells by overexpression of Kif2b or MCAK, two microtubule depolymerizers<sup>41</sup>. Contrary to a higher stability, higher plus-end microtubule assembly rates have also been linked to chromosomal instability in multiple colorectal cancer cell lines<sup>42</sup>. It is believed that both malfunctions are triggered by mutations in the well-known tumor suppressors APC or CHK2, respectively.

#### *Cohesion fatigue*

Loss of sister chromatid cohesion is a way through which cancer cells, but also oocytes can become chromosomally unstable. During mitosis, sister chromatids are held together at the centromere by the cohesin complex. Only when all chromosomes have bi-oriented can this cohesin be removed. Multiple reports demonstrated the presence of mutations in cohesin genes, which lead to premature separation of sister chromatids and chromosomal instability<sup>43,44</sup>. This phenotype could be rescued by restoring the wild-type sequence in two glioblastoma cell lines<sup>44</sup>. In human oocytes, premature separation of sister chromatids is the major reason for an age-dependent increase in aneuploidy in embryos<sup>16,28</sup>. Oocytes are in meiotic arrest starting from before birth until ovulation. During these years, cohesin molecules are gradually lost and are not replenished, resulting in weakened cohesi-

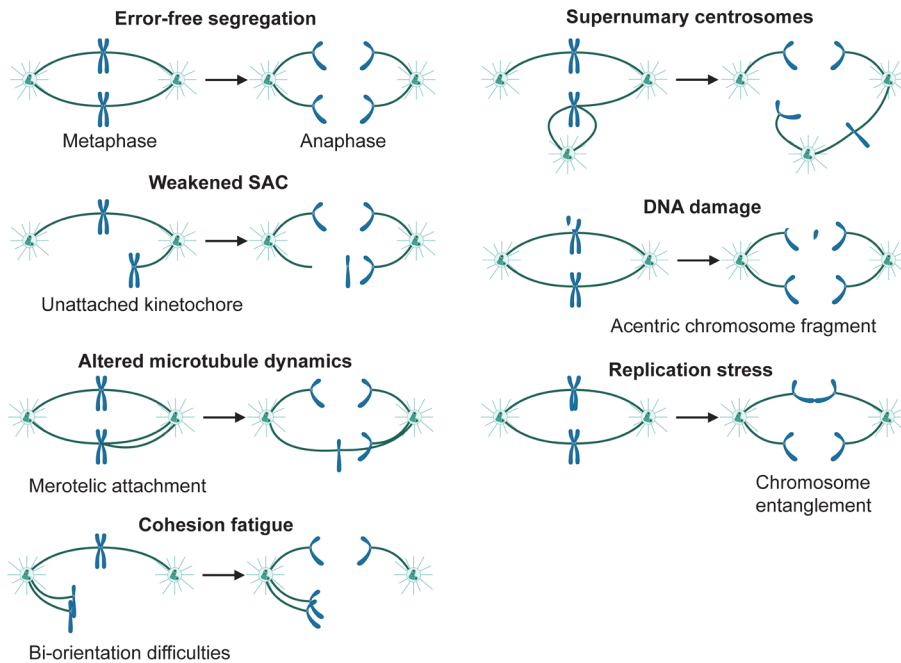


**Figure 4: Aneuploidy can be caused by many different mechanisms.** Graphical representation of an error-free (top left) and erroneous mitoses due to various issues. In all images, centrosomes are on the sides emanating microtubules towards chromosomes. Created with BioRender.com.

During these years, cohesin molecules are gradually lost and are not replenished, resulting in weakened cohesion and, ultimately, complete cohesion loss<sup>28,45</sup>. A failure to form chiasmata or their suboptimal positioning are other reasons why cohesion is affected, because these structures aid in cohesing the homologous chromosomes<sup>46–48</sup>. Interestingly, human oocytes have a much higher chance to fail crossover maturation than spermatocytes<sup>46</sup>.

### *Centrosome abnormalities*

Centrosomes are the most important microtubule nucleation facilitators in mammalian cells in mitosis. Right after mitosis, cells contain one centrosome, which in turn contain two cylindrical organelles called centrioles and is accompanied by a protein mass called the pericentriolar material<sup>49</sup>. The two centrioles must disengage in G1 to prepare for duplication during S phase. Before the onset of mitosis the centrosomes must again dissociate to create the characteristic bipolar mitotic

spindle. A delay or acceleration in mitotic centrosome disengagement is believed to increase the number of erroneous attachments, leading to mis-segregations<sup>50</sup>. Whether this phenomenon also occurs in human tumors is unknown. Furthermore, both defects in the structure and the number of centrosomes have been linked to increased levels of chromosomal instability<sup>18,51,52</sup>. Supernumerary centrosomes have the ability to form multipolar spindles, which lead to a massive number of mis-segregations. Multipolar spindles can also gradually become bipolar, but previously established erroneous attachments may persist in the following anaphase. Human tumors frequently have supernumerary centrosomes, supporting the hypothesis that centrosomes are responsible for chromosomal instability in some tumors<sup>53</sup>. Human oocytes do not have centrosomes and therefore rely on chromosome-dependent microtubule nucleation. Because of this, spindles frequently become multipolar and have many abnormal microtubule-kinetochore attachments<sup>18</sup>.

### *DNA damage*

Although aneuploidy occurs after an erroneous cell division, the cause of chromosomal instability could still lie in a problem occurring during interphase. For example, DNA damage could take place during any time in the cell cycle, go undetected and pass the G2 checkpoint<sup>54</sup>. This leads to the presence of acentric chromosomes, which are prone to mis-segregate<sup>55</sup>. Another problem that often arises, especially in cancer cells, is DNA replication stress<sup>56</sup>. Replication stress can be defined as the slowing down or stalling of replication forks. The resulting replication intermediates are sometimes not corrected before the onset of mitosis, leading to the generation of anaphase DNA bridges and subsequently aneuploidy<sup>57</sup>.

### **Consequences of aneuploidy**

Aneuploidy changes the gene dosage compared with diploid cells: a gain or a loss of a chromosome in a diploid cell increases or decreases the number of genes on the aneuploid chromosome by 50%. Transcriptomic and proteomic analyses on mouse and human cell lines with defined stable aneuploidies showed that the expression scales with copy number<sup>58–61</sup>. However, for about 25% of proteins their level gets adjusted to diploid levels (also known as dosage compensation)<sup>61,62</sup>.

In normal healthy cell lines, gene expression changes due to aneuploidy are frequently detrimental to their fitness<sup>59–61,63–65</sup>. This is supported by the observation that a large proportion of miscarriages are caused by aneuploidy and by the presence of aneuploidy-related syndromes, such as Down, Edward and Patau<sup>66</sup>. Why are cells so affected by this? Some proteins need to be present at the right number in order for a pathway to function properly. For example, Mad2 overexpression can lead to an overactive SAC and induce chromosomal instability<sup>67</sup>. The same is true for chromosomal losses. The large majority of chromosomes contain ribosomal genes, which means almost any loss of a chromosome affects ribosomal biogenesis and thus decreases translation<sup>60</sup>. Other proteins work in complexes and need proper stoichiometry in order to fulfill their function. Excess subunits are non-functional and may even be harmful. Too few subunits decrease the number of functional complexes<sup>68</sup>. Taking into account the above described consequences of aneuploidy, aneuploidy can thus in theory have an impact on an unlimited number of other pathways, depending on the affected protein.

Cells can also undergo a general aneuploidy stress response related to the sudden change in expression of hundreds of proteins at the same time. In case of chromosomal gains, cells undergo proteotoxic stress. Increased expression because of gene dosage changes overwhelms the protein folding machinery. Proteins are misfolded, not degraded and ultimately aggregate in the cytoplasm<sup>58,69</sup>. Protein aggregates impair cellular viability, which is why trisomic cell lines rely on increased proteasomal degradation and autophagy to clean up the mess<sup>61,70,71</sup>. Furthermore, gene dosage changes due to aneuploidy increase the number of free proteins, because proteins working in complexes lose stoichiometry. In turn, this increases intracellular solute concentration and therefore osmolarity in the cytoplasm, giving rise to hypo-osmotic stress<sup>72</sup>. Aneuploid human cell lines also have increased levels of replication stress and DNA damage regardless of karyotype<sup>73–75</sup>. For unknown reasons, lower expression of six subunits of the DNA helicase is behind this genetic instability<sup>73</sup>.

Despite the above described detrimental consequences, aneuploidy gives cells a proliferative advantage in certain contexts. For example, human tumors obtain clonal aneuploidies over time and tumor types share recurrent aneuploidy patterns<sup>64,76,77</sup>, suggesting cancer cells somehow benefit from their altered karyotype. This is supported by evidence from transgenic mouse models and patients with mutations in mitotic regulators, as both have elevated levels of chromosomal instability and incidence of cancer<sup>25,32,39,67,78,79</sup>. Furthermore, certain non-transformed cell lines such as embryonic stem cells obtain clonal copy number changes over time during culturing<sup>80,81</sup>. Aneuploidy also gives normal healthy and cancers cells an advantage when cultured under suboptimal conditions, such as when cells are treated with chemotherapeutics or cultured in low oxygen or serum<sup>82–84</sup>. Some of the proliferative advantages of aneuploidy may be explained by changes in expression of only a few genes. In a high CIN mouse model, T-cell lymphomas frequently gained chromosome 15, which harbors the lymphoma-inducing oncogene *Myc*<sup>85</sup>. Introducing the *Myc* oncogene to chromosome 6 greatly increased chromosome 6 gains. Deleting one copy of *Rad21* on chromosome 15 exacerbated this effect. Similarly, chromosome losses have the ability to decrease expression of tumor suppressors leading to haploinsufficiency or full loss of expression in case the other allele was already non-functional. This is for example the case in chronic lymphocytic leukemia, where a large proportion of tumors have a mutation in *TP53* on one allele and a deletion of the other<sup>86</sup>. Further supporting this notion, global analyses of aneuploidies in human tumors showed that copy number variations frequently colocalize with tumor type-specific driver mutations<sup>87</sup>. Taking everything together, aneuploidy is in general harmful for cells. However, depending on the context, such as the mutational landscape, cell type or environmental factors, some aneuploidies can suddenly become beneficial (Fig. 5).

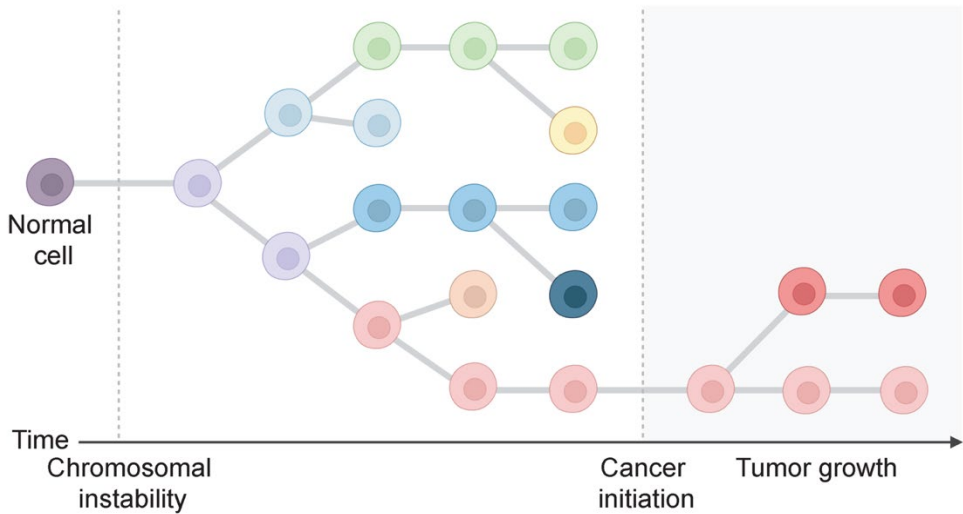


**Figure 5: The majority of aneuploidies are detrimental to the fitness of cells.** Illustration of how aneuploidy may be selected for during tumorigenesis. The different colors of the cells represent different karyotypes. At the start, a normal cell becomes chromosomally unstable and creates many different aneuploidies. Yet only one aneuploidy is beneficial for the tumorigenicity of cells and gives rise to a tumor. Adapted from “Cancer Evolution with Treatment”, by BioRender.com (2022). Retrieved from <https://app.biorender.com/biorender-templates>.

### Aneuploidy tolerance

Besides the pro-proliferative effects certain copy number variations can exert to overcome aneuploidy-related stresses, cells also find ways to tolerate it. p53 is one of the most commonly mutated tumor suppressors in cancer and aneuploidy correlates with mutations in p53<sup>64</sup>. In cell lines, a p53-dependent cell cycle arrest is frequently observed after aneuploidization, but why this happens remains unclear<sup>60,63</sup>. Abrogating p53 function therefore partially restores proliferation after pharmacological induction of CIN<sup>65,75,88</sup>. Another possible way through which cancer cells become tolerant to aneuploidy is by mutating *BCL9L*<sup>89</sup>. *BCL9L* is frequently mutated specifically in aneuploid tumor cells, is activated independent of p53 after aneuploidy induction and increases expression of the apoptotic factor caspase-2. Mutations in *BCL9L* thus inhibit apoptosis in aneuploid cells. Not only do cells sometimes turn a blind eye when it comes to aneuploidy-induced stresses, cells will over time also try to reduce them, such as by restoring normal protein homeostasis

by bringing back protein numbers to diploid levels<sup>61</sup>. Most of the proteins that are restored to normal levels are shown to work in complexes, suggesting that cells do this to return to normal protein stoichiometry. Since upregulation of lysosomal genes is a common response to aneuploidy<sup>61,74</sup>, it could be that an increase in autophagy is behind this. Cells are also able to buffer the negative consequences of aneuploidy by increasing their ploidy by whole-genome doubling. Whole-genome doubling is observed in 30-37% of cancers and correlates with increased levels of copy number variations<sup>90,91</sup>. It is believed that the extra chromosome copies present in these cells reduce the relative gene dosage changes after aneuploidization and therefore lower the stresses accompanied by aneuploidy. In conclusion, the detrimental effects of aneuploidy can be averted by mutating the pathways responsible for sensing the stresses or by buffering the expression changes.

### **Aneuploidy evolution**

In order for cells to become cancerous, they need to acquire a multitude of different hallmarks, such as sustained proliferative signaling, evade growth suppressors, avoid immune destruction, enable replicative immortality, activate invasion, induce angiogenesis, resist cell death and deregulate cellular energetics<sup>92</sup>. Chromosomal instability together with other types of genetic instability generate the genetic diversity that drives the acquisition of these hallmarks, since genes responsible for the proper regulation of pathways involved in for example cell proliferation become deregulated due to copy number aberrations. Aneuploidy is therefore a driver of the evolution of cancer. How then do aneuploidies evolve over time in cancer? First of all, aneuploidy can be a driver, passenger or detrimental. The presence of recurrent aneuploidy patterns and the fact that they colocalize with tumor-type specific cancer genes suggests that driver aneuploidies are all too common<sup>64,76,77</sup>. Detrimental aneuploidies are probably also frequent, because under normal culturing conditions the majority of aneuploidy-induced cell lines are outcompeted by their diploid counterpart<sup>59–61,64,65</sup>. To our knowledge, there are no reports describing passenger aneuploidies. This is probably because aneuploidy usually affects the expression of hundreds of genes at the same time, which means it will always have some kind of effect on cell viability. Perhaps that in certain contexts however, such as in incredibly



aneuploidy tolerant cell lines or when only a small portion of the chromosome is gained or lost, aneuploidy may be a passenger. Driver, passenger and detrimental aneuploidies shape the evolution of cancer karyotypes over time. Multiple models describe this evolution (Fig. 6)<sup>93</sup>: linear evolution postulates that aneuploidies are acquired linearly in a step-wise process. New driver aneuploidies will provide such a big selective advantage, that this karyotype will quickly take over the whole tumor. In branched evolution, cells will have shared aneuploidies but also generate new ones. Multiple aneuploidies confer a selective advantage, meaning multiple subclones will grow out and consist of a large part of the tumor. A different type of branching evolution, called neutral evolution, postulates that there is no selection, leading to the random accumulation of aneuploidies. This generates pervasive intratumor heterogeneity due to genetic drift. Perhaps that certain aneuploidy subclones are the result of such neutral evolution. The previously described models are frequently linked to small-scale mutations, such as single-nucleotide changes and not to aneuploidies. Aneuploidy however, is often associated with punctuated evolution<sup>94,95</sup>. Punctuated evolution describes a process where a large number of aneuploidies are generated in short bursts of time early during tumorigenesis. Selection subsequently leads to the outgrowth of a few clones.

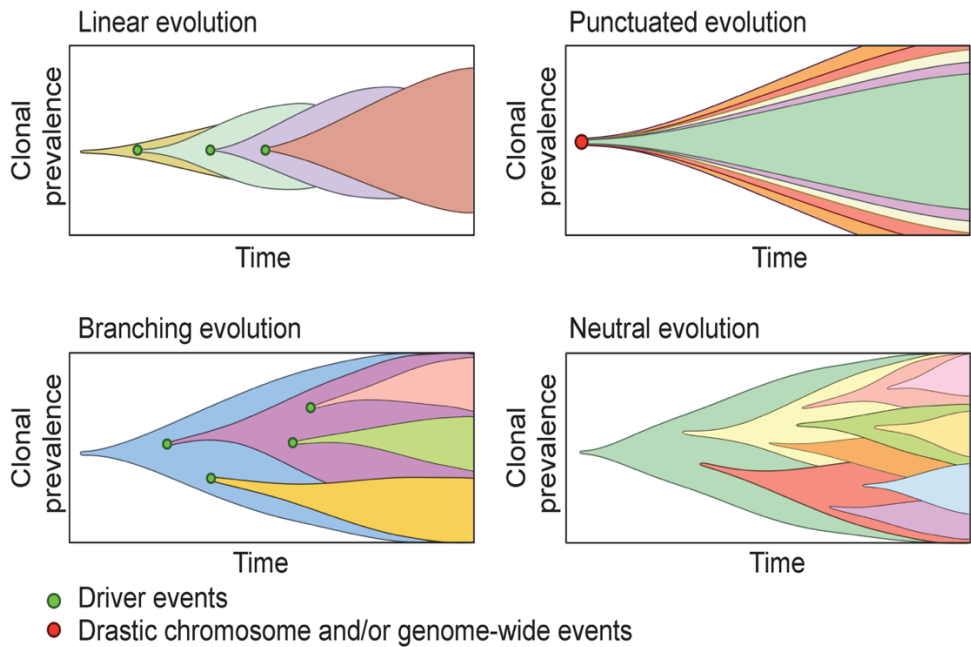


**Figure 6: Proposed models of evolution in cancer.** Illustration depicts the clonal prevalence over time. Each color represents a clone. Adapted from “Cancer Evolution”, by BioRender.com (2022). Retrieved from <https://app.biorender.com/biorender-templates>.

### Thesis outline

In this thesis we used state-of-the-art single-cell DNA sequencing to answer questions related to non-random chromosome mis-segregation frequencies, the consequences of aneuploidy and embryonic aneuploidy prevalence. In **Chapter 2** we review the causes and consequences of non-random segregation errors in both mitosis and meiosis. In **Chapter 3** we used our single-cell DNA sequencing technique to uncover that individual chromosomes have different probabilities of undergoing segregation errors. We found that the mis-segregation frequencies are dictated by the organization of chromosomes in the nucleus: peripheral chromosomes, which are usually larger in size, have a higher tendency to mis-segregate compared to central chromosomes. We hypothesize that this is the case because peripheral chromosomes bi-orient using the peripheral congression

pathway. In **Chapter 4** we designed and characterized a tool to enrich for the loss of a specific chromosome. We used this tool to follow the evolution of copy number changes in non-transformed cell lines over time and describe how tolerance to aneuploidy depends on the type of aberration and chromosome. We also find that cells have vastly different responses depending on which chromosome is lost. In **Chapter 5** we used our single-cell DNA sequencing technique to characterize aneuploidy in the trophectoderm and inner cell mass of 5 day old human embryos. We reveal that the large majority of embryos are chromosomally mosaic. In about half of embryos, mosaicism will not be picked up by bulk-sequencing approaches, because they are present in low levels or are reciprocal. In **Chapter 6** we briefly summarize and discuss the findings of the previous 3 chapters in the light of other literature and suggest interesting future research avenues.

## References

1. Haarhuis, J. H. I., Elbatsh, A. M. O. & Rowland, B. D. Cohesin and its regulation: On the logic of X-shaped chromosomes. *Dev. Cell* **31**, 7–18 (2014).
2. Heald, R. & Khodjakov, A. Thirty years of search and capture: The complex simplicity of mitotic spindle assembly. *J. Cell Biol.* **211**, 1103–1111 (2015).
3. Gudimchuk, N. B. & McIntosh, J. R. Regulation of microtubule dynamics, mechanics and function through the growing tip. *Nat. Rev. Mol. Cell Biol.* **22**, 777–795 (2021).
4. Sacristan, C. & Kops, G. J. P. L. Joined at the hip: Kinetochores, microtubules, and spindle assembly checkpoint signaling. *Trends Cell Biol.* **25**, 21–28 (2015).
5. Maiato, H., Gomes, A. M., Sousa, F. & Barisic, M. Mechanisms of chromosome congression during mitosis. *Biology (Basel)*. **6**, 1–56 (2017).
6. Barisic, M., Aguiar, P., Geley, S. & Maiato, H. Kinetochore motors drive congression of peripheral polar chromosomes by overcoming random arm-ejection forces. *Nat. Cell Biol.* **16**, 1249–1256 (2014).
7. Etemad, B. & Kops, G. J. P. L. Attachment issues: Kinetochore transformations and spindle checkpoint silencing. *Curr. Opin. Cell Biol.* **39**, 101–108 (2016).
8. Hiruma, Y. *et al.* Competition between MPS1 and microtubules at kinetochores regulates spindle checkpoint signaling. *Science* **348**, 1264–1267 (2015).
9. Etemad, B., Kuijt, T. E. F. & Kops, G. J. P. L. Kinetochore-microtubule

- attachment is sufficient to satisfy the human spindle assembly checkpoint. *Nat. Commun.* **6**, 1–8 (2015).
10. Thompson, S. L., Bakhoum, S. F. & Compton, D. A. Mechanisms of Chromosomal Instability. *Curr. Biol.* **20**, 285–295 (2010).
  11. Hindriksen, S., Lens, S. M. A. & Hadders, M. A. The ins and outs of Aurora B inner centromere localization. *Front. Cell Dev. Biol.* **5**, 1–21 (2017).
  12. Carmena, M., Wheelock, M., Funabiki, H. & Earnshaw, W. C. The Chromosomal Passenger Complex (CPC): From Easy Rider to the Godfather of Mitosis. *Nat. Rev. Mol. Cell Biol.* **13**, 789–803 (2012).
  13. Campbell, C. S. & Desai, A. Tension sensing by Aurora B kinase is independent of survivin-based centromere localization. *Nature* **497**, 118–121 (2013).
  14. Hengeveld, R. C. C., Vromans, M. J. M., Vleugel, M., Hadders, M. A. & Lens, S. M. A. Inner centromere localization of the CPC maintains centromere cohesion and allows mitotic checkpoint silencing. *Nat. Commun.* **8**, 1–12 (2017).
  15. Ohkura, H. Meiosis: An overview of key differences from mitosis. *Cold Spring Harb. Perspect. Biol.* **7**, 1–15 (2015).
  16. Webster, A. & Schuh, M. Mechanisms of Aneuploidy in Human Eggs. *Trends Cell Biol.* **27**, 55–68 (2017).
  17. Hunter, N. Meiotic recombination: The essence of heredity. *Cold Spring Harb. Perspect. Biol.* **7**, 1–35 (2015).
  18. Holubcová, Z., Blayney, M., Elder, K. & Schuh, M. Error-prone chromosome-mediated spindle assembly favors chromosome segregation defects in human oocytes. *Science* **348**, 1143–1147 (2015).
  19. Uttamantanin, R. *et al.* MetaSel: A metaphase selection tool using a Gaussian-based classification technique. *BMC Bioinformatics* **14**, 1–13 (2013).
  20. Liu, S. *et al.* Nuclear envelope assembly defects link mitotic errors to chromothripsis. *Nature* **561**, 551–555 (2018).
  21. Ly, P. *et al.* Chromosome segregation errors generate a diverse spectrum of simple and complex genomic rearrangements. *Nat. Genet.* **51**, 705–715 (2019).
  22. Zhang, C. Z. *et al.* Chromothripsis from DNA damage in micronuclei. *Nature* **522**, 179–184 (2015).
  23. Knouse, K. A., Wu, J., Whittaker, C. A. & Amon, A. Single cell sequencing reveals low levels of aneuploidy across mammalian tissues. *Proc. Natl. Acad. Sci.* **111**, 13409–13414 (2014).
  24. McConnell, M. J. *et al.* Mosaic Copy Number Variation in Human Neurons. *Science* **342**, 632–637 (2013).
  25. De Wolf, B. & Kops, G. J. P. L. *Kinetochore Malfunction in Human Pathologies. Advances in Experimental Medicine and Biology* **1002**, (2017).

26. Antonarakis, S. E. Down syndrome and the complexity of genome dosage imbalance. *Nat. Rev. Genet.* **18**, 147–163 (2017).
27. Duijf, P., Schultz, N. & Benezra, R. Cancer cells preferentially lose small chromosomes. *Int. J. Cancer* **132**, 1–20 (2013).
28. Gruhn, J. R. *et al.* Chromosome errors in human eggs shape natural fertility over reproductive life span. *Science* **365**, 1466–1469 (2019).
29. Baart, E. B. *et al.* Preimplantation genetic screening reveals a high incidence of aneuploidy and mosaicism in embryos from young women undergoing IVF. *Hum. Reprod.* **21**, 223–233 (2006).
30. McCoy, R. C. *et al.* Evidence of Selection against Complex Mitotic-Origin Aneuploidy during Preimplantation Development. *PLoS Genet.* **11**, 1–31 (2015).
31. Koch, A., Maia, A., Janssen, A. & Medema, R. H. Molecular basis underlying resistance to Mps1/TTK inhibitors. *Oncogene* **35**, 2518–2528 (2016).
32. Hoevenaar, W. H. M. *et al.* Degree and site of chromosomal instability define its oncogenic potential. *Nat. Commun.* **11**, 1–11 (2020).
33. Jeganathan, K., Malureanu, L., Baker, D. J., Abraham, S. C. & Van Deursen, J. M. Bub1 mediates cell death in response to chromosome missegregation and acts to suppress spontaneous tumorigenesis. *J. Cell Biol.* **179**, 255–267 (2007).
34. Gascoigne, K. E. & Taylor, S. S. Cancer Cells Display Profound Intra- and Interline Variation following Prolonged Exposure to Antimitotic Drugs. *Cancer Cell* **14**, 111–122 (2008).
35. Tighe, A., Johnson, V. L., Albertella, M. & Taylor, S. S. Aneuploid colon cancer cells have a robust spindle checkpoint. *EMBO Rep.* **2**, 609–614 (2001).
36. Kops, G. J. P. L., Weaver, B. A. A. & Cleveland, D. W. On the road to cancer: Aneuploidy and the mitotic checkpoint. *Nat. Rev. Cancer* **5**, 773–785 (2005).
37. Galli, M. & Morgan, D. O. Cell size determines the strength of the spindle assembly checkpoint during embryonic development. *Physiol. Behav.* **36**, 344–352 (2016).
38. Vázquez-Diez, C., Paim, L. M. G. & FitzHarris, G. Cell-Size-Independent Spindle Checkpoint Failure Underlies Chromosome Segregation Error in Mouse Embryos. *Curr. Biol.* **29**, 865–873 (2019).
39. Yost, S. *et al.* Biallelic TRIP13 mutations predispose to Wilms tumor and chromosome missegregation. *Nat. Genet.* **49**, 1148–1151 (2017).
40. Bakhoum, S. F., Genovese, G. & Compton, D. A. Deviant Kinetochore Microtubule Dynamics Underlie Chromosomal Instability. *Curr. Biol.* **19**, 1937–1942 (2009).
41. Bakhoum, S. F., Thompson, S. L., Manning, A. L. & Compton, D. A. Genome stability is ensured by temporal control of kinetochore- microtubule dynamics.

- Nat. Cell Biol.* **11**, 27–35 (2009).
42. Ertych, N. *et al.* Increased microtubule assembly rates influence chromosomal instability in colorectal cancer cells. *Nat. Cell Biol.* **16**, 779–791 (2014).
  43. Barber, T. D. *et al.* Chromatid cohesion defects may underlie chromosome instability in human colorectal cancers. *Proc. Natl. Acad. Sci. U. S. A.* **105**, 3443–3448 (2008).
  44. Solomon, D. A. *et al.* Mutational inactivation of STAG2 causes aneuploidy in human cancer. *Science* **333**, 1039–1043 (2011).
  45. Duncan, F. E. *et al.* Chromosome cohesion decreases in human eggs with advanced maternal age. *Aging Cell* **11**, 1121–1124 (2012).
  46. Wang, S. *et al.* Inefficient Crossover Maturation Underlies Elevated Aneuploidy in Human Female Meiosis. *Cell* **168**, 977–989 (2017).
  47. Lamb, N. E., Sherman, S. L. & Hassold, T. J. Effect of meiotic recombination on the production of aneuploid gametes in humans. *Cytogenet. Genome Res.* **111**, 250–255 (2005).
  48. Oliver, T. R. *et al.* Altered patterns of multiple recombinant events are associated with nondisjunction of chromosome 21. *Hum. Genet.* **131**, 1039–1046 (2012).
  49. Hoffmann, I. Centrosomes in mitotic spindle assembly and orientation. *Curr. Opin. Struct. Biol.* **66**, 193–198 (2021).
  50. Nam, H.-J., Naylor, R. & Deursen, J. M. Centrosome dynamics as a source of chromosomal instability. *Trends Cell Biol.* **25**, 65–73 (2015).
  51. Gönczy, P. Centrosomes and cancer: Revisiting a long-standing relationship. *Nat. Rev.* **15**, 639–652 (2015).
  52. Vitre, B. D. & Cleveland, D. W. Centrosomes, chromosome instability (CIN) and aneuploidy. *Curr. Opin. Cell Biol.* **24**, 809–815 (2012).
  53. Chan, J. Y. A Clinical Overview of Centrosome Amplification in Human Cancers. *Int. J. Biol. Sci.* **7**, 1122–1144 (2011).
  54. Löbrich, M. & Jeggo, P. a. The impact of a negligent G2/M checkpoint on genomic instability and cancer induction. *Nat. Rev.* **7**, 861–870 (2007).
  55. Warecki, B. & Sullivan, W. Mechanisms driving acentric chromosome transmission. *Chromosom. Res.* **28**, 229–246 (2020).
  56. Zeman, M. K. & Cimprich, K. A. Causes and consequences of replication stress. *Nat. Cell Biol.* **16**, 2–9 (2014).
  57. Burrell, R. A. *et al.* Replication stress links structural and numerical cancer chromosomal instability. *Nature* **494**, 492–496 (2013).
  58. Chunduri, N. K. & Storcková, Z. The diverse consequences of aneuploidy. *Nat. Cell Biol.* **21**, 54–62 (2019).
  59. Williams, B. R. *et al.* Aneuploidy Affects Proliferation and Spontaneous Immortalization in Mammalian Cells. *Science* **322**, 703–710 (2008).

60. Chunduri, N. K. *et al.* Systems approaches identify the consequences of monosomy in somatic human cells. *Nat. Commun.* **12**, 1–17 (2021).
61. Stingele, S. *et al.* Global analysis of genome, transcriptome and proteome reveals the response to aneuploidy in human cells. *Mol. Syst. Biol.* **8**, 1–12 (2012).
62. Liu, Y. *et al.* Systematic proteome and proteostasis profiling in human Trisomy 21 fibroblast cells. *Nat. Commun.* **8**, 1–15 (2017).
63. Thompson, S. L. & Compton, D. A. Proliferation of aneuploid human cells is limited by a p53-dependent mechanism. **188**, 369–381 (2010).
64. Taylor, A. M. *et al.* Genomic and Functional Approaches to Understanding Cancer Aneuploidy. *Cancer Cell* **33**, 676–689 (2018).
65. Sansregret, L. *et al.* APC/C Dysfunction Limits Excessive Cancer Chromosomal Instability. *Cancer Discov.* **7**, 218–233 (2017).
66. Hassold T & Hunt P. To err (meiotically) is human: the genesis of human aneuploidy. *Nat. Rev. Genet.* **2**, 280–291 (2001).
67. Sotillo, R. *et al.* Mad2 overexpression promotes aneuploidy and tumorigenesis in mice. *Cancer Cell* **11**, 9–23 (2007).
68. Taggart, J. C., Zaubner, H., Selbach, M., Li, G. W. & McShane, E. Keeping the Proportions of Protein Complex Components in Check. *Cell Syst.* **10**, 125–132 (2020).
69. Donnelly, N. & Storchová, Z. Causes and consequences of protein folding stress in aneuploid cells. *Cell Cycle* **14**, 495–501 (2015).
70. Ohashi, A. *et al.* Aneuploidy generates proteotoxic stress and DNA damage concurrently with p53-mediated post-mitotic apoptosis in SAC-impaired cells. *Nat. Commun.* **6**, 1–16 (2015).
71. Tang, Y. C., Williams, B. R., Siegel, J. J. & Amon, A. The energy and proteotoxic stress-inducing compounds AICAR and 17-AAG antagonize proliferation in aneuploid cells. *Cell* **144**, 499–512 (2011).
72. Tsai, H. J. *et al.* Hypo-osmotic-like stress underlies general cellular defects of aneuploidy. *Nature* **570**, 117–121 (2019).
73. Passerini, V. *et al.* The presence of extra chromosomes leads to genomic instability. *Nat. Commun.* **7**, 1–12 (2016).
74. Ariyoshi, K. *et al.* Induction of genomic instability and activation of autophagy in artificial human aneuploid cells. *Mutat. Res.* **790**, 19–30 (2016).
75. Santaguida, S. *et al.* Chromosome Mis-segregation Generates Cell-Cycle-Arrested Cells with Complex Karyotypes that Are Eliminated by the Immune System. *Dev. Cell* **41**, 638–651 (2017).
76. Hoadley, K. A. *et al.* Cell-of-Origin Patterns Dominate the Molecular Classification of 10,000 Tumors from 33 Types of Cancer. *Cell* **173**, 291–304 (2018).
77. Beroukhi, R. *et al.* The landscape of somatic copy-number alteration across

- human cancers. *Nature* **463**, 899–905 (2010).
78. de Wolf, B. *et al.* Chromosomal instability by mutations in the novel minor spliceosome component CENATAC. *EMBO J.* **40**, 1–18 (2021).
  79. Díaz-Rodríguez, E., Sotillo, R., Schvartzman, J. & Benezra, R. Hec1 overexpression hyperactivates the mitotic checkpoint and induces tumor formation in vivo. *Proc. Natl. Acad. Sci.* **105**, 16719–16724 (2008).
  80. Liu, X. *et al.* Trisomy eight in ES cells is a common potential problem in gene targeting and interferes with germ line transmission. *Dev. Dyn.* **209**, 85–91 (1997).
  81. Ben-David, U. *et al.* Aneuploidy induces profound changes in gene expression, proliferation and tumorigenicity of human pluripotent stem cells. *Nat. Commun.* **5**, 1–11 (2014).
  82. Rutledge, S. D. *et al.* Selective advantage of trisomic human cells cultured in non-standard conditions. *Sci. Rep.* **6**, 1–12 (2016).
  83. Replogle, J. M. *et al.* Aneuploidy increases resistance to chemotherapeutics by antagonizing cell division. *Proc. Natl. Acad. Sci.* **117**, 30566–30576 (2020).
  84. Ippolito, M. R. *et al.* Gene copy-number changes and chromosomal instability induced by aneuploidy confer resistance to chemotherapy. *Dev. Cell* **56**, 2440–2454 (2021).
  85. Trakala, M. *et al.* Clonal selection of stable aneuploidies in progenitor cells drives high-prevalence tumorigenesis. *Genes Dev.* **35**, 1079–1092 (2021).
  86. Zenz, T. *et al.* TP53 mutation profile in chronic lymphocytic leukemia: Evidence for a disease specific profile from a comprehensive analysis of 268 mutations. *Leukemia* **24**, 2072–2079 (2010).
  87. Davoli, T. *et al.* Cumulative haploinsufficiency and triplosensitivity drive aneuploidy patterns and shape the cancer genome. *Cell* **155**, 948–962 (2013).
  88. Soto, M. *et al.* p53 Prohibits Propagation of Chromosome Segregation Errors that Produce Structural Aneuploidies. *Cell Rep.* **19**, 2423–2431 (2017).
  89. López-García, C. *et al.* BCL9L Dysfunction Impairs Caspase-2 Expression Permitting Aneuploidy Tolerance in Colorectal Cancer. *Cancer Cell* **31**, 79–93 (2017).
  90. Zack, T. I. *et al.* Pan-cancer patterns of somatic copy-number alteration. *Nat. Genet.* **45**, 1134–1140 (2013).
  91. Bielski, C. M. *et al.* Genome doubling shapes the evolution and prognosis of advanced cancers. *Nat. Genet.* **50**, 1189–1195 (2019).
  92. Hanahan, D. & Weinberg, R. A. Hallmarks of cancer: The next generation. *Cell* **144**, 646–674 (2011).
  93. Davis, A., Gao, R. & Navin, N. Tumor evolution: Linear, branching, neutral or punctuated? *Biochim. Biophys. Acta* **1867**, 151–161 (2017).



94. Gao, R. *et al.* Punctuated copy number evolution and clonal stasis in triple-negative breast cancer. *Nat. Genet.* **48**, 1119–1130 (2016).
95. Sottoriva, A. *et al.* A Big Bang model of human colorectal tumor growth. *Nat. Genet.* **47**, 209–216 (2015).



## **Chapter 2**

# **Chromosome inequality: causes and consequences of non-random segregation errors in mitosis and meiosis**

Sjoerd J. Klaasen<sup>1,2</sup> & Geert J.P.L Kops<sup>1,2\*</sup>

### **Affiliations**

<sup>1</sup> Hubrecht Institute – KNAW (Royal Netherlands Academy of Arts and Sciences) and University Medical Centre Utrecht, Utrecht, the Netherlands.

<sup>2</sup> Oncode Institute, Utrecht, the Netherlands

**Published in *Cells*, vol. 11, 3564 (2022).**

**Aneuploidy is a hallmark of cancer and a major cause of miscarriages in humans. It is caused by chromosome segregation errors during cell divisions. Evidence is mounting that the probability of specific chromosomes to undergo a segregation error is non-random. In other words, some chromosomes have a higher chance to contribute to aneuploid karyotypes than others. This could have important implications for the origins of recurrent aneuploidy patterns in cancer and the developing embryo. Here, we review recent progress in understanding the prevalence and causes of non-random chromosome segregation errors in mitosis and meiosis. We evaluate its potential impact on cancer and human reproduction and discuss possible research avenues.**

Every mitotic or meiotic division, cells must accurately segregate their chromosomes into two new daughter cells. Failure to do so leads to aneuploidy, which is here defined as copy number aberrations from the diploid state of whole or large parts of chromosomes. Aneuploidy is one of the most striking genomic abnormalities in cancer and embryos and is surprisingly common during embryonic development. Depending on the cell type, normal cells *in vitro* mis-segregate chromosomes between 0.5-5.0 times per 100 cell divisions<sup>1-3</sup>. These low segregation error frequencies are supported by the observation that 2.2-4.0% of cells in healthy human liver, brain and skin are aneuploid<sup>4</sup>, although neurons in the brain have also been reported to be much more aneuploid<sup>5</sup>. Certain cancer cell lines *in vitro* mis-segregate chromosomes orders of magnitude more frequently than healthy cells, are highly aneuploid and display karyotype heterogeneity<sup>1,3,6,7</sup>. Aneuploidy is also surprisingly common during human embryonic development: around 50-80% of early embryos from *in-vitro* fertilization procedures exhibit chromosomal copy number changes<sup>8-10</sup>. It is estimated that 31% of embryos possess aneuploidies from segregation errors made during meiosis, while 74% of embryos possess mosaic aneuploidies from mis-segregations made during the first few mitotic divisions after fertilization<sup>9</sup>. Because aneuploidy often induces miscarriages, aneuploidy percentages rapidly decline when more developed embryos are assessed<sup>11</sup>. Nevertheless, certain trisomies, such as for chromosome 13, 18 or 21, are compatible with life.

Why is aneuploidy so common in cancer, but not in healthy adult tissue? First, cancer cells more frequently mis-segregate chromosomes during cell divisions, a phenotype known as chromosomal instability (CIN)<sup>12</sup>. Despite much effort, it remains unclear what the molecular causes for this are, and there could be many<sup>13</sup>. It is thought though, that CIN provides cancer cells with various advantages, and indeed inducing CIN can initiate cancer and promote metastasis<sup>14–16</sup>. Second, cancer cells have evolved to deal with the problematic consequences of aneuploidy. Expression levels of genes on a given chromosome scale with its copy number state<sup>17–20</sup>. In normal cells, this leads to an array of stresses of, for example, proteotoxic or genotoxic origin<sup>18,21–25</sup>, often leading to a p53-dependent arrest<sup>18,26</sup>. Because of this, non-transformed cells with experimentally-induced aneuploidies have a proliferative disadvantage over their diploid counterparts<sup>18,20</sup>. Many cancers however have evolved mechanisms to cope with these disadvantages. These include mutations in the p53 pathway, whole genome doublings that buffer against gene dosage changes, increased expression of pathways responsible for resolving the stresses, or gene dosage compensation of stress-inducing proteins<sup>27–30</sup>.

Whole and arm-level aneuploidy profiles of cancers are similar within tissue type but different between tissues<sup>28,31,32</sup>. For example, colorectal cancers typically gain chromosomes 7, 8 and 13 but lose chromosome 18, while squamous cancers lose chromosome arm 3p but gain 3q<sup>28,33</sup>. One type of structural aneuploidy, called chromothripsis-like patterns, also preferentially resides on certain chromosomes<sup>34–36</sup>. Chromothripsis occurs due to the rupture of micronuclei, which originate from mis-segregation events and is characterized by extensive genomic rearrangements and oscillating copy number patterns restricted to a single chromosome<sup>37,38</sup>. Likewise, only certain chromosomes can be found at altered copy number states at late stages of human development (gain of chromosome 13, 18, 21 and X and loss of the X or Y chromosome)<sup>39</sup>. How do cells develop such recurrent aneuploidy patterns? One likely explanation is selection. In cancer, tissue-specific aneuploidies can achieve amplifications of oncogenes and loss of tumor suppressors that result in an increased fitness of cells from that particular tissue<sup>40,41</sup>. Similarly, during embryogenesis only cells with aneuploidies of small chromosomes are able to

propagate, since these contain relatively few genes and thus suffer less from cellular stresses<sup>17</sup>. However, it is becoming clear that another factor may have important contributions: the non-random mis-segregation frequencies of specific chromosomes that impacts which chromosomes are more or less likely to be lost or gained. Chromosomes differ in various ways (Fig. 1) and several of these can impact their behavior in mitosis. This review focuses on recent progress in understanding non-random chromosome segregation errors. We discuss the current evidence for a chromosome segregation error bias in mitosis and meiosis and its various proposed causes. Furthermore, we will highlight the importance of non-random segregation errors in tumor evolution and human reproduction.

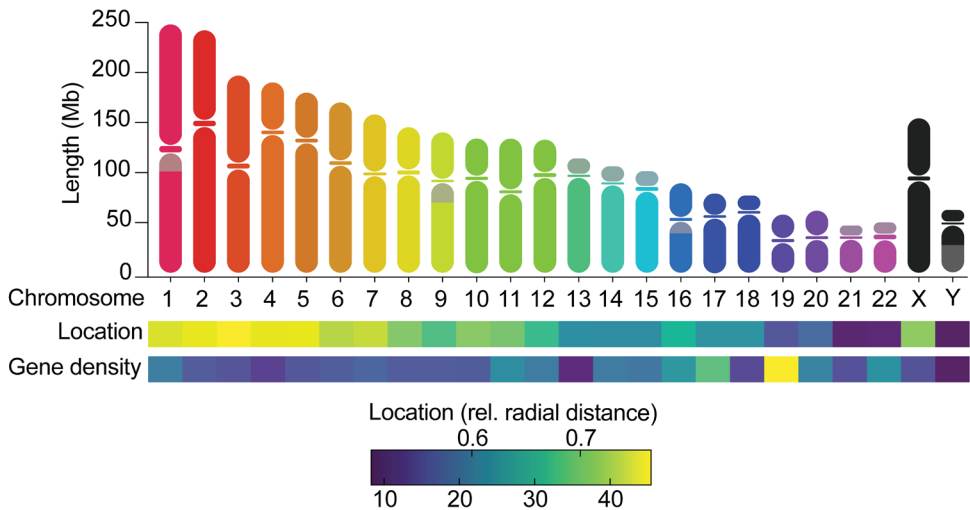


**Figure 1: Chromosomes differ in many ways.** Graph shows the length of chromosome arms and centromeres, its relative radial distances towards the center of the nucleus<sup>136</sup> and gene densities calculated from Ensembl (GRCh38.p13). Large heterochromatin blocks are shown in grey.

## Evidence for non-random chromosome segregation error frequencies

### *In mitosis*

The first observations of non-random segregation errors came from micronucleus assays, which measure the genotoxicity of compounds by quantifying the number of micronuclei in cell culture<sup>42</sup>. Micronuclei in lymphocytes treated with different

clastogenic and aneugenic agents were shown to have various non-random chromosomal contents, depending on the agents used or the set-ups of the experiments (for an extensive list see Norppa *et al.* (2003))<sup>42</sup>. Although certain chromosomes may be more prone to become micronucleated<sup>43,44</sup>, micronuclei originate from recent segregation error events and are therefore regarded as a proxy for recently mis-segregated chromosomes. As such, non-random micronuclear content in these assays is indicative of non-random segregation errors upon treatment with the toxic agents. Interestingly, chromosomes that end up in micronuclei have a higher probability to improperly segregate in the following mitoses. Around half of micronuclei undergo membrane rupture<sup>45</sup>, causing defective replication, inadequate nuclear protein import, epigenetic rewiring, exposure to cytosolic proteins<sup>46–48</sup>, and mis-segregations during the next cell cycle<sup>45,49</sup>. Micronuclei therefore catalyze the formation of chromosome-specific supernumerary and complex aneuploidies.

In recent years, advances in single-cell technologies such as fluorescence in-situ hybridization (FISH) and single-cell DNA sequencing allowed researchers to assess segregation error rates per chromosome by looking at the complete chromosome content of cells following disrupted mitosis. Release from a nocodazole-induced 8h mitotic arrest specifically increased the mis-segregation frequencies of chromosomes 1 and 2 maximally 11-fold in human cells<sup>50</sup>. A similar treatment in rat kangaroo kidney epithelial (PtK1) cells caused non-disjunction for six chromosomes, but less so for chromosomes 1 and 5<sup>51</sup>. Release from an arrest induced by monastrol, an Eg5 kinesin inhibitor, enriched for anaphase lagging chromosomes 1 and 2 in human cells, chromosome 4 in PtK1 cells and chromosome 3+X in Indian Muntjac cells<sup>51,52</sup>. Compromising attachment error correction and the spindle assembly checkpoint (SAC) by inhibiting the kinase Mps1 revealed a high mis-segregation frequency of larger chromosomes by up to a 3-fold difference in human cells and of chromosome 3+X in Indian Muntjac cells<sup>38,52,53</sup>. Larger chromosomes were also found to mis-segregate more frequently in human cells when attachment error correction was compromised by inhibiting Aurora B kinase, when microtubules were stabilized by low concentrations of taxol, or when chromosome congression

was compromised by inhibition of the mitotic kinesin CENP-E<sup>53,54</sup>. Interestingly, generating DNA damage in human cells during interphase using ionizing radiation or replication stress, which is defined as the slowing down or stalling of the replication fork machinery, specifically elevated structural rearrangements and micronuclear incorporation of larger chromosomes as well<sup>38,55,56</sup>. Lastly, auxin-inducible degradation of CENP-A in human cells increased the segregation error frequency of chromosomes 6, X and Y<sup>57,58</sup>. In conclusion, segregation error biases are frequently observed when chromosomal instability is experimentally induced.

Can non-random mis-segregation events also be observed under more natural conditions? Small (<2.7Mb) human artificial chromosomes in HT1080 cells mis-segregated and were lost maximally 5 times more often than their larger natural and artificial counterparts<sup>59</sup>. In human embryos, segregation errors during the first few divisions are frequent. Preimplantation genetic testing on single cells of 3 day old human embryos showed that the frequency at which a given chromosome was found as aneuploid correlated with its size<sup>60</sup>. Likewise, in cancer cells, larger chromosomes were preferentially entrapped in the micronuclei of glioblastoma, colorectal cancer and cervical cancer cell lines<sup>53,61</sup>, and other biases were observed in three other cancer lines<sup>53</sup>. Furthermore, FISH for five chromosomes on anaphase figures in five glioma and one breast cancer cell line also found that larger chromosomes mis-segregated more often than smaller ones<sup>62</sup>. Taken together, a mis-segregation bias is also frequently observed in natural conditions of chromosomal instability, and tends to correlate with chromosome size.

### *In meiosis*

Male meiosis is relatively error-free with around 1-5% of spermatozoa containing aneuploidies<sup>63</sup>. Single cell DNA sequencing of 31,228 spermatozoa from 20 healthy donors established that the smaller acrocentric chromosomes and the sex chromosomes were ~2-to-6-fold more likely to be aneuploid, which was in line with FISH studies on spermatozoa and testicular biopsies<sup>63-65</sup>. Unlike male meiosis, female meiosis is notoriously erroneous and is therefore responsible for the large majority of meiotic-associated aneuploidies in embryos<sup>63,66</sup>. Observations using



leftover oocytes from *in vitro* fertilization and *in vitro* and *in vivo* matured oocytes from biopsies of small antral follicles showed that the aneuploidy level is relatively high in females compared with males<sup>63,67</sup>. Like in spermatocytes, sex or acrocentric chromosomes are often found aneuploid in oocytes<sup>67</sup>. Chromosome 16 is a notable exception, as it seems to mis-segregate most often in female meiosis<sup>68</sup>. Oocytes in meiosis II of women below the age of 20 are ~1.7 times more frequently aneuploid compared to those of women between the ages of 20 to 33 (22% versus 37%)<sup>67</sup>. The errors mostly originate from non-disjunction events and are ~4 times more likely to affect large chromosomes compared to acrocentric ones<sup>67</sup>. Oocytes of women above the age of 33 are 2.3 times more frequently aneuploid compared to those of women between the ages of 20 to 33 (24% versus 54%) and often involve premature separation of sister chromatids or reverse segregation of acrocentric or smaller chromosomes<sup>67</sup>. The observation that smaller chromosomes more often mis-segregate during meiosis in older individuals is corroborated by similar studies also using human oocytes and embryos<sup>60,69–73</sup>.

## Chromosome segregation mechanisms

In order to understand what causes non-random mis-segregation of chromosomes one must understand the basic principles governing chromosome segregation during cell division. We will therefore briefly discuss the general steps of mitosis and meiosis (Fig. 2).

Before cells can enter mitosis, all chromosomes must be replicated and sister chromatids must be tightly bound to each other by a protein complex called cohesin. The start of mitosis is defined by the start of condensation of chromosomes into their characteristic X-shaped structures. When condensation is completed, the nuclear envelope breaks down and highly dynamic tubulin proteins will polymerize into microtubules. These microtubules organize into a spindle with two focused poles on opposite sides of the cell. In most cells, except oocytes<sup>74</sup>, these poles are organized by centrosomes. Microtubules physically interact with chromosomes via kinetochores, which are multiprotein structures located on centromeres<sup>75</sup>. An

intricate balance of pulling and pushing forces direct the movement of chromosomes to the metaphase plate, a process known as congression<sup>76</sup>. These movements are generated by the depolymerization or polymerization of microtubules, but also by microtubule motors such as CENP-E and dynein, which allow for gliding of chromosomes on microtubules. Chromosomes located in the center of the nucleus almost instantaneously acquire the proper end-on attachments, meaning interactions of kinetochores with the +-ends of microtubules, and therefore achieve correct bi-orientation without the need for error-correction mechanisms<sup>77</sup>. The more peripheral ones however tend to first connect to the lattices of microtubules, and need the help of motor proteins and attachment error-correction mechanisms for conversion to end-on interactions and correct biorientation<sup>76,78–80</sup>. Only when all chromosomes have bioriented and congressed on the metaphase plate, will anaphase commence: centromeric cohesin is released and sister chromatids are pulled to opposite sides. To make sure that anaphase does not start until all chromosomes are properly bioriented, cells employ the spindle assembly checkpoint (SAC) pathway. This pathway, dependent on the kinase Mps1<sup>81</sup>, senses lack of interactions between kinetochores and microtubules, and halts anaphase initiation accordingly<sup>82</sup>. Interestingly, the SAC is not activated when specific erroneous attachments are present, such as when one kinetochore is captured by both poles (merotely) or both kinetochores are captured by one pole (syntely)<sup>83,84</sup>. Instead, these attachment types are corrected by an error-correction pathway involving the kinase Aurora B<sup>85–88</sup>.

Many of the mechanistic principles of chromosome segregation in mitosis also apply to meiosis<sup>89</sup>. Nevertheless, meiosis differs in several aspects. Meiosis occurs over two distinct steps: separation of homologs (meiosis I) and separation of sister chromatids (meiosis II, similar to mitosis). A defining step during meiosis I is the pairing of homologs through the recombination of chromosome arms into chiasmata. This process should take place at least once on every homolog as it is important for driving genetic variation and for keeping homologs together until anaphase I<sup>90</sup>. Probably the most striking feature of meiosis is its sexual dimorphism. In humans,

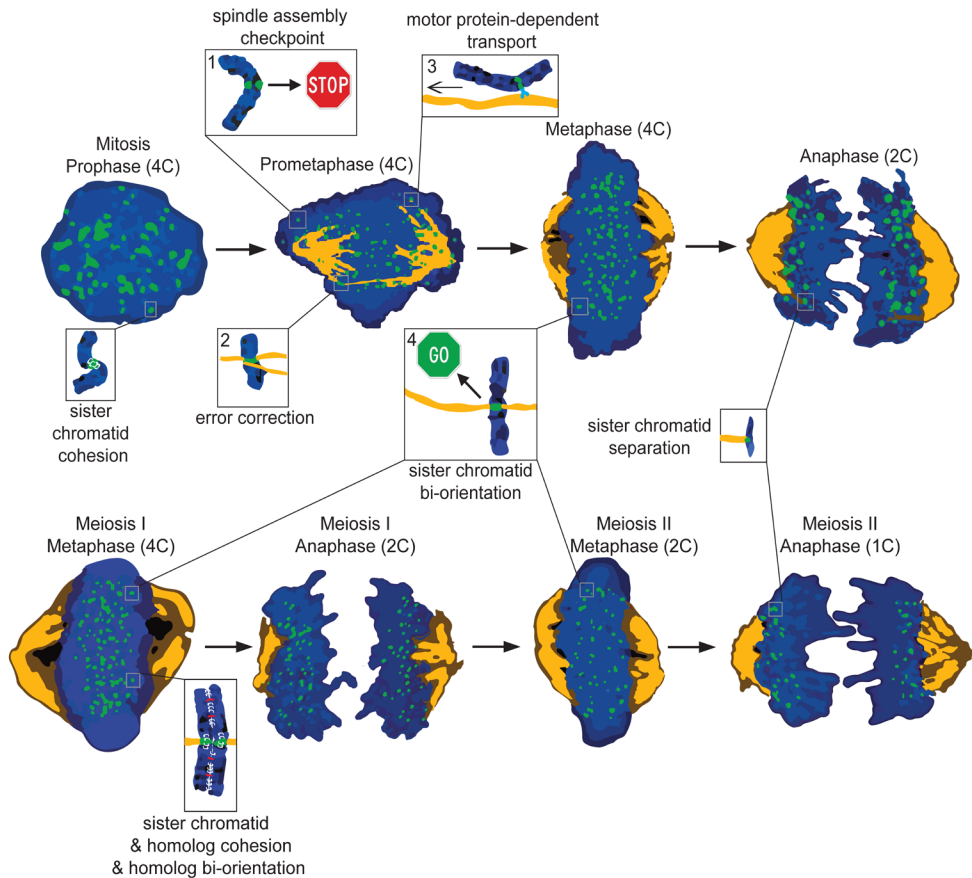


**Figure 2:** Cartoon illustrating different phases of mitosis (top) and meiosis (bottom). During mitosis, all the DNA is supposed to evenly split, creating two genetically identical daughter cells. Chromosomes (blue) are brought to the metaphase plate with the help of microtubules (orange) or motor proteins (light blue). During this phase, sister kinetochores (green) could be: 1. Unattached, leading to the activation of the spindle assembly checkpoint (SAC). 2. Erroneously attached, which is resolved by the error correction machinery. 3. Laterally attached, which allows for transport towards the metaphase plate. 4. End-on attached, which favors proper segregation. Only when all sister kinetochores are bi-oriented the SAC is silenced, causing the removal of centromeric cohesin (white) and the movement of sisters to opposite poles. Meiosis follows many of the same principles as mitosis, but differs as well. Instead of creating two genetically identical diploid daughter cells, meiosis generates four genetically different haploid cells. Furthermore, homologous chromosomes are not only cohesed by cohesin, but also by chiasmata (red), which are physical links created during genetic recombination. During meiosis, the homologous chromosomes are separated first followed by separation of the sisters. Zoom-ins in the figure highlight some of the mechanisms responsible for proper chromosome segregation. 4C, 2C and 1C refers to DNA content.

female meiosis I starts in the germ cells during fetal development, is followed by a prolonged metaphase I arrest (also called dictyate arrest), and continues after ovulation to metaphase II until fertilization triggers the final steps. Male meiosis on the other hand takes place throughout adult life<sup>90</sup>.

## **Segregation error bias mechanisms**

### *Centromeric and centromere-proximal features*

Centromeres are vital for proper chromosome segregation since they assemble the kinetochore and are the site of sister chromatin cohesion. They have thus been implicated in multiple mis-segregation biases. For example, treating cells with the microtubule poison nocodazole or with the kinesin inhibitor monastrol causes a mitotic arrest, leading to cohesion fatigue at the centromeres of specific chromosomes<sup>50,91</sup>. It is tempting to speculate that the frequently mis-segregating chromosomes have lower levels of centromeric cohesin molecules and that these are therefore more susceptible to cohesion fatigue, but this remains to be determined. Some cancers (e.g. glioblastoma) have mutations in cohesin-related genes and correcting these mutations in glioblastoma cell lines reduced CIN<sup>92</sup>. It would be of interest to establish if the mis-segregation frequencies in these cells are similar to those with experimentally induced cohesion fatigue.

Aside from a cohesion-related bias, the size of centromeres has also been implicated in affecting individual chromosome segregation error frequencies. In Indian Muntjac cells, mis-segregation frequencies after SAC inhibition and monastrol treatment were larger for chromosomes with larger centromeres<sup>52</sup>. Large centromeres bind more microtubules and are therefore perhaps more likely to make merotelic attachments, leading to mis-segregations. Whether this phenomenon also takes place in other species is unclear. However, human kinetochores differ substantially in size, and computational modelling suggest that larger kinetochores may make more erroneous attachments<sup>93,94</sup>. Paradoxically, smaller centromeric domains may also increase mis-segregation probabilities. The centromeric proteins CENP-A and CENP-B are responsible for determining the location of kinetochores. As such, CENP-A degradation forces cells to rely solely on CENP-B for assembling kinetochores, and this caused higher frequency of segregation errors for

chromosomes whose centromeres had lower CENP-B levels<sup>57,58</sup>. In conclusion, centromeres were found to impact mis-segregation frequencies in multiple settings.

### *Chromosome size*

As outlined in section 2, depending on the mode of induction, an increase in chromosome size was found to increase or decrease mis-segregation frequencies. Larger chromosomes are more often found near the periphery of the nucleus, which complicates their eventual biorientation (see section 4.3). In addition, simply by chance, larger chromosomes have a higher likelihood to become damaged or contain elements prone to damage. For example, random DNA damage, such as ionizing radiation, more often induced structural rearrangements and the formation of micronuclei of larger chromosomes<sup>38,56</sup>. Furthermore, replication stress relatively frequently induced the formation of micronuclei containing larger chromosomes, because these are more likely to contain replication stress-sensitive sequences<sup>55,95,96</sup>. Replication stress is a common phenotype in cancer as it is induced by overexpression of various oncogenes<sup>97</sup>.

On the other hand, smaller chromosomes contain a lower number of certain protein structures and therefore depend more on them. As discussed before, it is vital for every homolog in meiosis to have at least one chiasma. A lack of chiasmata (achiasmate) on a single pair of homologs allows them to drift apart and has been proposed to contribute to segregation errors in meiosis<sup>11</sup>. Chiasmata distribute evenly across DNA, meaning larger chromosomes such as 1 have on average ~4 chiasmata, while smaller chromosomes such as the acrocentric and Y chromosomes only have 1 or 2. An exception is the X chromosome, which only has 1 chiasma<sup>98,99</sup>. Therefore, if every crossover has an equal chance to fail maturation, larger chromosomes are less likely to be achiasmate as other chiasmata compensate for a failed crossover event. Supporting this, smaller chromosomes in murine spermatocytes and human oocytes are more likely to be achiasmate, and mis-segregated chromosomes in human spermatozoa or oocytes have a decreased number of crossovers<sup>100–102</sup>. It is also believed that the female age-related increase in aneuploidy is related to chromosome size. Cohesin is lost over time in oocytes

and is not replenished<sup>67,103,104,105,106</sup>. Loss of cohesin abolishes chiasmata and creates gaps between homologs and sister chromatids leading to erroneous kinetochore-microtubule attachments or even a complete loss of cohesion between chromosomes<sup>103,107</sup>. Progressive loss of cohesin between the homologs as well as the sister chromatids first affects chromosomes with shorter arms, because these have less overall cohesin. This model also explains why oocytes of women of 35-39 years old mis-segregate smaller chromosomes even more frequently than oocytes of women above 39 years old<sup>108,109</sup>. Early age-related loss of cohesin in oocytes first substantially decreases cohesion on smaller chromosomes, while even more loss of cohesin in older women eventually also affects proper cohesion of larger chromosomes. In short, chromosome size can be an important cause for non-random segregation errors, especially in meiosis.

### *Chromosome location*

Chromosomes are not organized randomly in the interphase nucleus, which significantly impacts mis-segregation frequencies in multiple contexts. Larger chromosomes are frequently positioned in the periphery of the nucleus, while smaller chromosomes occupy a more central position<sup>53,110</sup>. Because of this, peripheral and thus larger chromosomes often end up behind the poles at the start of mitosis<sup>78,111</sup>. In turn, they need to travel a longer distance to the metaphase plate, are more likely to make non-amphitelic attachments, such as lateral or erroneous ones<sup>77,78,112</sup> or might have difficulties crossing centrosomes. They thus need more time to bi-orient, in contrast to the almost instantaneously biorienting central chromosomes<sup>113</sup>. When cells were forced to prematurely enter anaphase due to SAC inhibition these larger peripheral chromosomes mis-segregated more frequently<sup>38,53</sup>. Increased mis-segregations of these chromosomes was not due to other chromosome-specific differences, because the same chromosomes had different mis-segregation frequencies when their location naturally or experimentally changed<sup>53</sup>. Larger chromosomes also mis-segregated more after inhibition of Aurora B, the master regulator of the error correction pathway, and misaligned more after altering microtubule dynamics or inhibiting CENP-E, a motor protein necessary for congression<sup>53,54</sup>. Whether chromosome locations affect mis-segregation biases

when chromosomal instability occurs naturally is unclear. Interestingly though, micronuclear entrapment of chromosomes in cancer cells, as well as mis-segregation frequencies during mitosis in human embryos and certain cancer cells correlate with chromosome size and thus location. In mice, SAC weakening occurs during the first error-prone mitotic divisions<sup>114</sup>. The mitotic mis-segregation bias found in human embryos may therefore be similar to the one found in SAC-compromised human somatic cells, and thus be a consequence of the 3-dimensional chromosome organization. This, however, remains to be determined since mis-segregations during these divisions have also been linked to difficulties clustering the parental genomes<sup>115</sup>.

## **Consequences of a chromosome segregation error bias**

### *Karyotype evolution in cancer*

Given the many observations of non-random segregation error frequencies for various chromosomes and the resulting non-random aneuploidy landscapes in cell populations following segregation error events, a major question is how this impacts genome evolution in cancer and human reproduction. Non-random segregation errors could, for example, contribute to the emergence of recurrent aneuploidy patterns observed in tumors (Fig. 3a). Chromosome 1 mis-segregates frequently in intestinal cancer cell lines and in error-induced intestinal organoids<sup>53</sup>, which could impact the probability and timing by which the often-observed loss of 1p in colorectal adenocarcinomas occurs<sup>116</sup>. How much the biased mis-segregation contributes to emergence of such patterns is unknown. Clonal outgrowth of cells that underwent the high-probability event of loss of chromosome 1 in this scenario could be due to neutral drift dynamics or to positive selection. The former is not uncommon for single nucleotide variants<sup>117,118</sup> and has been seen for copy number variations as well<sup>119</sup>. Which evolutionary dynamics underlie aneuploidy patterns in the various cancers remains to be resolved. However, copy number variations regularly colocalize with cancer genes<sup>40,41</sup>, which makes it likely that at least some aneuploidies are the result of positive selection. Although it has been investigated in only a limited number of settings in humans, this hypothesis is supported by the observation that the

proliferation rates of diploid cells are higher than that of trisomic or monosomic cells in normal culturing conditions, and that in certain challenging conditions specific aneuploidies are favored<sup>18,20,120,121</sup>. This suggests that selection of aneuploidies is inherently non-neutral. Such observations were done from a relatively normal ground state, and it therefore remains to be determined if this holds true for all chromosomes and chromosome combinations, in different aneuploidy-tolerant non-transformed and transformed cell types and under different selection pressures.

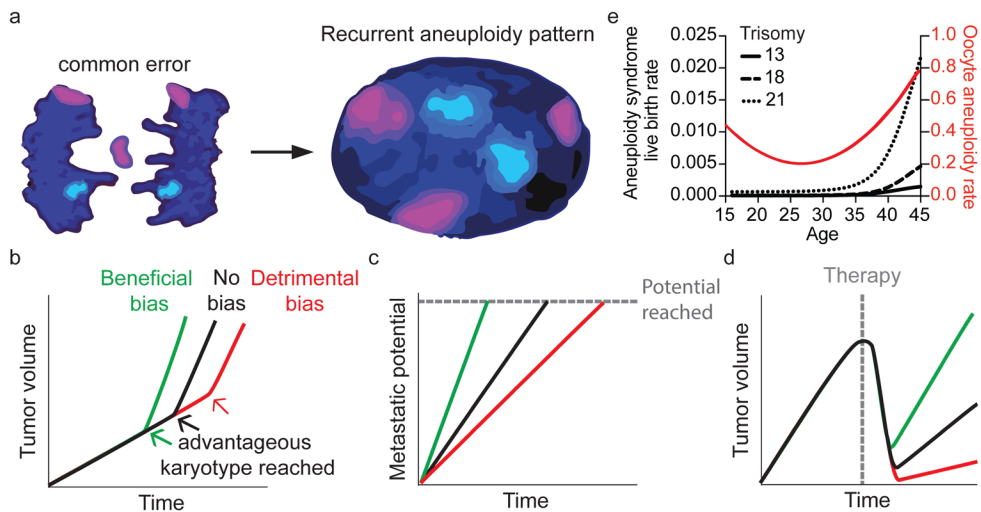


**Figure 3: Hypothesized consequences of a segregation error bias.** **a.** Frequently mis-segregating chromosomes gives rise to the recurrent aneuploidy pattern seen in cancer. **b,c,d,** Graphs depicting influence of a mis-segregation bias on the speed by which a tumor grows (**b**), it reaches metastatic potential (**c**) or is able to grow out after therapy (**d**). **e.** Graph showing the relationship between age and oocyte aneuploidy rate<sup>67</sup> or the aneuploidy syndrome live-birth rate<sup>126</sup>.

Another potential way through which a segregation error bias can affect the evolution of karyotypes is by creating the initial aneuploidy landscapes on which selection acts, thereby impacting the time it takes to reach the recurrent aneuploidy patterns seen in cancer. Accordingly, non-random mis-segregations could impact multiple aspects of tumorigenesis, since specific recurrent aneuploidy patterns are associated with tumor proliferation, metastasis formation and therapy resistance (Fig. 3b-d)<sup>27,122</sup>. For example, clear cell renal carcinoma metastases have often lost



chromosome arm 9p compared with the primary tumor<sup>123</sup>. If chromosome 9 is mis-segregated relatively often, a cancer could quickly obtain a cell with this potentially beneficial aneuploid state. On the other hand, it would take substantially longer if chromosome 9 would have a low mis-segregation probability.

A mis-segregation bias may not only be important for the acquisition of aneuploidies, but also for their maintenance. For example, imagine a cancer with a chromosome 20 trisomy, which provides a proliferative advantage and has therefore been selected for. As stated before, reaching this state is easier if chromosome 20 mis-segregates more frequently. However, after this aneuploidy is acquired the high mis-segregation frequency would tend to result in deviation away from this trisomic state. Selection for reduced CIN rates or altered segregation error biases could in principle provide solutions to this. Unfortunately, experimental or theoretical examinations of the potential consequences of a mis-segregation bias have yet to be done. Genome evolution studies following the karyotypes of chromosomally unstable cells with different mis-segregation biases or mathematical models of aneuploidy evolution that incorporate experimental data (such as known mis-segregation biases, cancer chromosomal instability levels, recurrent aneuploidy patterns and the proliferative advantage of specific aneuploidies) should shed more light on these questions<sup>124,125</sup>.

### *Aneuploid live births*

In human embryos, non-random mis-segregations could potentially determine frequencies of aneuploidies in live births. Larger chromosomes mis-segregate more frequently in oocytes of younger women and therefore are not expected to increase aneuploid live births, because only small chromosome aneuploidies are compatible with life (chromosome 13, 18 or 21). Younger women indeed do not have an increased chance to give birth to children with trisomies of chromosome 13, 18 or 21 (Fig. 3e)<sup>67,126</sup>. On the other hand, smaller chromosomes mis-segregate more frequently in oocytes of older women, and in that population of women the amount of aneuploid live births increases drastically. Nonetheless, trisomy of chromosome 13, 18 and 21 often result in miscarriage<sup>39</sup>, and aneuploidies in human embryos are often of mitotic origin, which comes with its own segregation error bias<sup>9,60</sup>. The latter

are however usually mosaic, meaning they may not be a source of aneuploidy in births as they are likely outcompeted by diploid cells in the embryo<sup>60,127</sup>. It therefore remains an interesting question to what extent biased segregation errors of the small chromosomes contributes to increased rates of live aneuploid births from older women.

## Concluding remarks and future directions

As outlined above, more and more accumulating evidence indicates that segregation errors in mitosis and meiosis can be non-random, and some of the molecular explanations for this are emerging. These insights open up many fascinating new questions. For example, does compromising different pathways implicated in chromosomal instability, such as hyperstable microtubule-kinetochore attachments, centrosomal defects/amplification, polyploidization or cohesion fatigue<sup>92,128–132</sup>, cause non-random segregation errors and if so, what kinds? Does this differ between cell types (e.g. oocytes have a weak SAC and are acentrosomal)<sup>133–135</sup>? Do chromosomally unstable cancers experience non-random segregation errors and if so, can cancer types be distinguished by their bias? What are the consequences of a segregation error bias on the evolution of karyotypes and therefore the evolution of cancer? Large-scale single-cell sequencing research efforts, new mathematical models for chromosome copy number evolution and in-depth molecular characterization of chromosome-specific behaviors during division of various cell types will shed more light on these questions.

## References

1. Thompson, S. L. & Compton, D. A. Examining the link between chromosomal instability and aneuploidy in human cells. *J. Cell Biol.* **180**, 665–672 (2008).
2. Janssen, A., Burg, M. Van Der, Szuhai, K., Kops, G. J. P. L. & Medema, R. H. Chromosome Segregation Errors as a Cause of DNA Damage and Structural. **333**, 1895–1899 (2011).
3. Bolhaqueiro, A. C. F. *et al.* Ongoing chromosomal instability and karyotype evolution in human colorectal cancer organoids. *Nat. Genet.* **51**, 824–834

- (2019).
4. Knouse, K. A., Wu, J., Whittaker, C. A. & Amon, A. Single cell sequencing reveals low levels of aneuploidy across mammalian tissues. *Proc. Natl. Acad. Sci.* **111**, 13409–13414 (2014).
  5. McConnell, M. J. *et al.* Mosaic Copy Number Variation in Human Neurons. *Science* **342**, 632–637 (2013).
  6. Burrell, R. a *et al.* Replication stress links structural and numerical cancer chromosomal instability. *Nature* **494**, 492–496 (2013).
  7. Lengauer, C., Kinzler, K. W. & Vogelstein, B. Genetic instability in colorectal cancers. *Nature* **386**, 623–627 (1997).
  8. McCoy, R. C. Mosaicism in Preimplantation Human Embryos: When Chromosomal Abnormalities Are the Norm. *Trends Genet.* **33**, 448–463 (2017).
  9. Starostik, M. R., Sosina, O. A. & McCoy, R. C. Single-cell analysis of human embryos reveals diverse patterns of aneuploidy and mosaicism. *Genome Res.* **30**, 814–826 (2020).
  10. Vanneste, E. *et al.* Chromosome instability is common in human cleavage-stage embryos. *Nat. Med.* **15**, 577–583 (2009).
  11. Webster, A. & Schuh, M. Mechanisms of Aneuploidy in Human Eggs. *Trends Cell Biol.* **27**, 55–68 (2017).
  12. Bakhoum, S. F. & Compton, D. A. Chromosomal instability and cancer: a complex relationship with therapeutic potential. *J. Clin. Invest.* **122**, 1138–1143 (2012).
  13. Gordon, D. J., Resio, B. & Pellman, D. Causes and consequences of aneuploidy in cancer. *Nat. Rev. Genet.* **13**, 189–203 (2012).
  14. Hoevenaar, W. H. M. *et al.* Degree and site of chromosomal instability define its oncogenic potential. *Nat. Commun.* **11**, 1–11 (2020).
  15. Bakhoum, S. F. *et al.* Chromosomal instability drives metastasis through a cytosolic DNA response. *Nat. Publ. Gr.* **553**, 467–472 (2018).
  16. Diaz-Rodríguez, E., Sotillo, R., Schvartzman, J. & Benezra, R. Hec1 overexpression hyperactivates the mitotic checkpoint and induces tumor formation in vivo. *Proc. Natl. Acad. Sci.* **105**, 16719–16724 (2008).
  17. Sheltzer, J. M. & Amon, A. The Aneuploidy Paradox: Costs and Benefits of an Incorrect Karyotype. *Trends Genet.* **27**, 446–453 (2011).

18. Chunduri, N. K. *et al.* Systems approaches identify the consequences of monosomy in somatic human cells. *Nat. Commun.* **12**, 1–17 (2021).
19. Stingele, S. *et al.* Global analysis of genome, transcriptome and proteome reveals the response to aneuploidy in human cells. *Mol. Syst. Biol.* **8**, 1–12 (2012).
20. Williams, B. R. *et al.* Aneuploidy Affects Proliferation and Spontaneous Immortalization in Mammalian Cells. *Science* **322**, 703–710 (2008).
21. Donnelly, N. & Storchová, Z. Causes and consequences of protein folding stress in aneuploid cells. *Cell Cycle* **14**, 495–501 (2015).
22. Passerini, V. *et al.* The presence of extra chromosomes leads to genomic instability. *Nat. Commun.* **7**, 1–12 (2016).
23. Oromendia, A. B., Dodgson, S. E. & Amon, A. Aneuploidy causes proteotoxic stress in yeast. *Genes Dev.* **26**, 2696–2708 (2012).
24. Sheltzer, J. M. *et al.* Aneuploidy drives genomic instability in yeast. *Science* **333**, 1026–1030 (2011).
25. Torres, E. M. *et al.* Effects of aneuploidy on cellular physiology and cell division in haploid yeast. *Science* **317**, 916–924 (2007).
26. Chunduri, N. K. & Storchová, Z. The diverse consequences of aneuploidy. *Nat. Cell Biol.* **21**, 54–62 (2019).
27. Ben-David, U. & Amon, A. Context is everything: aneuploidy in cancer. *Nat. Rev. Genet.* **21**, 44–62 (2020).
28. Taylor, A. M. *et al.* Genomic and Functional Approaches to Understanding Cancer Aneuploidy. *Cancer Cell* **33**, 676–689 (2018).
29. Schukken, K. M. & Sheltzer, J. Extensive protein dosage compensation in aneuploid human cancers. *Genome Res.* **32**, 1–31 (2022).
30. Gronroos, E. & López-García, C. Tolerance of chromosomal instability in cancer: Mechanisms and therapeutic opportunities. *Cancer Res.* **78**, 6529–6535 (2018).
31. Hoadley, K. A. *et al.* Cell-of-Origin Patterns Dominate the Molecular Classification of 10,000 Tumors from 33 Types of Cancer. *Cell* **173**, 291–304 (2018).
32. Beroukhi, R. *et al.* The landscape of somatic copy-number alteration across human cancers. *Nature* **463**, 899–905 (2010).
33. Muzny, D. M. *et al.* Comprehensive molecular characterization of human

- colon and rectal cancer. *Nature* **487**, 330–337 (2012).
34. Cai, H. *et al.* Chromothripsis-like patterns are recurring but heterogeneously distributed features in a survey of 22,347 cancer genome screens. *BMC Genomics* **15**, 1–13 (2014).
  35. Cortés-Ciriano, I. *et al.* Comprehensive analysis of chromothripsis in 2,658 human cancers using whole-genome sequencing. *Nat. Genet.* **52**, 331–341 (2020).
  36. Voronina, N. *et al.* The landscape of chromothripsis across adult cancer types. *Nat. Commun.* **11**, 1–13 (2020).
  37. Zhang, C. Z. *et al.* Chromothripsis from DNA damage in micronuclei. *Nature* **522**, 179–184 (2015).
  38. Ly, P. *et al.* Chromosome segregation errors generate a diverse spectrum of simple and complex genomic rearrangements. *Nat. Genet.* **51**, 705–715 (2019).
  39. Hassold T & Hunt P. To err (meiotically) is human: the genesis of human aneuploidy. *Nat. Rev. Genet.* **2**, 280–291 (2001).
  40. Davoli, T. *et al.* Cumulative haploinsufficiency and triplosensitivity drive aneuploidy patterns and shape the cancer genome. *Cell* **155**, 948–962 (2013).
  41. Sack, L. M. *et al.* Profound Tissue Specificity in Proliferation Control Underlies Cancer Drivers and Aneuploidy Patterns. *Cell* **173**, 499–514 (2018).
  42. Norppa, H. & Falck, G. C. M. What do human micronuclei contain? *Mutagenesis* **18**, 221–233 (2003).
  43. Catalán, J., Falck, G. C. M. & Norppa, H. The X chromosome frequently lags behind in female lymphocyte anaphase. *Am. J. Hum. Genet.* **66**, 687–691 (2000).
  44. Falck, G. C., Catala, J. & Norppa, H. Nature of anaphase laggards and micronuclei in female cytokinesis-blocked lymphocytes. *Mutagenesis* **17**, 111–117 (2002).
  45. Hatch, E. M., Fischer, A. H., Deerinck, T. J. & Hetzer, M. W. Catastrophic Nuclear Envelope Collapse in Cancer Cell Micronuclei. *Cell* **154**, 47–60 (2013).
  46. Agustinus, A. S. *et al.* Epigenetic dysregulation from chromosomal transit in

- micronuclei. *bioRxiv* (2022). doi:10.1158/1538-7445.am2022-3768
47. Crasta, K. *et al.* DNA breaks and chromosome pulverization from errors in mitosis. *Nature* **482**, 53–58 (2012).
  48. MacKenzie, K. J. *et al.* CGAS surveillance of micronuclei links genome instability to innate immunity. *Nature* **548**, 461–465 (2017).
  49. Soto, M., García-Santisteban, I., Krenning, L., Medema, R. H. & Raaijmakers, J. A. Chromosomes trapped in micronuclei are liable to segregation errors. *J. Cell Sci.* **131**, 1–8 (2018).
  50. Worrall, J. T. *et al.* Non-random Mis-segregation of Human Chromosomes. *Cell Rep.* **23**, 3366–3380 (2018).
  51. Torosantucci, L., De Santis Puzzon, M., Cenciarelli, C., Rens, W. & Degrossi, F. Aneuploidy in mitosis of PtK1 cells is generated by random loss and nondisjunction of individual chromosomes. *J. Cell Sci.* **122**, 3455–3461 (2009).
  52. Drpic, D. *et al.* Chromosome Segregation Is Biased by Kinetochore Size. *Curr. Biol.* **28**, 1344–1356 (2018).
  53. Klaasen, S. J. *et al.* Nuclear chromosome locations dictate segregation error frequencies. *Nature* **607**, 604–609 (2022).
  54. Tovini, L. & McClelland, S. E. Impaired CENP-E function renders large chromosomes more vulnerable to congression failure. *Biomolecules* **9**, 1–15 (2019).
  55. Shaikh, N. *et al.* Replication Stress Generates Multiple Distinct Classes of Copy Number Alterations. *bioRxiv Mol. Biol.* (2019). doi:10.1101/743658
  56. Balajee, A. S., Bertucci, A., Taveras, M. & Brenner, D. J. Multicolour FISH analysis of ionising radiation induced micronucleus formation in human lymphocytes. *Mutagenesis* **29**, 447–455 (2014).
  57. Fachinetti, D. *et al.* DNA sequence-specific binding of CENP-B enhances the fidelity of human centromere function. *Dev. Cell* **33**, 314–327 (2015).
  58. Dumont, M. *et al.* Human chromosome-specific aneuploidy is influenced by DNA-dependent centromeric features. *EMBO J.* **39**, 1–21 (2020).
  59. Spence, J. M., Mills, W., Mann, K., Huxley, C. & Farr, C. J. Increased missegregation and chromosome loss with decreasing chromosome size in vertebrate cells. *Chromosoma* **115**, 60–74 (2006).
  60. McCoy, R. C. *et al.* Evidence of Selection against Complex Mitotic-Origin

- Aneuploidy during Preimplantation Development. *PLoS Genet.* **11**, 1–31 (2015).
61. Bochtler, T. *et al.* Micronucleus formation in human cancer cells is biased by chromosome size. *Genes Chromosom. Cancer* **58**, 392–395 (2019).
  62. Klein, A., Zang, K. D., Steudel, W. I. & Urbschat, S. Different mechanisms of mitotic instability in cancer cell lines. *Int. J. Oncol.* **29**, 1389–1396 (2006).
  63. Bell, A. D. *et al.* Insights into variation in meiosis from 31,228 human sperm genomes. *Nature* **583**, 259–264 (2020).
  64. Ioannou, D., Fortun, J. & Tempest, H. G. Meiotic nondisjunction and sperm aneuploidy in humans. *Reproduction* **157**, 15–31 (2019).
  65. Uroz, L. & Templado, C. Meiotic non-disjunction mechanisms in human fertile males. *Hum. Reprod.* **27**, 1518–1524 (2012).
  66. Kuliev, A., Zlatopolsky, Z., Kirillova, I., Spivakova, J. & Cieslak Janzen, J. Meiosis errors in over 20,000 oocytes studied in the practice of preimplantation aneuploidy testing. *Reprod. Biomed. Online* **22**, 2–8 (2011).
  67. Gruhn, J. R. *et al.* Chromosome errors in human eggs shape natural fertility over reproductive life span. *Science* **365**, 1466–1469 (2019).
  68. Hassold, T., Merrill, M., Adkins, K., Freeman, S. & Sherman, S. Recombination and maternal age-dependent nondisjunction: Molecular studies of trisomy 16. *Am. J. Hum. Genet.* **57**, 867–874 (1995).
  69. Fragouli, E. *et al.* Comparative genomic hybridization analysis of human oocytes and polar bodies. *Hum. Reprod.* **21**, 2319–2328 (2006).
  70. Rodriguez-Purata, J. *et al.* Embryo selection versus natural selection: How do outcomes of comprehensive chromosome screening of blastocysts compare with the analysis of products of conception from early pregnancy loss (dilation and curettage) among an assisted reproductive technolog. *Fertil. Steril.* **104**, 1460–1466 (2015).
  71. Gabriel, A. S. *et al.* Array comparative genomic hybridisation on first polar bodies suggests that non-disjunction is not the predominant mechanism leading to aneuploidy in humans. *J. Med. Genet.* **48**, 433–437 (2011).
  72. Feichtinger, M. *et al.* Increasing live birth rate by preimplantation genetic screening of pooled polar bodies using array comparative genomic hybridization. *PLoS One* **10**, 1–13 (2015).
  73. Handyside, A. H. *et al.* Multiple meiotic errors caused by predivision of

- chromatids in women of advanced maternal age undergoing in vitro fertilisation. *Eur. J. Hum. Genet.* **20**, 742–747 (2012).
74. Binyam, M., Scheffler, K. & Schuh, M. Assembly and Positioning of the Oocyte Meiotic Spindle. *Annu. Rev. Cell Dev. Biol.* **34**, 381–403 (2018).
  75. Sacristan, C. & Kops, G. J. P. L. Joined at the hip: Kinetochores, microtubules, and spindle assembly checkpoint signaling. *Trends Cell Biol.* **25**, 21–28 (2015).
  76. Kops, G. J. P. L., Saurin, A. T. & Meraldi, P. Finding the middle ground : how kinetochores power chromosome congression. *Cell. Mol. Life Sci.* **67**, 2145–2161 (2010).
  77. Vukušić, K. & Tolic, I. M. Polar Chromosomes — Challenges of a Risky Path. *Cells* **11**, 1–27 (2022).
  78. Barisic, M., Aguiar, P., Geley, S. & Maiato, H. Kinetochore motors drive congression of peripheral polar chromosomes by overcoming random arm-ejection forces. *Nat. Cell Biol.* **16**, 1249–1256 (2014).
  79. Roos, U.-P. Light and Electron Microscopy of Rat Kangaroo Cells in Mitosis III. Patterns of Chromosome Behavior during Prometaphase. *Chromosoma* **54**, 363–385 (1976).
  80. Itoh, G. *et al.* Lateral attachment of kinetochores to microtubules is enriched in prometaphase rosette and facilitates chromosome alignment and bi-orientation establishment. *Sci. Rep.* **8**, 1–18 (2018).
  81. Pachis, S. T. & Kops, G. J. P. L. Leader of the SAC: Molecular mechanisms of Mps1/TTK regulation in mitosis. *Open Biol.* **8**, 1–10 (2018).
  82. London, N. & Biggins, S. Signalling dynamics in the spindle checkpoint response. *Nat. Rev. Mol. Cell Biol.* **15**, 735–747 (2014).
  83. Etemad, B., Kuijt, T. E. F. & Kops, G. J. P. L. Kinetochore-microtubule attachment is sufficient to satisfy the human spindle assembly checkpoint. *Nat. Commun.* **6**, 1–8 (2015).
  84. Tauchman, E. C., Boehm, F. J. & DeLuca, J. G. Stable kinetochore-microtubule attachment is sufficient to silence the spindle assembly checkpoint in human cells. *Nat. Commun.* **6**, 1–9 (2015).
  85. Lampson, M. A., Renduchitala, K., Khodjakov, A. & Kapoor, T. M. Correcting improper chromosomes-spindle attachments during cell division. *Nat. Cell Biol.* **6**, 232–237 (2004).



86. Liu, D., Vader, G., Vromans, M. J. M., Lampson, M. A. & Lens, S. M. A. Sensing Chromosome Bi-Orientation Kinase from Kinetochore Substrates. *Science* **323**, 1350–1353 (2009).
87. Carmena, M., Wheelock, M., Funabiki, H. & Earnshaw, W. C. The Chromosomal Passenger Complex (CPC): From Easy Rider to the Godfather of Mitosis. *Nat. Rev. Mol. Cell Biol.* **13**, 789–803 (2012).
88. Hindriksen, S., Lens, S. M. A. & Hadders, M. A. The ins and outs of Aurora B inner centromere localization. *Front. Cell Dev. Biol.* **5**, 1–21 (2017).
89. Ohkura, H. Meiosis: An overview of key differences from mitosis. *Cold Spring Harb. Perspect. Biol.* **7**, 1–15 (2015).
90. Bolcun-Filas, E. & Handel, M. A. Meiosis: The chromosomal foundation of reproduction. *Biol. Reprod.* **99**, 112–126 (2018).
91. Hengeveld, R. C. C., Vromans, M. J. M., Vleugel, M., Hadders, M. A. & Lens, S. M. A. Inner centromere localization of the CPC maintains centromere cohesion and allows mitotic checkpoint silencing. *Nat. Commun.* **8**, 1–12 (2017).
92. Solomon, D. A. *et al.* Mutational inactivation of STAG2 causes aneuploidy in human cancer. *Science* **333**, 1039–1043 (2011).
93. Magidson, V. *et al.* Adaptive changes in the kinetochore architecture facilitate proper spindle assembly. *Nat. Cell Biol.* **17**, 1134–1144 (2015).
94. Cherry, L. M. & Johnston, D. A. Size variation in kinetochores of human chromosomes. *Hum. Genet.* **75**, 155–158 (1987).
95. Kumar, R. *et al.* HumCFS: A database of fragile sites in human chromosomes. *BMC Genomics* **19**, 1–8 (2019).
96. Burrell, R. A. *et al.* Replication stress links structural and numerical cancer chromosomal instability. *Nature* **494**, 492–496 (2013).
97. Bartkova, J. *et al.* DNA damage response as a candidate anti-cancer barrier in early human tumorigenesis. *Nature* **434**, 864–870 (2005).
98. Laurie, D. A. & Hulten, M. A. Further studies on bivalent chiasma frequency in human males with normal karyotypes. *Ann. Hum. Genet.* **49**, 189–201 (1985).
99. Falek, A. & Chiarelli, B. Meiotic chromosomes of man. *Am. J. Phys. Anthropol.* **28**, 351–354 (1943).
100. Zelazowski, M. J. *et al.* Age-Dependent Alterations in Meiotic Recombination

- Cause Chromosome Segregation Errors in Spermatocytes. *Cell* **171**, 601–614 (2017).
101. Lu, S. *et al.* Probing Meiotic Recombination and Aneuploidy of Single Sperm Cells by Whole-Genome Sequencing. *Science* **338**, 1627–1631 (2012).
  102. Wang, S. *et al.* Inefficient Crossover Maturation Underlies Elevated Aneuploidy in Human Female Meiosis. *Cell* **168**, 977–989 (2017).
  103. Sakakibara, Y. *et al.* Bivalent separation into univalents precedes age-related meiosis i errors in oocytes. *Nat. Commun.* **6**, 1–8 (2015).
  104. Duncan, F. E. *et al.* Chromosome cohesion decreases in human eggs with advanced maternal age. *Aging Cell* **11**, 1121–1124 (2012).
  105. Revenkova, E., Herrmann, K., Adelfalk, C. & Jessberger, R. Oocyte cohesin expression restricted to predictyate stages provides full fertility and prevents aneuploidy. *Curr. Biol.* **20**, 1529–1533 (2010).
  106. Burkhardt, S. *et al.* Chromosome Cohesion Established by Rec8-Cohesin in Fetal Oocytes is Maintained without Detectable Turnover in Oocytes Arrested for Months in Mice. *Curr. Biol.* **26**, 678–685 (2016).
  107. Zielinska, A. P., Holubcova, Z., Blayney, M., Elder, K. & Schuh, M. Sister kinetochore splitting and precocious disintegration of bivalents could explain the maternal age effect. *Elife* **4**, 1–19 (2015).
  108. Wang, S. *et al.* Crossover Interference, Crossover Maturation, and Human Aneuploidy. *BioEssays* **41**, 1–13 (2019).
  109. Capalbo, A., Hoffmann, E. R., Cimadomo, D., Ubaldi, F. M. & Rienzi, L. Human female meiosis revised: New insights into the mechanisms of chromosome segregation and aneuploidies from advanced genomics and time-lapse imaging. *Hum. Reprod. Update* **23**, 706–722 (2017).
  110. Bolzer, A. *et al.* Three-dimensional maps of all chromosomes in human male fibroblast nuclei and prometaphase rosettes. *PLoS Biol.* **3**, 0826–0842 (2005).
  111. Magidson, V. *et al.* The spatial arrangement of chromosomes during prometaphase facilitates spindle assembly. *Cell* **146**, 555–567 (2011).
  112. Cimini, D., Cameron, L. A. & Salmon, E. D. Anaphase Spindle Mechanics Prevent Mis-Segregation of Merotelically Oriented Chromosomes. *Curr. Biol.* **14**, 2149–2155 (2004).
  113. Maiato, H., Gomes, A. M., Sousa, F. & Barisic, M. Mechanisms of

- chromosome congression during mitosis. *Biology (Basel)*. **6**, 1–56 (2017).
114. Vázquez-Diez, C., Paim, L. M. G. & FitzHarris, G. Cell-Size-Independent Spindle Checkpoint Failure Underlies Chromosome Segregation Error in Mouse Embryos. *Curr. Biol.* **29**, 865–873 (2019).
  115. Cavazza, T. *et al.* Parental genome unification is highly error-prone in mammalian embryos. *Cell* **184**, 2860–2877.e22 (2021).
  116. Liu, Y. *et al.* Comparative Molecular Analysis of Gastrointestinal Adenocarcinomas. *Cancer Cell* **33**, 721–735 (2019).
  117. Williams, M. J., Werner, B., Barnes, C. P., Graham, T. A. & Sottoriva, A. Identification of neutral tumor evolution across cancer types. *Nat. Genet.* **48**, 238–244 (2016).
  118. Davis, A., Gao, R. & Navin, N. Tumor evolution: Linear, branching, neutral or punctuated? *Biochim. Biophys. Acta* **1867**, 151–161 (2017).
  119. Sottoriva, A. *et al.* A Big Bang model of human colorectal tumor growth. *Nat. Genet.* **47**, 209–216 (2015).
  120. Rutledge, S. D. *et al.* Selective advantage of trisomic human cells cultured in non-standard conditions. *Sci. Rep.* **6**, 1–12 (2016).
  121. Replogle, J. M. *et al.* Aneuploidy increases resistance to chemotherapeutics by antagonizing cell division. *Proc. Natl. Acad. Sci.* **117**, 30566–30576 (2020).
  122. van Jaarsveld, R. H. & Kops, G. J. P. L. Difference Makers : Chromosomal Instability versus Aneuploidy in Cancer. *Trends in Cancer* **2**, 561–571 (2016).
  123. Turajlic, S. *et al.* Tracking Cancer Evolution Reveals Constrained Routes to Metastases: TRACERx Renal. *Cell* **173**, 581–594 (2018).
  124. Araujo, A., Bentley, P. & Baum, B. Modelling the role of aneuploidy in tumour evolution. *Alife* 488–495 (2010).
  125. Valind, A., Jin, Y. & Gisselsson, D. Elevated Tolerance to Aneuploidy in Cancer Cells: Estimating the Fitness Effects of Chromosome Number Alterations by In Silico Modelling of Somatic Genome Evolution. *PLoS One* **8**, 1–17 (2013).
  126. Savva, G. M., Walker, K. & Morris, J. K. The maternal age-specific live birth prevalence of trisomies 13 and 18 compared to trisomy 21 (Down syndrome). *Prenat. Diagn.* **30**, 57–64 (2010).
  127. Bolton, H. *et al.* Mouse model of chromosome mosaicism reveals lineage-

- specific depletion of aneuploid cells and normal developmental potential. *Nat. Commun.* **7**, 1–12 (2016).
128. Bakhoun, S. F., Genovese, G. & Compton, D. A. Deviant Kinetochore Microtubule Dynamics Underlie Chromosomal Instability. *Curr. Biol.* **19**, 1937–1942 (2009).
  129. Bakhoun, S. F., Thompson, S. L., Manning, A. L. & Compton, D. A. Genome stability is ensured by temporal control of kinetochore- microtubule dynamics. *Nat. Cell Biol.* **11**, 27–35 (2009).
  130. Pihan, G. A., Wallace, J., Zhou, Y. & Doxsey, S. J. Centrosome abnormalities and chromosome instability occur together in pre-invasive carcinomas. *Cancer Res.* **63**, 1398–1404 (2003).
  131. Chan, J. Y. A Clinical Overview of Centrosome Amplification in Human Cancers. *Int. J. Biol. Sci.* **7**, 1122–1144 (2011).
  132. Neil J. Ganem, S. A. G. and D. P. A Mechanism Linking Extra Centrosomes to Chromosomal Instability. *Physiol. Behav.* **176**, 139–148 (2011).
  133. Kolano, A., Brunet, S., Silk, A. D., Cleveland, D. W. & Verlhac, M. H. Error-prone mammalian female meiosis from silencing the spindle assembly checkpoint without normal interkinetochore tension. *Proc. Natl. Acad. Sci.* **109**, 1858–1867 (2012).
  134. Kyogoku, H. & Kitajima, T. S. Large Cytoplasm Is Linked to the Error-Prone Nature of Oocytes. *Dev. Cell* **41**, 287–298 (2017).
  135. Holubcová, Z., Blayney, M., Elder, K. & Schuh, M. Error-prone chromosome-mediated spindle assembly favors chromosome segregation defects in human oocytes. *Science* **348**, 1143–1147 (2015).
  136. Payne, A. C. *et al.* In situ genome sequencing resolves DNA sequence and structure in intact biological samples. *Science* **371**, (2021).

# Chapter 3

## Nuclear chromosome locations dictate segregation error frequencies

Sjoerd J. Klaasen<sup>1</sup>, My Anh Truong<sup>2#</sup>, Richard H. van Jaarsveld<sup>1#</sup>, Isabella Koprivec<sup>3</sup>, Valentina Štimac<sup>3</sup>, Sippe G. de Vries<sup>2</sup>, Patrik Risteski<sup>3</sup>, Snježana Kodba<sup>3</sup>, Krno Vukušić<sup>3</sup>, Kim de Luca<sup>1</sup>, Joana F. Marques<sup>1</sup>, Elianne M. Gerrits<sup>1</sup>, Bjorn Bakker<sup>4</sup>, Floris Foijer<sup>4</sup>, Jop Kind<sup>1,5</sup>, Iva M. Tolić<sup>3</sup>, Susanne M.A. Lens<sup>2</sup> & Geert J.P.L. Kops<sup>1\*</sup>

### Affiliations

<sup>1</sup> Oncode Institute, Hubrecht Institute - Royal Academy of Arts and Sciences and University Medical Centre Utrecht, Utrecht, the Netherlands.

<sup>2</sup> Oncode Institute, Center for Molecular Medicine, University Medical Center Utrecht, Utrecht University, Utrecht, The Netherlands

<sup>3</sup> Ruđer Bošković Institute, Zagreb, Croatia

<sup>4</sup> Department of Ageing Biology/ERIBA, University of Groningen, University Medical Center Groningen, Groningen, the Netherlands.

<sup>5</sup> Department of Molecular Biology, Faculty of Science, Radboud Institute for Molecular Life Sciences, Radboud University Nijmegen, The Netherlands

#These authors contributed equally

\*Correspondence to: g.kops@hubrecht.eu.

Published in *Nature*, vol. 607, 604–609 (2022).

Chromosome segregation errors during cell divisions generate aneuploidies and micronuclei, which can undergo extensive chromosomal rearrangements such as chromothripsis<sup>1–5</sup>. Selective pressures then shape distinct aneuploidy and rearrangement patterns, for example in cancer<sup>6,7</sup>, but it is unknown if initial biases in segregation errors and micronucleation for particular chromosomes exist. Using single-cell DNA sequencing<sup>8</sup> after an error-prone mitosis in untransformed, diploid cell lines and organoids, we here show that chromosomes have different segregation error frequencies that result in non-random aneuploidy landscapes. Isolation and sequencing of single micronuclei from these cells showed that chromosomes missegregating frequently also preferentially become entrapped in micronuclei. A similar bias was found in naturally occurring micronuclei of two cancer cell lines. We find that segregation error frequencies of individual chromosomes correlate with their location in the interphase nucleus, and show that this is highest for peripheral chromosomes behind spindle poles. Randomization of chromosome positions, Cas9-mediated live tracking and forced repositioning of individual chromosomes showed that a greater distance from the nuclear center directly increases the propensity to missegregate. Accordingly, chromothripsis in cancer genomes<sup>9</sup> and aneuploidies in early development<sup>10</sup> occur more frequently for larger chromosomes, which are preferentially located near the nuclear periphery. Our findings reveal a direct link between nuclear chromosome positions, segregation error frequencies, and micronucleus content, with implications for our understanding of tumor genome evolution and the origins of specific aneuploidies during development.

Aneuploidy, a state in which the genome content of cells deviates from an integer multiple of the haploid set, can cause miscarriages and developmental syndromes, and is strongly associated with tumorigenesis<sup>7,11–13</sup>. Aneuploidies typically result from chromosome segregation errors during cell divisions. Such errors can be caused by, for example, altered microtubule dynamics, hyperstable kinetochore-microtubule attachments, cohesion problems or weakened spindle assembly

checkpoint (SAC) activity<sup>2,14–17</sup>. Mitotic errors also lead to the formation of micronuclei, which are prone to nuclear envelope rupturing, leading to extensive genomic rearrangements<sup>3–5,18</sup>. Cancers exhibit distinct aneuploidy and rearrangement patterns, for instance when originating from different organs, after colonizing distant sites, or after relapse, suggesting convergent evolution towards an optimal karyotype under distinct selective pressures<sup>11,19–23</sup>. Aneuploidies found in preimplantation or aborted embryos are likewise not random<sup>10,24</sup>. Although selection likely plays a crucial role, it is unknown if the process that causes aneuploidy is biased and may create a non-random genomic substrate for selection. In support of this possibility, severe perturbations of the spindle or centromere can affect segregation of some chromosomes more than others<sup>25–27</sup>.

## Results

### Chromosome segregation error frequencies

To examine the propensity of individual chromosomes for missegregation, we used single-cell karyotype sequencing (scKaryo-seq<sup>8</sup>) to assess hundreds of karyotypes from diploid cells that underwent an aberrant mitosis. scKaryo-seq allows for high fidelity and high-throughput determination of the copy number state of all chromosomes in single cells. RPE1-hTERT cells synchronized in G2 (Extended Data Fig. 1a) were allowed to proceed into mitosis in the presence or absence of a low concentration of Cpd-5 (62.5 nM), a small molecule inhibitor of the mitotic kinase MPS1<sup>28</sup>. Low Cpd-5 compromises attachment error-correction and the SAC response (Extended Data Fig. 1b-d), leading to nearly all cells undergoing anaphase with a few misaligned and lagging chromosomes (Fig. 1a, Extended Data Fig. 1e-f, Supplementary Video 1 and 2). These are among the most common mitotic errors observed in cancer cells<sup>2,8,29</sup>. Our synchronization and release procedure did not affect short-term viability (Extended Data Fig. 2a-b). Individual nuclei isolated four hours following error-prone mitosis were subjected to scKaryo-seq. Low Cpd-5 had caused an average of 5.5 segregation error events per aneuploid cell, totaling 2417 quantifiable whole and structural chromosome copy number alterations (Fig. 1b). Strikingly, the aneuploidy landscapes revealed that segregation error probabilities were not equal between chromosomes: chromosomes 1-5, 8, 11, and X had a

significantly higher probability to missegregate than expected from a random error frequency of 4.3% (Bonferroni correction;  $P = 0.0022$ ). Chromosomes 14, 15, and 19-22 on the other hand had significantly lower probabilities (Fig. 1c). A similarly biased distribution of aneuploidies was seen in diploid BJ-hTERT fibroblasts and human intestinal organoids, and in a near-tetraploid clone of RPE1-hTERT cells (Extended Data Fig. 2c-g, Extended Data Fig. 3a-f), showing the missegregation bias occurs in different cell types and culture conditions.

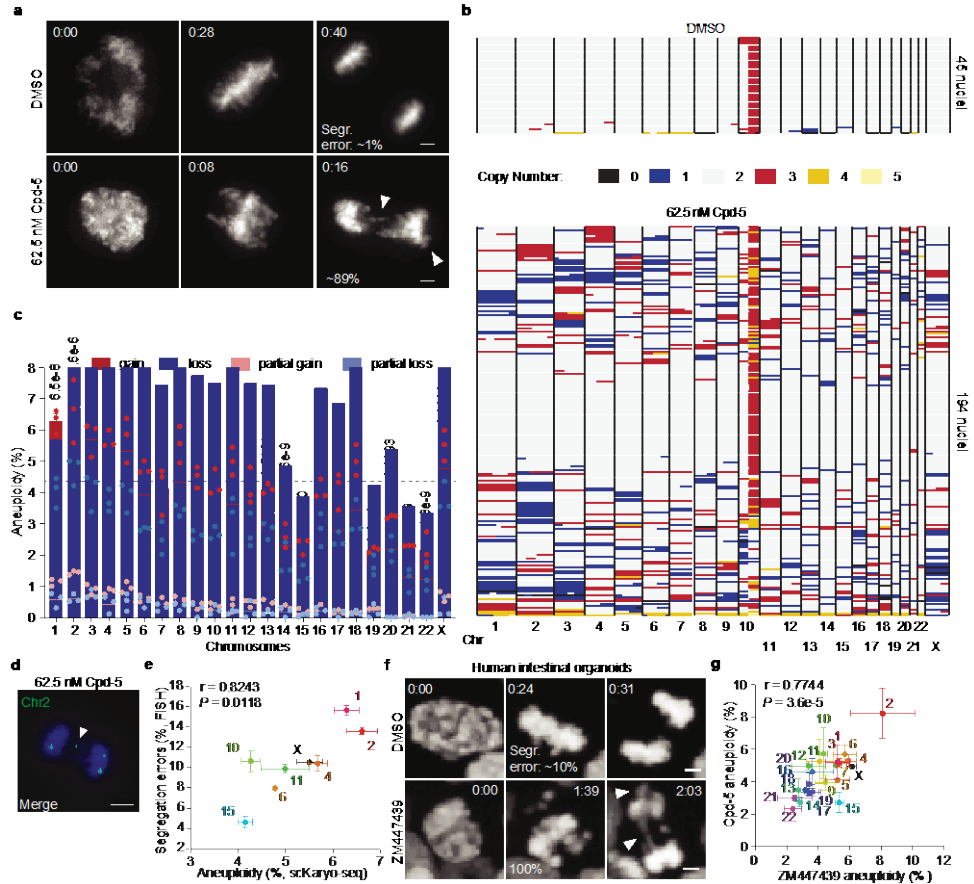


**Figure 1: Segregation error frequencies of chromosomes during error-prone mitosis are non-random.** **a**, Representative stills of synchronous RPE1-hTERT H2B-mNeon cells going through mitosis in the presence of Cpd-5. Triangles indicate missegregating chromosomes. **b,c**, Representative replicate (**b**) and quantification (**c**) showing the copy number states of synchronized RPE1-hTERT cells treated with DMSO or Cpd-5. Each row in the figure represents one nucleus. The different colors represent copy number states. The graph shows the aneuploidy percentages per chromosome for three independent



experiments (mean  $\pm$  s.e.m., two-tailed binomial test,  $n = 410$  aneuploid cells). The different colors represent if the chromosome has been lost, gained or partially lost or gained. The horizontal black line at 4.34% depicts the expected random chance to missegregate each chromosome. Numbers on top are p-values. **d,e**, Representative FISH image (**d**) and quantification (**e**) of RPE1-hTERT cells as treated in **b**, but fixed 45 min after release from RO-3306 (scale bar = 5  $\mu$ m). The triangle shows a lagging chromosome 2. The graph plots the percentage of chromosomes positive for corresponding FISH probes on the y-axis versus the aneuploidy percentages determined in **c**. (mean  $\pm$  s.e.m., two-tailed Pearson correlation coefficient,  $n = \text{chr1}; 327, \text{chr2}; 307, \text{chr4}; 311, \text{chr6}; 290, \text{chr10}; 322, \text{chr11}; 313, \text{chr15}; 286$  and  $\text{chrX}; 314$ ). Three independent experiments were performed. **f**, Representative stills of human intestinal organoids treated with DMSO as a control or the aurora B inhibitor ZM447439 (scale bar = 5  $\mu$ m). Triangles point at missegregating chromosomes. **g**, Plot comparing aneuploidy percentages of human intestinal organoids after overnight Cpd-5 versus ZM447439 treatment (mean  $\pm$  s.e.m., two-tailed Pearson correlation coefficient,  $n = 217$  or 64 aneuploid cells, respectively). Experiment was performed in duplo.

Fluorescence in-situ hybridization (FISH) for centromeres of chromosomes 1, 2, 4, 6, 10, 11, 15 and X on anaphase figures further verified that the non-random aneuploidy landscapes observed by scKaryo-seq were due to biased segregation errors in anaphase (Fig. 1d-e). Importantly, similar segregation error probabilities were seen when mitotic errors were induced by other means. First, small molecule inhibition of Aurora B, while inducing severe errors in 2D cultures<sup>30,31</sup>, caused mild segregation errors in human intestinal organoids, allowing isolation of daughter nuclei (Supplementary Video 3). scKaryo-seq of these nuclei showed a highly similar segregation error bias to Cpd-5-treated cells (Fig. 1f-g). Second, a low concentration of nocodazole perturbs microtubule assembly rates, a proposed cause of chromosomal instability in colorectal cancer cells<sup>15</sup>. Low nocodazole caused misaligned chromosomes in RPE1-hTERT cells that subsequently frequently missegregated in anaphase (Extended Data Fig. 3g-h, Supplementary Video 4)<sup>32</sup>. Although scKaryo-seq was not possible due to rarity of segregation errors in this condition, centromere FISH for six chromosomes (1, 6, 7, 15, 18 and X) showed that misalignment frequencies were significantly different between chromosomes and followed a similar trend to Cpd-5/AurBi-induced aneuploidy landscapes (Extended Data Fig. 3i-j). Taken together, we conclude that chromosome segregation errors of various origins in non-transformed cells are non-random.

### **Chromosome micronucleation frequencies**

Erroneously segregated chromosomes frequently become encapsulated in micronuclei. Chromosomes in micronuclei can undergo extensive rearrangements like chromothripsis, which plays an important role in tumor evolution<sup>3–5,18</sup>. Because we observed a bias in initial aneuploidy landscapes after segregation errors, we examined if this translated into a biased micronuclear content. We therefore adapted a FACS-based approach<sup>33</sup> to isolate micronuclei and assess their content by sequencing, a protocol we refer to as MN-seq. MN-seq performed on single- or bulk-sorted micronuclei from Cpd-5-treated cells revealed a striking non-random content that correlated strongly with the pattern of missegregation frequencies of chromosomes (Fig. 2a-d, Extended Data Fig. 4a-c). This was verified by FISH (Extended Data Fig. 4d-e). A similarly biased micronuclear content was observed for cells treated with a low dose of nocodazole (Extended Data Fig. 4f-h). We next examined if micronuclear content was non-random in naturally occurring micronuclei of cancer cells. MN-seq of five chromosomally unstable cancer cell lines uncovered that non-random micronuclear content existed in all lines, and that two lines (Caco-2 and HeLa) displayed a bias highly similar to that of Cpd-5/AurBi-treated diploid cells (Fig. 2e-f, Extended Data Fig. 4i-k). Of note, recent FISH analysis showed a similar micronucleus content bias in glioblastoma cells<sup>34</sup>. These data indicate that chromosomes with a higher missegregation probability more frequently become entrapped in micronuclei. Since naturally occurring micronuclei most likely arise from relatively recent missegregation events, our data further suggest that segregation errors in various cancer cells are non-random and may be caused by similar underlying mechanisms.

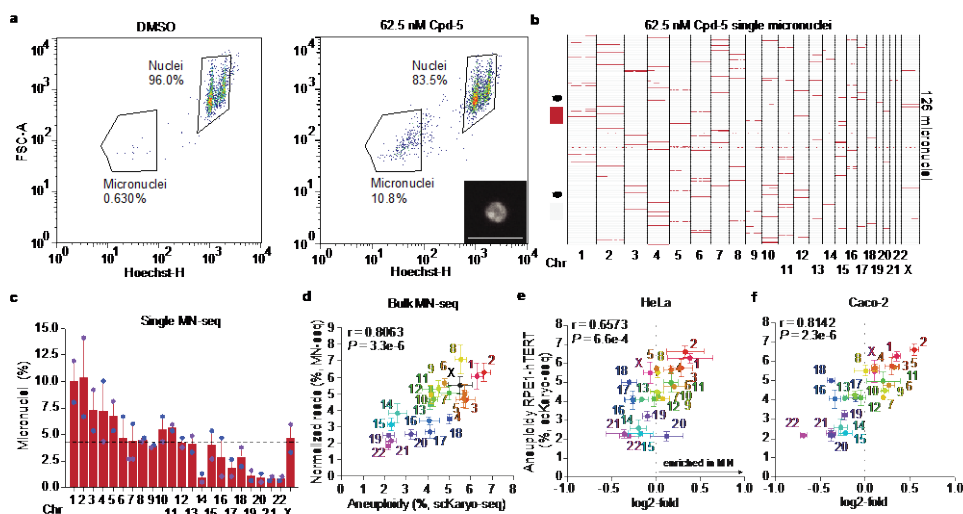


**Figure 2: Micronuclear content reflects segregation error bias.** **a.** Representative flow cytometry plots of RPE1-hTERT nuclei and micronuclei. Image depicts micronucleus imaged after sorting (scale bar =  $5\mu\text{m}$ ) **b,c.** Representative MN-seq data (**b**) and quantification (**c**) of single micronuclei isolated from cells treated with Cpd-5 (mean  $\pm$  s.e.m., two independent experiments,  $n = 222$  micronuclei). Every line in **b.** represents a single micronucleus. Red shows the presence of a chromosomal region. **d.** Plot comparing bulk MN-seq data of  $\sim 8000$  micronuclei shown as the percentage of reads mapped to a certain chromosome normalized for chromosome size and the aneuploidy percentages determined in Fig. 1c (mean  $\pm$  s.e.m., two-tailed Pearson correlation coefficient). Four independent experiments were performed. **e,f.** Plots comparing log2-fold enrichment of micronuclear DNA determined from bulk sequencing of two chromosomally unstable cancer cell lines versus the aneuploidy percentages from Fig. 1c (mean  $\pm$  s.e.m., two-tailed Pearson correlation coefficient,  $n = \sim 6000$  MN). Three independent experiments were performed for each cell line.

## Origin of non-random segregation errors

Having established that frequencies of missegregation and entrapment in micronuclei are not equal for all chromosomes, we next wished to understand the origins of this bias. We therefore compared segregation error frequencies to chromosome characteristics such as centromere size or the ratio of p- to q arm lengths, but did not find any correlation (Extended Data Fig. 5a-b). Chromosome size and gene density, on the other hand, did correlate (directly and inversely, respectively) with segregation error frequencies (Extended Data Fig. 5c-d). Chromosome size was nonetheless unlikely to be a direct cause for the observed

bias, because the two X chromosomes that differ in size by 24.4% in RPE1-hTERT cells due to one being fused to a q-arm of chromosome 10 had identical missegregation frequencies (Extended Data Fig. 5e). Moreover, some chromosomes with near-identical sizes had profoundly different missegregation frequencies (e.g. 13 vs 14, 15 vs 16 or 18 vs 19) (Fig. 1c). We next considered the location of chromosomes in interphase nuclei, as this correlates directly with chromosome size and inversely with gene density<sup>35–37</sup>, but can differ between chromosomes of near-identical size. In support of this, four out of five acrocentric chromosomes (14, 15, 21 and 22), which reside near the centrally located nucleoli, had low missegregation frequencies (Fig. 1c). Segregation error frequencies of chromosomes in RPE1-hTERT cells strongly correlated with the densities of lamina-associated chromosome domains (LADs) (Fig. 3a), and with published distances of chromosomes from the center of the nucleus (Extended Data Fig. 5f)<sup>37</sup>. Chromosome size correlated to LAD densities in RPE1-hTERT and other cells, both diploid (TIG3-hTERT and hESCs) and aneuploid (HeLa, U2OS, K562 and HT1080), showing that in a wide array of cell lines larger chromosomes reside in the nuclear periphery more frequently than smaller ones (Extended Data Fig. 5g-m)<sup>38–42</sup>. Centromere FISH of six chromosomes (1, 2, 6, 15, 17, 18) further verified this in non-transformed and transformed cell lines (Fig. 3b-c, Extended Data Fig. 6a-e).

To further explore the hypothesis that chromosome location can cause a segregation error bias, we live imaged chromosome movement during mitosis in cells with labelled centromeres and centrosomes (Fig. 3d, Extended Data Fig. 6f, Supplemental Video 5 and 6), and analyzed the trajectories of three categories of chromosomes: centrally located ones (central), peripheral ones located behind a spindle pole (polar), and peripheral ones located in between the spindle pole planes (non-polar peripheral) (Fig. 3d). This revealed that peripheral chromosomes took significantly longer to congress than central ones in unperturbed conditions, and more readily missegregated as misaligned or lagging chromosomes upon treatment with Cpd-5 (Fig. 3e-h). Of the peripheral chromosomes, the polar ones congressed slower and missegregated more frequently than the non-polar ones. This was true

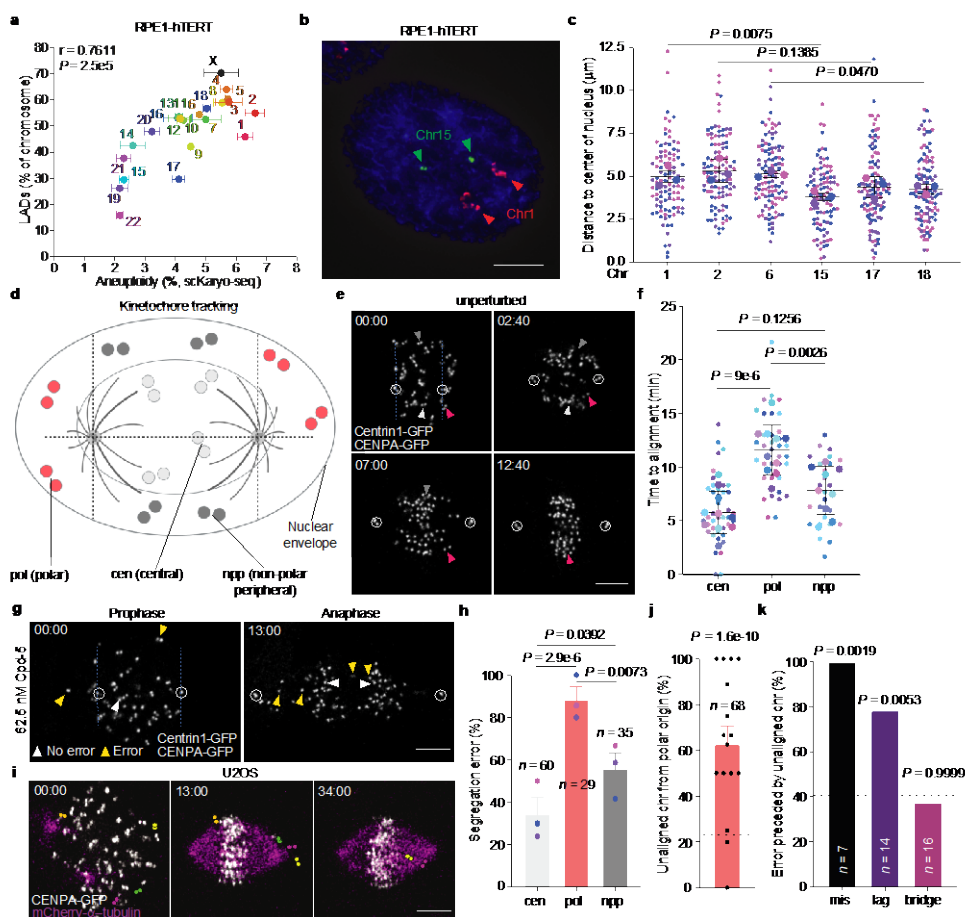


**Figure 3: Segregation error probabilities correlate with nuclear chromosome locations.** **a.** Plot comparing aneuploidy percentages after Cpd-5 treatment as in Fig. 1c and the percentage of lamina-associated domains (LAD) for every chromosome in RPE1-hTERT cells (mean + s.e.m., two-tailed Pearson correlation coefficient,  $n = 2$  independent DamID experiments). **b,c.** Representative FISH image of RPE1-hTERT cells (**b**) and quantification (**c**) of the distance of chromosomes to the center of the nucleus (mean  $\pm$  s.d., two-tailed ratio t-test,  $n = 99, 106, 108, 98, 106$  or  $107$  chromosomes, respectively. Scale bar =  $5 \mu\text{m}$ ). Experiment was performed in triplicate. **d.** Schematic depicting the nucleus of a cell with kinetochore pairs in different colored circles depending on their location relative to the two centrosomes. **e,f.** Representative stills (**e**) and quantification (**f**) of the alignment time of kinetochores in RPE1-hTERT CENPA-GFP/Centrin1-GFP cells (scale bar =  $5 \mu\text{m}$ ). Triangles follow specific kinetochore pairs. Circles follow centrosomes. Experiment was performed ten times (mean  $\pm$  s.d., one-way ANOVA with Tukey's post-hoc test,  $n = 38, 29$  and  $35$  chromosome pairs, respectively). **g,h.** As in **e-f**, but instead cells were treated with  $62.5 \text{ nM}$  Cpd-5 and missegregations were quantified (**h**). Triangles follow kinetochore pairs (scale bar =  $5 \mu\text{m}$ , white = no error, yellow = error). Experiment was performed in

triplicate (mean  $\pm$  s.e.m., two-tailed Fisher's exact test,  $n = 43, 35$  and  $26$  chromosomes). **i,j,k**, Representative stills (**i**) and quantification (**j-k**) of kinetochore behavior in U2OS cells expressing CENPA-GFP/mCherry- $\alpha$ -tubulin (scale bar =  $5\ \mu\text{m}$ ). The dashed lines represent the expected percentage of unaligned chromosomes (**j**) or errors (**k**), which are based on the number of polar kinetochore pairs at the start of NEBD and the number of unaligned chromosomes at the start of metaphase. Experiment was performed sixteen times (mean  $\pm$  s.e.m., two-tailed Fisher's exact test).

also when only polar and non-polar peripheral chromosomes with an equal starting distance from the metaphase plate were compared (Extended Data Fig. 6f-k). We observed a similar phenomenon in chromosomally unstable cancer cells, in which peripheral, polar chromosomes had a 3-fold higher probability to be misaligned than expected based on the frequency of polars (Fig. 3i-j, Supplemental Video 7). Moreover, misalignments and laggards in anaphase were observed significantly more frequently in cells with such misaligned metaphase chromosome than in cells without them ( $18/77$  versus  $3/112$ , respectively) (Fig. 3k), suggesting missegregating chromosomes may often arise from misaligned chromosomes. These observations suggest that the peripheral location of chromosomes and even more so how this location relates to the spindle poles delays biorientation and congression and thereby contributes to the high frequency of missegregation of peripheral chromosomes.

### **The role of nuclear chromosome location**

We next wished to examine if the distinct locations of chromosomes in an interphase nucleus are directly responsible for the different segregation error probabilities. In a first approach, we randomized the location of chromosomes in mitosis before inducing erroneous anaphases. This was done by a short treatment with monastrol, which allows for microtubule-based chromosome movements in a monopolar spindle and simultaneously makes most if not all chromosomes essentially spindle pole-proximal (Fig. 4a-b). scKaryo-seq of cells released from monastrol into low Cpd-5 showed that the probability of chromosomes to missegregate was substantially altered in two different cell lines (Fig. 4c, Extended Data Fig. 7a-e). In a second approach, we leveraged the ability to image specific chromosomes using repeat-specific gRNAs and fluorescently labelled dCas9<sup>27,43</sup>. Chromosomes that are

on average mostly peripheral can occasionally be found in the nuclear interior and vice versa. This allowed us to directly relate the location of a specific chromosome to its behavior in mitosis (Fig. 4d). Live imaging of chromosome 1 (small foci) and 9 (big foci) verified that prior to nuclear envelop breakdown chromosome 1 was more often peripheral compared to chromosome 9, but was centrally located in ~20% of cells (Extended Data Fig. 8a-b, Supplementary Video 8)<sup>27</sup>. Conversely, chromosome 9 could be found near the nuclear periphery in ~35% of cells. Regardless of identity, chromosomes starting from a peripheral location were significantly more often misaligned before anaphase onset in Cpd-5-treated cells compared to when they started from a more central position (3-fold for chromosome 1; 4-fold for chromosome 9) (Fig. 4e). Importantly, a peripheral starting position substantially increased missegregation rates (misalignments and laggards) compared to a central starting position (1.8-fold for chromosome 1 and 2.5-fold for chromosome 9) (Fig. 4f). A similar result was obtained when tracking chr11 using the LacO/LacI-GFP system in fibrosarcoma HT1080 cells (Extended Data Fig. 8c-d)<sup>44</sup>.

In a final approach, we forced relocation of chromosome 9 from a central location to the periphery by conditionally tethering it to the nuclear lamina via rapalog-controlled dimerization of dCas9 and Lamin B1. 24 hours of incubation with rapalog increased the frequency by which chromosome 9 was found near the periphery nearly two-fold (Fig. 4g-h), which by itself did not compromise its correct segregation during normal divisions (Fig. 4i). Upon error-prone divisions after addition of Cpd-5, however, relocation of chromosome 9 resulted in a nearly two-fold increase in its missegregation rate compared to non-relocated chromosome 9 (Fig. 4i). Taken together, these data lead us to conclude that chromosome segregation error probabilities are directly influenced by the location in the interphase nucleus prior to the onset of mitosis.

## Discussion

Our data are consistent with a model in which the location of chromosomes in the nucleus dictates probabilities of segregation errors of individual chromosomes and their entrapment in micronuclei (Extended Data Fig. 9). We hypothesize that

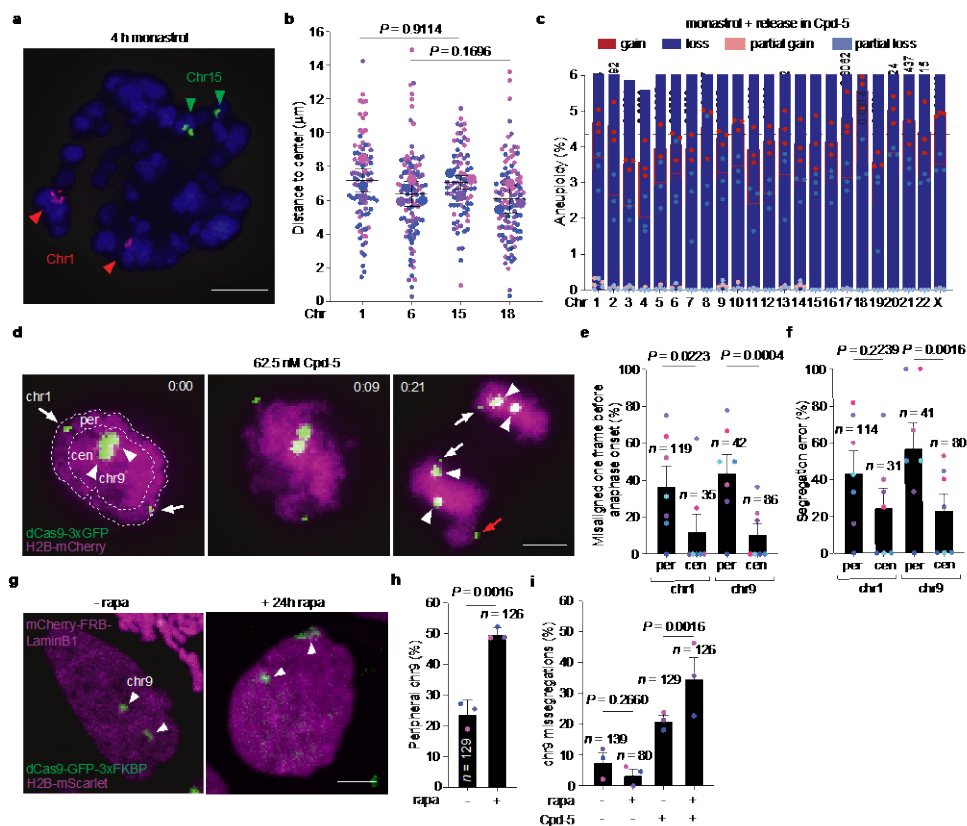


**Figure 4: Distance of chromosomes from the nuclear center dictates missegregation probability.**

**a,b**, Representative FISH images (**a**) and quantification (**b**) of the distance of FISH probes to the center in RPE1-hTERT cells synchronized as before and treated for 4h with monastrol (mean  $\pm$  s.d., two-tailed ratio t-test,  $n = 89, 110, 87$  and  $109$  chromosomes, respectively). Data was pooled from three independent experiments. **c**, Quantification of aneuploidy levels determined by scKaryo-seq of RPE1-hTERT cells treated as in **i**, followed by a release in Cpd-5, a shake-off and replating. Data is pooled from three independent experiments (mean  $\pm$  s.e.m., two-tailed binomial test,  $n = 373$  aneuploid cells). **d,e,f**, Stills (**d**) and quantification of central versus peripheral chromosomes 1 (arrow) and 9 (triangle) misaligned right before anaphase onset (**e**) and subsequently missegregating in RPE1-hTERT cells (**f**). Experiment was performed in septuplicate (mean  $\pm$  s.d., two-tailed Fisher's exact test). **g,h,i**, Stills (**g**) and quantification of the peripheralness (**h**) of chromosome 9 in DLD1 expressing dCas9-GFP-3xFKBP mCherry-FRB-LaminB1 after 24h of rapalog (scale bar =  $5 \mu\text{m}$ ). Cells were followed live to determine missegregations in Cpd-5 (**i**). Experiment was performed in triplicate (mean  $\pm$  s.e.m., two-tailed Fisher's exact test).



peripheral chromosomes missegregate more often than central ones because they need to travel longer distances to reach the metaphase plate, more regularly undergo lateral or merotelic microtubule interactions, and/or experience additional delays by being behind spindle poles<sup>45–49</sup>. It may therefore be a common outcome of processes that cause chromosomal instability, consistent with inducing the bias when we disrupt the SAC, attachment error-correction, or microtubule dynamics. Additional biases from different underlying processes are nonetheless likely to exist<sup>25–27</sup>, and could for example impact aneuploidies in human female meiosis<sup>24</sup>. Of note, chromosome size also correlates with aneuploidy landscapes after the first few error-prone mitotic divisions of human embryos<sup>10</sup>. In mice, errors during these divisions have been attributed to a weakened SAC<sup>17</sup>. The nuclear location of chromosomes may thus also explain non-random aneuploidies during embryonic development. Interestingly, a recent survey of chromothriptic events in 2,658 human cancers showed their occurrence correlates with chromosomes size and thus with nuclear position (Extended Data Fig. 10)<sup>9</sup>. Non-random segregation errors may therefore impact the dynamics of recurring aneuploidy and genomic rearrangement patterns seen in cancer, and thereby influence tumor growth, metastasis and relapse. Tissue-specific chromosome locations<sup>50</sup> are likely to differentially impact these dynamics.

## Acknowledgments

We thank Judith Vivié, Lennart Kester and Dylan Mooijman for help with scKaryo-seq, Sarah Tammouhi for help with organoid culturing and live imaging, the Hubrecht Flow Cytometry facility for help with sorting, the Hubrecht Imaging Centre for help with microscopy and the Utrecht Sequencing Facility for providing sequencing service and data. We thank the Kops, Lens and Tolić lab members for discussions and comments on the manuscript. Figures 3d, S6f and S9 were created with Biorender.com. This study was funded by the Cancer Genomics Centre and the European Research Council (ERC-SyG 855158). The Kops, Lens and Kind labs are part of the Oncode Institute, which is partly funded by the Dutch Cancer Society (KWF Kankerbestrijding). The Tolić lab is funded by the Croatian Science

Foundation (PZS-2019-02-7653) and European Regional Development Fund (KK.01.1.1.04.0057 and KK.01.1.1.0004).

### **Author contributions**

S.J.K., R.H.J. and G.J.P.L.K. conceived the project and S.J.K. and G.J.P.L.K. wrote the manuscript. S.J.K. designed, performed and analyzed all experiments unless specified otherwise. E.M.G. and R.H.J. set up RPE1-hTERT cell synchronization procedure. R.H.J. performed and analyzed RPE1-hTERT synchronization for filming and scKaryo-seq and performed and analyzed FISH on anaphase figures. J.F.M. generated tetraploid RPE1 cell line. Live tracking experiments of figure 3d-k, supervised by I.M.T., were performed and analyzed by I.K. and V.Š. (RPE1 cells) and performed by P.R. and S.K. and analyzed by K.V. (U2OS cells). M.A.T. and S.V. designed, performed and analyzed dCas9-imaging experiments. S.J.K. and M.A.T. performed and analyzed dCas9-tethering experiments. K.L. performed and analyzed U2OS DamID experiments. B.B. and F.F. provided help with setting up scKaryo-seq analysis. All authors provided input on the manuscript. J.K. and S.L. supervised experiments by K.L. and M.A.T./S.V., respectively and G.J.P.L.K. supervised all aspects of the work.

### **Competing interests**

The authors declare no competing interests.

### **Additional information**

All requests for reprints or materials should be addressed to GJPLK (g.kops@hubrecht.eu)

### **Data availability**

Raw sequencing data can be found at the European Nucleotide Archive: PRJEB52892.

Source data are available at <https://doi.org/10.6084/m9.figshare.19779736>.

Previously published Dam- and Mad-Lamin B1 sequencing data for RPE1-hTERT can be found at GSM3904483, GSM3904484, GSM3904548 and GSM3904549, for hESC at GSM557443 and GSM557444, for TIG3-hTERT at GSM2030834, for HeLa at E-MTAB-6888, for K562 at GSM1612855, GSM1612856 and for HT1080 at GSM984848.

### **Code availability**

Code to generate figures from raw sequencing data can be found at <https://github.com/sjklansen/scKaryo-seq.git>.

## **Methods**

### **Cloning**

FRB-mCherry-LaminB1 construct was generated using Gibson assembly by replacing AID-BirA from the hPGK-AID-BirA-hsLmnB1-P2A-BLAST construct (gift from Jop Kind lab) with FRB-mCherry (gift from Adrian Saurin). Next, P2A-BLAST was removed. LacI-GFP-FKBP construct was also generated using Gibson assembly. The Tet-On-GFP from a Tet-On-GFP-FKBP construct (gift from Susanne Lens lab) was replaced with LacI-GFP<sup>51</sup>.

### **Cell culture**

RPE1-hTERT (Flip-In) (gift from the Prasad Jallepalli lab), Caco-2 (gift from Hans Clevers lab), HeLa (gift from Michiel Vermeulen lab), HT-29 (gift from Hans Clevers lab), U2OS (gift from Susanne Lens lab) and WiDr (gift from Hans Clevers lab) cells were cultured in DMEM/F12, GlutaMAX supplement (Gibco) supplemented with 9% foetal bovine serum (Sigma-Aldrich) and 1% penicillin/streptomycin (Sigma-Aldrich). U2OS DamID, U2OS CENPA, BJ-hTERT (gift from Rene Medema lab), HCT116 (gift from Hans clevers lab) and HT1080 cells were cultured in DMEM, high glucose, GlutaMAX supplement, pyruvate (Gibco), supplemented with 10% fetal bovine serum and 1% penicillin/streptomycin. Human small intestine duodenum and ileum organoids (gift from Hans Clevers lab) were cultured as described previously<sup>52</sup>. Instead of WNT conditioned media, WNT surrogate was used (0.15 nM, U-Protein Express). DLD1 (gift from Daniella Cimini) cells were cultured in RPMI, GlutaMAX

supplement (Gibco) supplemented with 9% foetal bovine serum and 50 µg/ml penicillin/streptomycin. To generate RPE1-hTERT Flp-in H2B-mNeon cells, cells were transduced with a lentivirus containing an H2B-mNeon-IRES-puromycin construct. Selection was performed with 10 µg/ml puromycin (Sigma-Aldrich) for 48 hours. Organoids were transduced with the same construct without selection. Tetraploid RPE1-hTERT cells were generated by treating original RPE1-hTERT cells with 62.5 nM Cpd-5 for 48h every 7 days for 4 weeks, after which tetraploid colonies grew out for an additional 22 weeks. Monoclonal RPE1-hTERT dCas9-3xGFP and DLD1 dCas9-GFP-3xFKBP FRB-mCherry-LaminB1 lines were generated by transduction with a dCas9-3xGFP or dCas9-GFP-3xFKBP lentivirus<sup>53</sup>, followed by single-cell sorting. Next, FRB-mCherry-LaminB1 was lentivirally introduced in DLD1 cells. HT1080 cells containing a LacO-array in chromosome 11 (a gift from Wendy Bickmore) were transduced with LacI-GFP-FKBP and FRB-mCherry-LaminB1 and cloned by single cell sorting. Cell lines were not authenticated.

### **scKaryo-seq**

RPE1-hTERT Flp-in cells were plated in a 6-well plate (Corning) at 40% confluency and treated with palbociclib (250 nM; Selleck Chemicals LLC). After 24 hours, cells were washed 3x with warm medium and treated with RO-3306 (5 µM; Tocris Bioscience). After 16h, cells were washed 3x for 5 min at 37 °C with warm medium containing DMSO, Cpd-5 (62.5 nM; gift from René Medema) or monastrol (200 µM; Sigma-Aldrich). Cpd-5-treated cells were cultured for another 4 hours before harvesting. Monastrol-treated cells were washed 3x with warm medium containing 62.5 nM Cpd-5. Mitotic cells were collected by shake-off and plated in a new well of a 6-well plate for 4 h. BJ-hTERT cells were plated in a 6-well plate at 40% confluency and treated with 31.25 nM of Cpd-5 for 16h. All cells were trypsinized and stored at -20 °C for further processing. Single G1 nuclei of RPE1-hTERT Flp-in cells or single nuclei of BJ-hTERT cells were sorted as described before<sup>54</sup>. Human intestinal organoids were plated 1 day before being treated for 16h with 5 µM ZM447439 (Selleck Chemicals LLC) or 10 µM EdU (Thermofisher) for 3h, washed 3x for 5 min with warm medium, incubated with 62.5 nM Cpd-5 for 16h and fixed using 70% ice-

cold ethanol. Ethanol was removed by one wash with PBS and cells were incubated for 10 min with the Click-iT reaction cocktail (see Click-iT EdU proliferation assay). The reaction cocktail was washed away and replaced with a PBS/DAPI mix. Single G1 nuclei in case of ZM447439 or EdU-positive G1 cells were sorted in 384-well plates. Tetraploid RPE1-hTERT cells were plated at 40% confluency and treated with 62.5 nM Cpd-5 for 24 hours. G1 nuclei were sorted. HCT116 cells were synchronized for 16 h using monastrol, released and treated with Cpd-5 as described for RPE1-hTERT cells. Plates were stored at -20 °C. NLAIII-based library prep was performed as described previously with a few modifications<sup>54</sup>. Cell lysis was performed for 2 hours at 55 °C with 8 mg/ml of Proteinase K (Fisher Scientific) in 1× CutSmart (New England Biolabs) and heat inactivation at 80 °C for 10 min. Adapters were ligated with 100 nl of 100 nM barcoded double-stranded NLAIII adapters and 400 nl of 10 U T4 DNA ligase (New England Biolabs) in 1× T4 DNA ligase buffer (New England Biolabs) supplemented with 3 mM ATP (Invitrogen) at 16 °C overnight. Samples were sequenced on an Illumina NextSeq500 or 2000 at 1x75bp or 1x100bp, respectively. After sequencing, mapping (bwa aln 0.7.12 and python 2.7.5) and Aneufinder (version 1.2.0) plotting, copy number variations of whole and partial chromosomes were determined manually. Chromosome 8 of the human intestinal organoids was not quantified as this chromosome was heterogeneously aneuploid in the control condition.

### Centromere FISH

Cells were plated on 12-mm round glass coverslips (Superior Marienfeld). To validate scKaryo-seq segregation error bias, cells were synchronized and treated with Cpd-5 as described above. Cells were fixed 45 min after release from RO-3306 with -20 °C 75% methanol and 25% acetic acid. To determine the distance of chromosomes to the center of the nucleus, cells were plated one day before fixation. To determine nuclear chromosome territories of monastrol-treated mitotic cells, cells were synchronized as described above and incubated for 4 h in monastrol and subsequently fixed. After fixation, coverslips were airdried and incubated for 2 min with 2x SSC at RT. Coverslips were washed in series with 70%, 85% and 100 % ethanol and airdried. 1.2 µl of a red and green satellite enumeration probe (Cytocell)

and 1.6  $\mu$ l of hybridization solution per coverslip were spotted on a glass slide. The coverslips were placed upside down on the probe solution and incubated at 75 °C for 2 min. Coverslips were incubated at RT for 4-16 h followed by a 2 min incubation at 72 °C with 0.25x SSC (pH 7.0). Coverslips were washed for 30 sec with 2x SSC 0.5% Tween-20 at RT, incubated with DAPI and mounted using ProLong Gold antifade (Molecular Probes).

Image acquisition was done on a DeltaVision RT system (Applied Precision/GE Healthcare) with a 100  $\times$  1.40 numerical aperture (NA) UplanSApo objective (Olympus) as z stacks at 0.5  $\mu$ m intervals. For deconvolution SoftWorx (Applied Precision/GE Healthcare, version 6.5.2) was used. Image analysis and quantification was done using Fiji ImageJ (version 2.0.0).

FISH segregation error frequencies were determined by counting the number of missegregating FISH-positive chromosomes and dividing it by the total number of missegregating chromosomes.

Chromosomes in low nocodazole were considered misaligned when FISH-positive chromosomes were physically separated from the metaphase plate. This number was then divided by the total number of FISH-positive chromosomes.

To measure the distance of chromosomes to the center of the nucleus, we determined the centroid X and Y coordinates of the three different thresholded channels (DAPI, red probe and green probe). The center of monastrol-treated cells was determined using a custom ImageJ script, which measures the center of mass of thresholded DAPI particles.

### **Live imaging**

To time mitotic phases, RPE1-hTERT Flp-in H2B-mNeon cells were plated in a black glass-bottom 96-well plate (Corning) at 40% confluency and synchronized as described for scKaryo-seq. Cells were imaged on an Andor CSU-W1 spinning disk (50  $\mu$ m disk) with 20x 0.75 NA dry objective lens (Nikon). A 488 nm laser was used

for sample excitation and filters between 540 nm-50 bandpass for emission. Images were acquired using an Andor iXon-888 EMCCD camera. 9 Z-slices of 2  $\mu\text{m}$  were imaged for 4 h every 1 min. Nuclear envelope breakdown (NEBD) was defined as 1 frame before extensive chromosome movement. Images were acquired using NIS-elements (Nikon, version 5.30.04).

To determine time from condensation to anaphase onset and segregation errors, we used a Nikon Ti-E motorized microscope equipped with a Zyla 4.2Mpx sCMOS camera (Andor) and 40  $\times$  1.3 NA oil objective lens (Nikon). Fluorescence excitation was done using a Spectra X LED illumination system (Lumencor) and Chroma-ET filtersets. 9 Z-slices of 2  $\mu\text{m}$  were imaged every 4 min for 4 h. The same videos were also used to determine cell survival.

In order to examine cell survival for MN-seq, RPE1-hTERT Flp-in and BJ-hTERT cells were plated at 40% confluency. Cells were imaged on the same microscope used for determining segregation errors. DIC and a 10x 0.45 NA objective lens (Nikon) were used to visualize cells every 3-5 minutes for 16 h.

Human intestinal organoids were imaged as described previously<sup>54</sup>.

To determine missegregations in cells treated with low nocodazole, RPE1-hTERT H2B-eYFP cells were plated at 40% confluency one day before imaging. Next, cells were treated with nocodazole (48 nM; Sigma-Aldrich) and imaged on an Andor CSU-W1 spinning disk (50  $\mu\text{m}$  disk) with 100x 1.45 NA oil objective lens (Nikon). A 488 nm laser was used for sample excitation and filters between 540 nm-50 bandpass for emission. Images were acquired using an Andor iXon-888 EMCCD camera. 9 Z-slices of 2  $\mu\text{m}$  were imaged for 16 h every 3 min.

To compare the behavior of polar and non-polar chromosomes, RPE1-hTERT cells stably expressing both CENPA-GFP and Centrin1-GFP (a gift from Alexey Khodjakov) were imaged on the Expert Line easy3D STED microscope system (Abberior Instruments) using Prairie View (5.4.64.500) and Inspector (Abberior

Instruments GmbH, version 16.3) with 485nm and 640nm lasers using a 60x/1.2 UPLSAPO 60XW water objective (Olympus) and an avalanche photodiode (APD) detector. Low dose (1:100,000) SPY-595-DNA was added to detect the moment of nuclear envelope breakdown and low dose (1:50,000) SPY-640-tubulin (Spirochrome, AG) was added to easily distinguish between the poles and the kinetochores, as well as to enable pole tracking when Centrin1 signal was not easily detectable in a specific frame. 6 Z-slices of 1  $\mu\text{m}$  were taken every 20 seconds. Right after nuclear envelope breakdown the edges of the nucleus were manually drawn to determine the relative nuclear position of tracked chromosomes by dividing the nucleus into 3 equally spaced concentric areas. Chromosomes were considered central if they resided in the two innermost shells or were touching the second most outer ring. Positions of both centrosomes were also determined at that point. Each kinetochore pair was followed manually in a maximum intensity projection. The positions and trajectories of the kinetochore pairs were additionally verified in single Z-planes of a Z-stack in Fiji (version 1.53f51/1.53s30/1.53r), as well as in Imaris 3D Viewer (version 9.8.0). One pair each of polar and non-polar peripheral chromosome with the same distance to the metaphase plate were selected from the same cell.

U2OS kinetochore tracking experiments were performed with a U2OS cell line stably expressing CENPA-GFP, mCherry- $\alpha$ -tubulin, and photoactivatable-GFP- $\alpha$ -tubulin (a gift from Marin Barisic and Helder Maiato). Cells were imaged using a Bruker Opterra I multipoint scanning confocal microscope system, as previously described<sup>55</sup>. Image acquisition was performed at 1 min intervals with Z-stacks of 15 slices at a 1  $\mu\text{m}$ -spacing. Misaligned kinetochores included all pairs of kinetochores displaced from the metaphase plate in the frame when the elongation of the prometaphase spindle reached its peak, which was defined as the last point in which the separation of two centrosomes showed a continuous increase in spindle length for two consecutive frames for more than 1  $\mu\text{m}$ . Spatial x and y coordinates of unaligned kinetochores were extracted in every time frame using the Low Light Tracking Tool (version 0.10), an ImageJ plugin, as previously described<sup>56</sup>. The tracking of kinetochores in the x and y planes was performed on individual imaging z-planes. Around 10-15% of unaligned kinetochore pairs could not be successfully tracked in all frames, mainly



due to cell and spindle movements in the z-direction over time. Spindle poles were manually tracked with points placed in the center of the pole structure, in the z-plane where the tubulin signal was highest. Aligned kinetochore pairs were manually tracked in 2D. All unaligned pairs in NEBD frame were double-checked to be 'behind spindle poles' by using 3D Imaris Viewer. Lagging chromosomes were defined as a single kinetochore that was stuck and stretched between the separating mass of kinetochores during early anaphase. Chromosome bridges included cells with a kinetochore pair that was well separated but remained between the separating mass of kinetochores during early anaphase. Misalignments included cells that had at least one pair of kinetochores at the pole during anaphase, and the 'no error' phenotype was defined as the cell that had the absence of the aforementioned phenotypes. Multipolar cells (1 out of 190) were not included in the analysis. Quantitative analysis of all parameters was performed using custom-made MATLAB (MatlabR2021a 9.10.0) scripts.

For live-tracking of individual chromosomes, RPE1-hTERT dCas9-3xGFP were transduced with lentiviruses containing sgRNAs targeting chromosome 1 (ATGCTCACCT) and chromosome 9 (TGGAATGGAATGGAATGGAA). 24-hour post-transduction, cells were plated in an optical-quality plastic 8-well slide (IBIDI, cat. No. 80826) at 50% confluency. After 16 hours, asynchronous mitotic cells were treated with 62.5 nM Cpd-5 and immediately imaged using a 40x 1.4 NA oil PLAN Apochromat lens on a Zeiss Cell Observer microscope equipped with a AxioImager Z1 stand, a Hamamatsu ORCA-flash 4.0 camera, and a Colibri 7 LED. Images were acquired every 2.5 minutes for 4.2 hours. Videos were subsequently processed and analyzed using ZEN software (Zeiss, version 3.3). To see if chromosomes were either peripheral or central, we followed the same procedure as described for the analysis of RPE1-hTERT CENPA-GFP and Centrin1-GFP experiments.

Chromosome 9 tracking and tethering experiments were performed on the spinning disk system as described before with a few adaptations. 500 nM rapalog (Takara) was added 24 h before imaging DLD1 cells. 62.5 nM Cpd-5 was added right before

imaging. We used a 60 x 1.20 NA water phase immersion oil lens and 16 Z-slices of 1  $\mu\text{m}$  were imaged every 3 min overnight.

Cells were imaged at 37 °C in 5% CO<sub>2</sub> for all imaging experiments.

### **MN-seq**

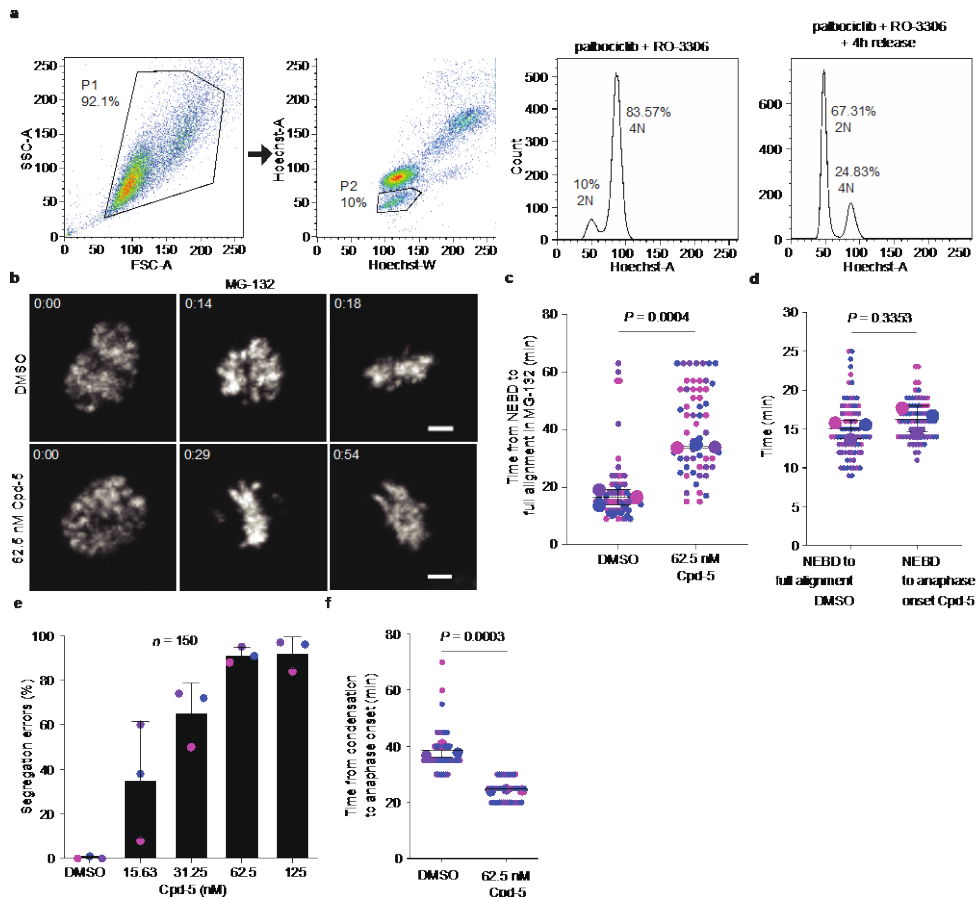
RPE1-hTERT Flp-in cells were plated in a 6-well plate at 40% confluency and treated with Cpd-5 or nocodazole for 16 h. Cancer cell lines were plated in a similar fashion, but were not treated with any drugs. Preparations for FACS was performed similarly as described previously<sup>57</sup>. In short, cells were incubated on ice for 30 min under light with PBS/2% FBS and 12.5  $\mu\text{g}/\text{ml}$  EMA (Thermofisher). EMA was washed 4x using PBS and (micro)nuclei were harvested from the cells using the same nuclear staining buffer used for scKaryo-seq. EMA-negative and Hoechst-positive (micro)nuclei were sorted in bulk in a PCR strip containing mineral oil and stored at -20 °C for further processing. Library preparation was performed similarly to scKaryo-seq, but with a few modifications. Every 5  $\mu\text{l}$  of sorted (micro)nuclei were incubated with 5  $\mu\text{l}$  of lysis buffer (final concentration: 0.02 U Proteinase K per  $\mu\text{l}$  (NEB) in 1x CutSmart Buffer (NEB)) for 2 h at 55 °C and 10 min at 80 °C. Genomic DNA was digested by incubating (micro)nuclei with 10  $\mu\text{l}$  of digestion mix (final concentration: 0.5 U NLAIII (New England Biolabs) per  $\mu\text{l}$  in 1x CutSmart Buffer) for 2h at 37 °C followed by 20 min at 65 °C. Genomic DNA fragments were subsequently ligated to adapters by adding 20  $\mu\text{l}$  ligation mix (final concentration: 20 U per  $\mu\text{l}$  T4 DNA ligase (New England Biolabs), 0.5 mM ATP (Thermofisher) and 25 nM adapter in 0.5x T4 DNA ligase buffer (New England Biolabs) and incubating at 16 °C overnight. After ligation, the rest of the library preparation, sequencing and analysis was performed as described for scKaryo-seq. To get the percentage of reads per chromosome, all the reads mapped to a specific chromosome were summed and normalized by dividing it to the number of bins for that specific chromosome. The percentage of reads for chromosome 10 in RPE1-hTERT cells were normalized using bulk-sequenced nuclei as the q-arm of this chromosome is present in 3 copies.

### **DamID**

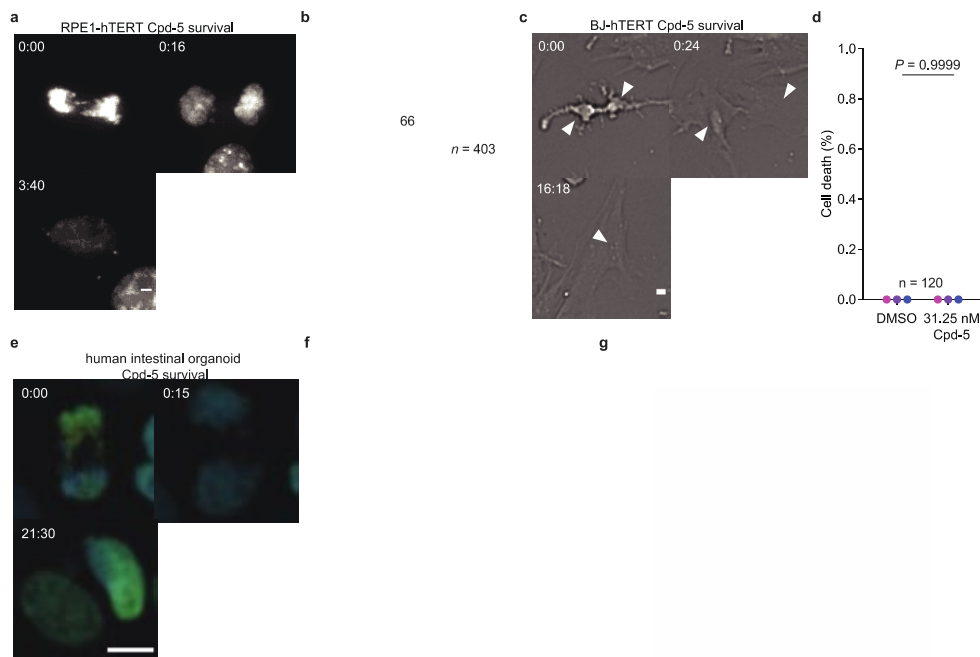
DamID data from Shield1-inducible DamID U2OS cells were derived by transfection of Dam-LaminB1 or Dam constructs (cloned into the **pPTuner IRES2 vector** (Clontech, Takara)), antibiotic resistance selection with 500 µg/mL G418 (Gibco), and subsequent characterization of monoclonal cell populations. Selection of suitable clones was based on methylation levels at known LAD or iLAD genomic regions, measured by Mbol-qPCR and DamID as previously described<sup>58</sup>. Stabilization of Dam proteins was achieved by addition of Shield1 ligand (AOBIOUS) to the cell culture medium at 500 nM final concentration for 18-24 h before cell collection. Multiplexed DamID was performed as previously described<sup>58</sup> and sequenced on an Illumina HiSeq2500 platform (1x50 bp). Raw reads were demultiplexed by their library-specific index and sample-specific DamID barcode, universal DamID adapter sequence was trimmed with cutadapt (version 2.5), and reads were aligned to reference genome hg19 using bowtie2 (version 2.3.4.2). Reads mapping to annotated GATC sites were counted and aggregated in genomic bins of 100 kb. Computation of observed over expected (OE) values per bin was performed as described<sup>59</sup>.

## Statistics

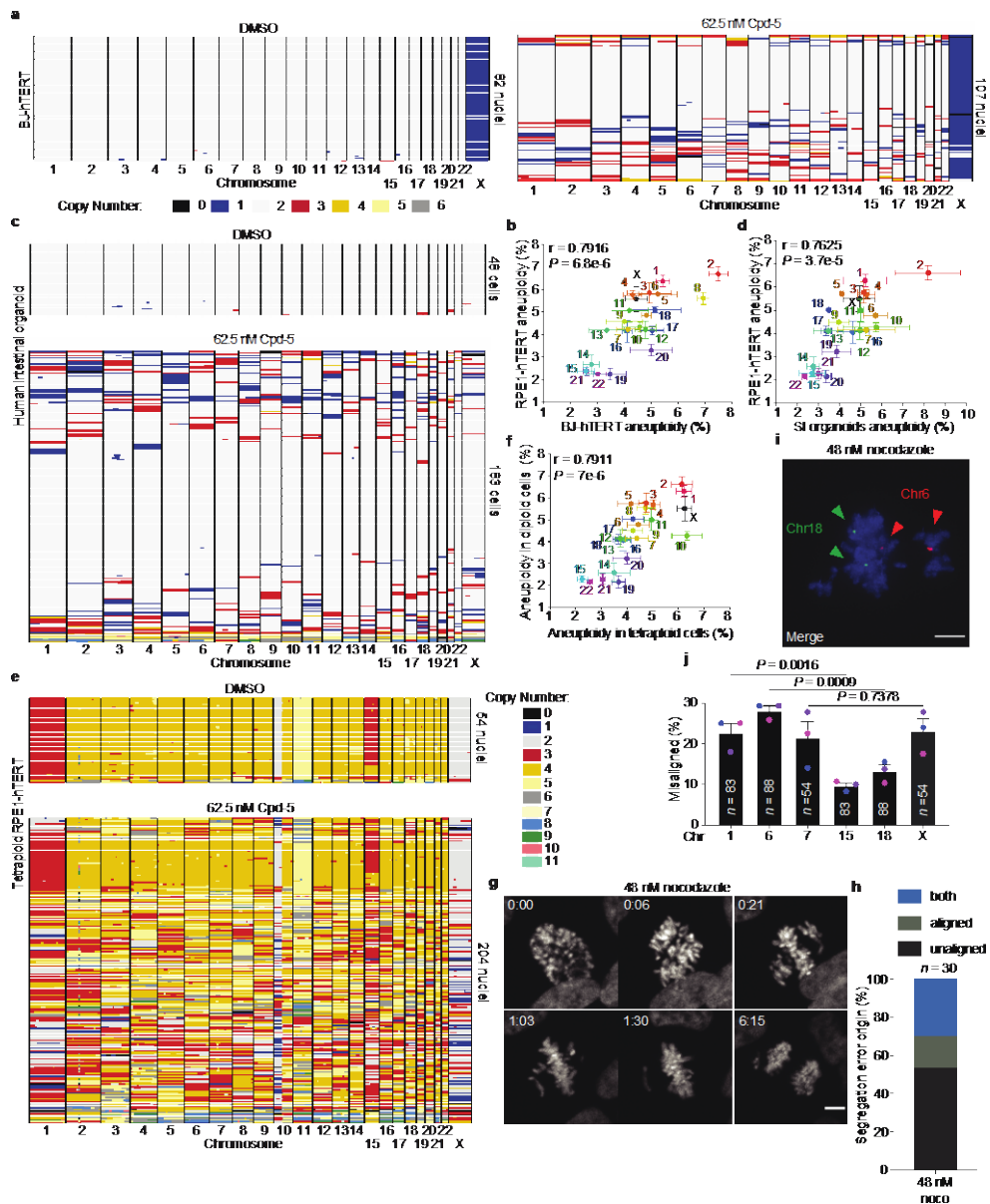
Statistical analyses were performed using GraphPad Prism software (8.4.3). Superplots were used in many of the graphs in which each color represents a replicate, the small dots are the individual measurements and the large dots indicate the mean of each replicate.



**Extended Data Fig. 1: Characterization of RPE1-hTERT missegregations.** **a.** Representative gating strategy for flow cytometry and the DNA content of RPE1-hTERT cells synchronized using palbociclib and RO-3306. Fourth graph on the right shows the DNA content 4 h after washing out RO-3306. **b,c,** Stills (**b**) and quantification (**c**) of the time of alignment in synchronized and MG-132-treated RPE1-hTERT H2B-mNeon cells (scale bar = 5  $\mu$ m). Experiment was performed in triplicate (mean  $\pm$  s.d., two-tailed unpaired t-test,  $n = 60$  and  $58$ , respectively). **d.** Quantification of the time from condensation to full alignment or anaphase onset in DMSO or Cpd-5, respectively. Experiment was performed in triplicate (mean  $\pm$  s.d., two-tailed unpaired t-test,  $n = 75$ ). **e.** Quantification of the segregation error percentages of RPE1-hTERT H2B-mNeon treated with different concentrations of Cpd-5. Three independent experiments were performed (mean  $\pm$  s.e.m.). **f.** Quantification of the time from condensation to anaphase onset of cells treated with DMSO or 62.5 nM Cpd-5. Three independent experiments were performed (mean  $\pm$  s.d., two-tailed unpaired t-test,  $n = 45$  cells).

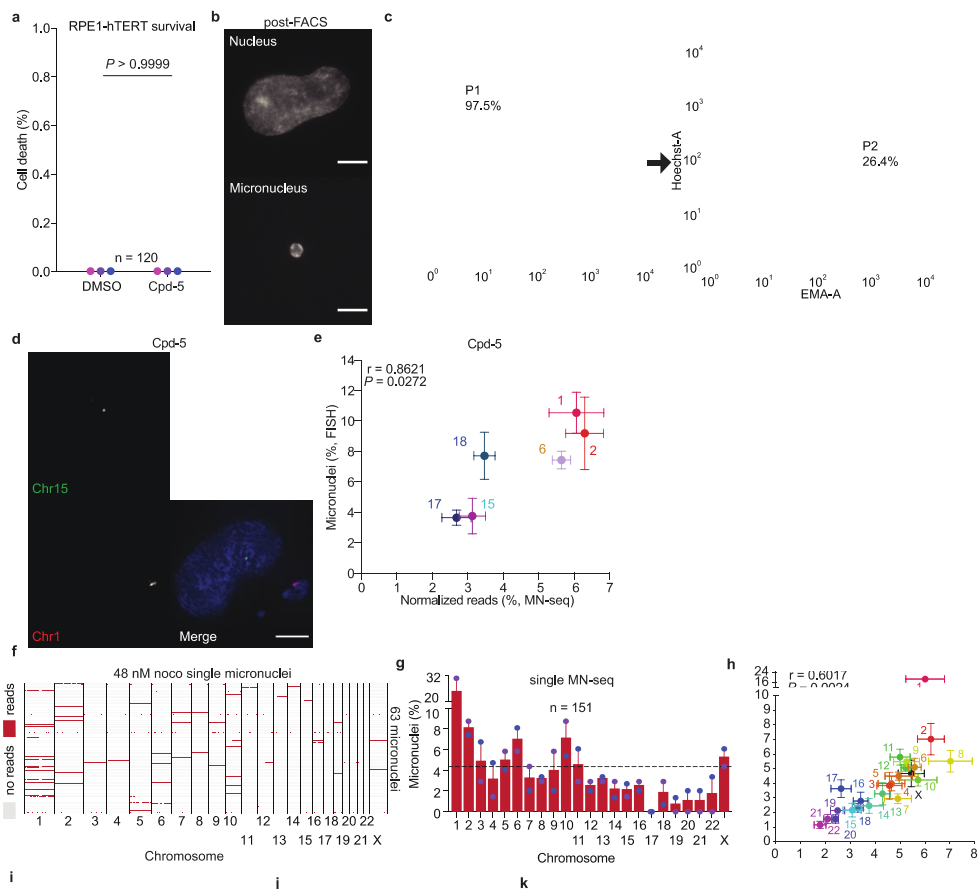


**Extended Data Fig. 2: Characterization of survival after Cpd-5 treatment of multiple cell lines.** **a,b,** Representative stills of a RPE1-hTERT H2B-mNeon cell going through mitosis after synchronization and release in 62.5 nM Cpd-5 (**a**) and quantification of cell death (**b**). Three independent experiments were performed (scale bar = 5  $\mu$ m, mean  $\pm$  s.e.m., unpaired t-test). **c,d,** Stills of BJ-hTERT cells in 31.25 nM Cpd-5 (**c**) and quantification of cell death (**d**). Experiment was performed in triplicate (scale bar = 5  $\mu$ m, mean  $\pm$  s.e.m., two-tailed Fisher's exact test,  $n = 120$  daughter cells per condition). **e,f,** Stills (**e**) and quantification (**f**) of human intestinal organoids going through mitosis in the presence of Cpd-5. Two independent experiments were performed (mean  $\pm$  s.e.m., two-tailed Fisher's exact test). **g.** Graph illustrating sorting strategy of human intestinal organoids to enrich for cells with aneuploidies. Organoids were treated with EdU for 3h, washed and treated overnight with 62.5 nM Cpd-5. EdU-positive G1 cells were sorted.



**Extended Data Fig. 3: Similar missegregation frequencies in different cell lines and after different perturbations.** **a.** Representative scKaryo-seq replicate of BJ-hTERT cells treated for 16 h with Cpd-5. **b.** Plot comparing aneuploidy percentages of RPE1-hTERT cells after Cpd-5 treatment (see Fig. 1c) and quantification of BJ-hTERT aneuploidy percentages (mean  $\pm$  s.e.m., two-tailed Pearson correlation coefficient,  $n = 180$  aneuploid cells). Three independent experiments were performed. **c.** Representative scKaryo-seq replicate of a human intestinal organoid line treated with or without Cpd-5 for 16 h. **d.** Plot comparing aneuploidy percentages of RPE1-hTERT cells (see Fig. 1c) and human intestinal organoid

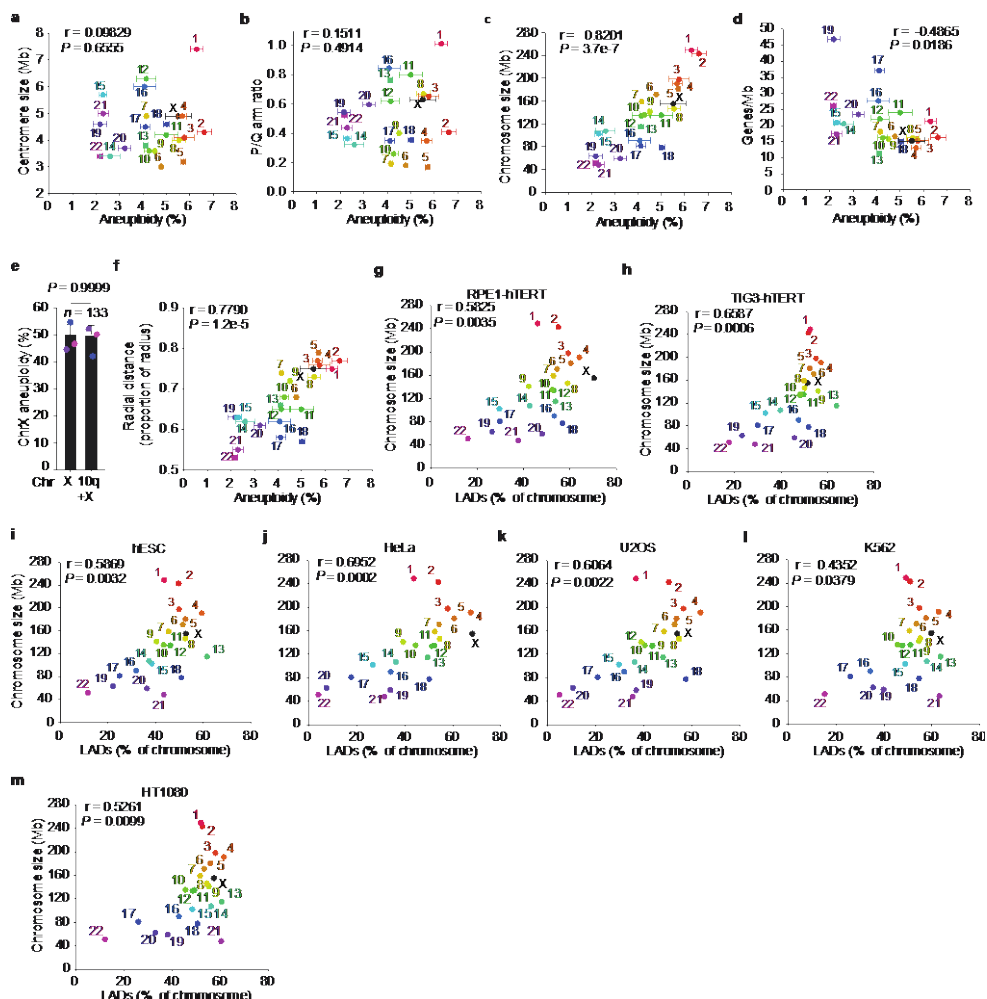
aneuploidy percentages after Cpd-5 treatment. (mean  $\pm$  s.e.m., two-tailed Pearson correlation coefficient,  $n = 217$  aneuploid cells). Two independent organoid lines originating from the duodenum and ileum were used for this experiment. Chromosome 8 was not included in the analysis, because this chromosome was heterogeneously aneuploid in the ileum organoid line. **e.** Representative scKaryo-seq replicate of tetraploid RPE1-hTERT cells treated with and without Cpd-5 for 24 h. **f.** Plot comparing aneuploidy percentages of Fig. 1c versus quantification of the aneuploidy percentages after Cpd-5 treatment in tetraploid RPE1-hTERT cells (mean  $\pm$  s.e.m., two-tailed Pearson correlation coefficient,  $n = 180$  aneuploid cells). Experiment was performed in triplicate. **g,h,** Stills (**g**) and quantification (**h**) looking at the location of missegregating chromosomes just before anaphase onset after 48 nM nocodazole treatment (scale bar = 5  $\mu$ m). Experiment was performed in triplicate ( $n = 30$  segregation error events). **i,j,** Representative FISH images (**i**) and quantification (**j**) of RPE1-hTERT cells synchronized as before and released in mitosis with 48 nM nocodazole (scale bar = 5  $\mu$ m). Measured is the percentage of misaligned FISH probes (mean  $\pm$  s.e.m., two-tailed Fisher's exact test). Three independent experiments were performed.



**Extended Data Fig. 4: MN-seq characterization and micronucleus content bias in nocodazole-treated and cancer cells.** **a**, Live-cell imaging of RPE1-hTERT cells to determine survival when treated for 16 h with 62.5 nM Cpd-5. Experiment was performed in triplicate (scale bar = 5  $\mu$ m, mean  $\pm$  s.e.m., two-tailed Fisher's exact test). **b**, Representative images of a FAC-sorted nucleus and micronucleus (scale bar = 5  $\mu$ m). **c**, Gating strategy for micronuclei. **d,e**, Representative FISH images (**d**) and quantification (**e**) of micronucleated RPE1-hTERT cells treated with Cpd-5 for 16 hours (scale bar = 5  $\mu$ m). The graph shows the percentage of micronuclei containing a certain chromosome (s.e.m., two-tailed Pearson correlation coefficient, 1/15 ( $n = 371$  micronuclei), 2/17 ( $n = 277$  micronuclei) and 6/18 ( $n = 376$



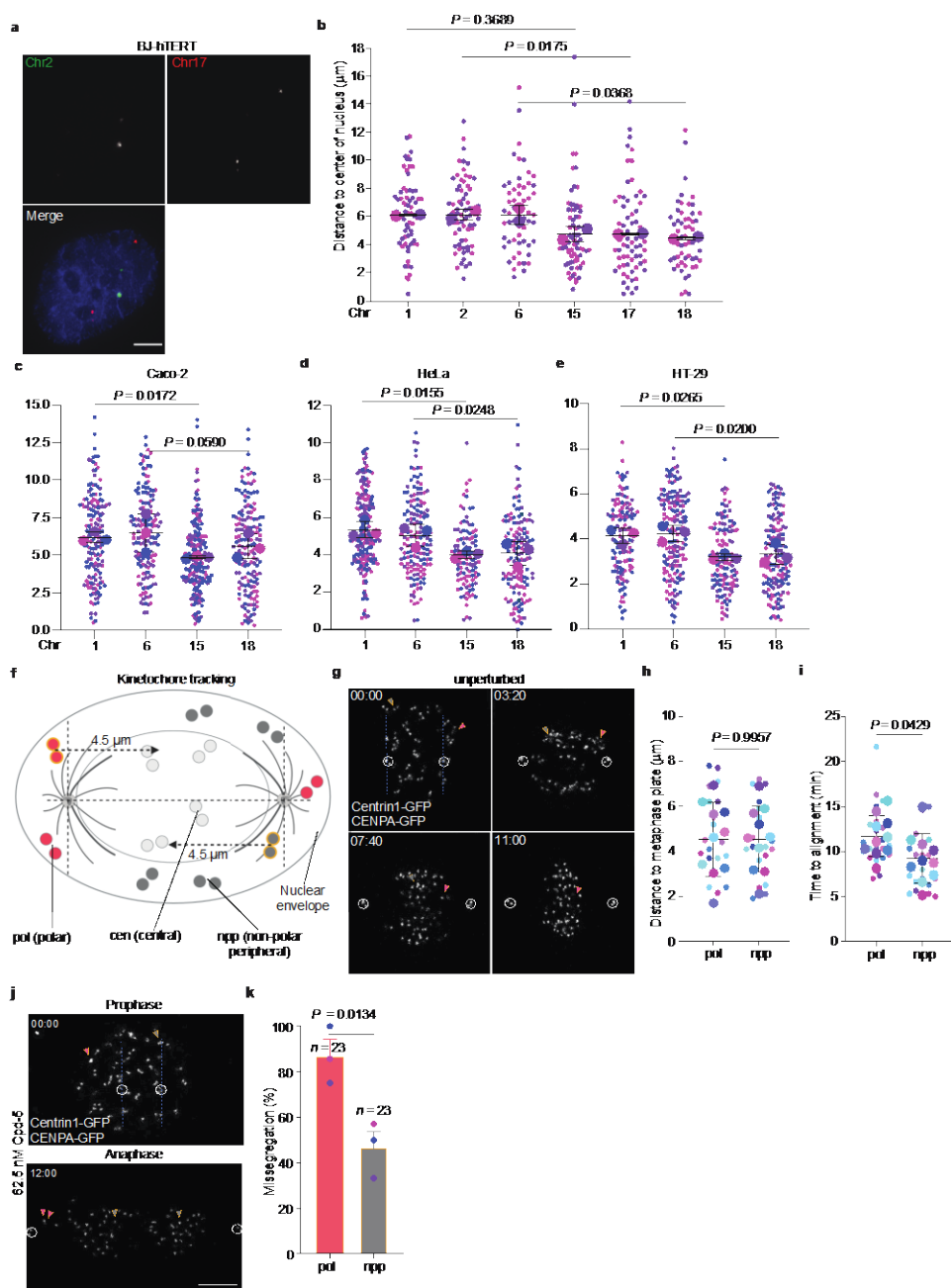
micronuclei)). Three independent experiments were performed. **f,g,h**, as in Fig. 2b-d but instead cells were treated with low nocodazole (single micronuclei; mean  $\pm$  s.e.m, two independent experiments,  $n = 151$ , bulk micronuclei; mean  $\pm$  s.e.m., four independent experiments, two-tailed Pearson correlation coefficient,  $n = \sim 8000$  micronuclei). **i,j,k**, Log2-fold enrichment of chromosomes in MN determined from bulk MN-seq data sorted from three chromosomally unstable cancer cell lines (mean  $\pm$  s.e.m., two-tailed Pearson correlation coefficient,  $n = \sim 1500$  MN for HT-29 and WiDr and 6000 for U2OS). Three independent experiments were performed for each cell line.



**Extended Data Fig. 5: Mis segregation frequency correlates with chromosome organization and organization is similar between cell lines. a,b,c,d**, Plots comparing aneuploidy percentages after Cpd-5 treatment (see Fig. 1c) in RPE1-hTERT cells to centromere sizes (**a**), ratio of P- over Q arm sizes (**b**), chromosome sizes (**c**), and gene densities (**d**) (two-tailed Pearson correlation coefficient). **e**.

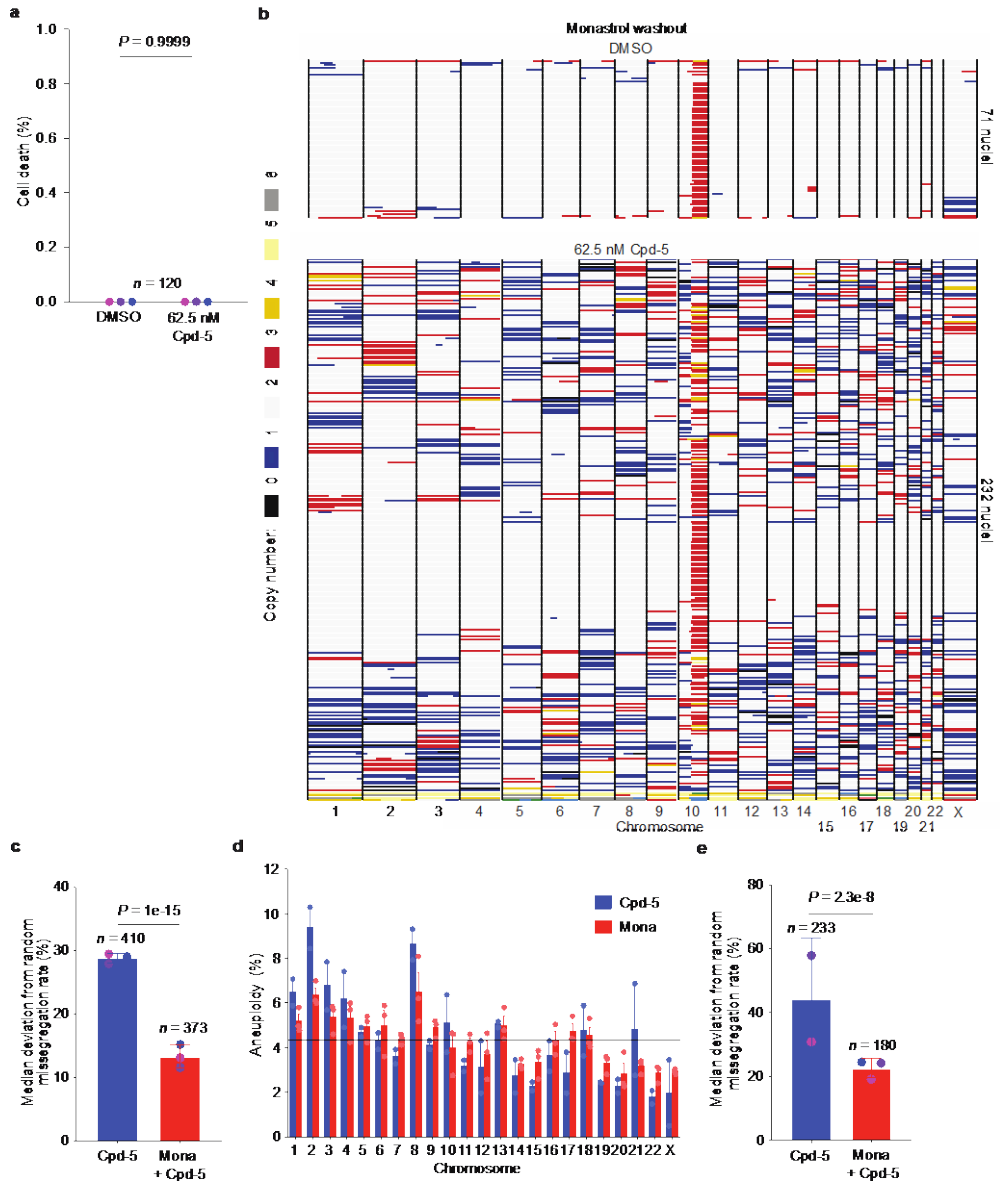
Quantification of aneuploidy percentages of both X chromosomes in RPE1-hTERT cells after Cpd-5 treatment (mean  $\pm$  s.e.m., two-tailed Fisher's exact test,  $n = 133$  cells with an X chromosome aneuploidy).

**f.** Plot comparing aneuploidy percentages after Cpd-5 treatment versus previously determined radial distances (two-tailed Pearson correlation coefficient)<sup>37</sup>. **g,h,i,j,k,l,m,** Plots comparing the percentage of LADs per chromosome for indicated cell lines to chromosome size (two-tailed Pearson correlation coefficient).



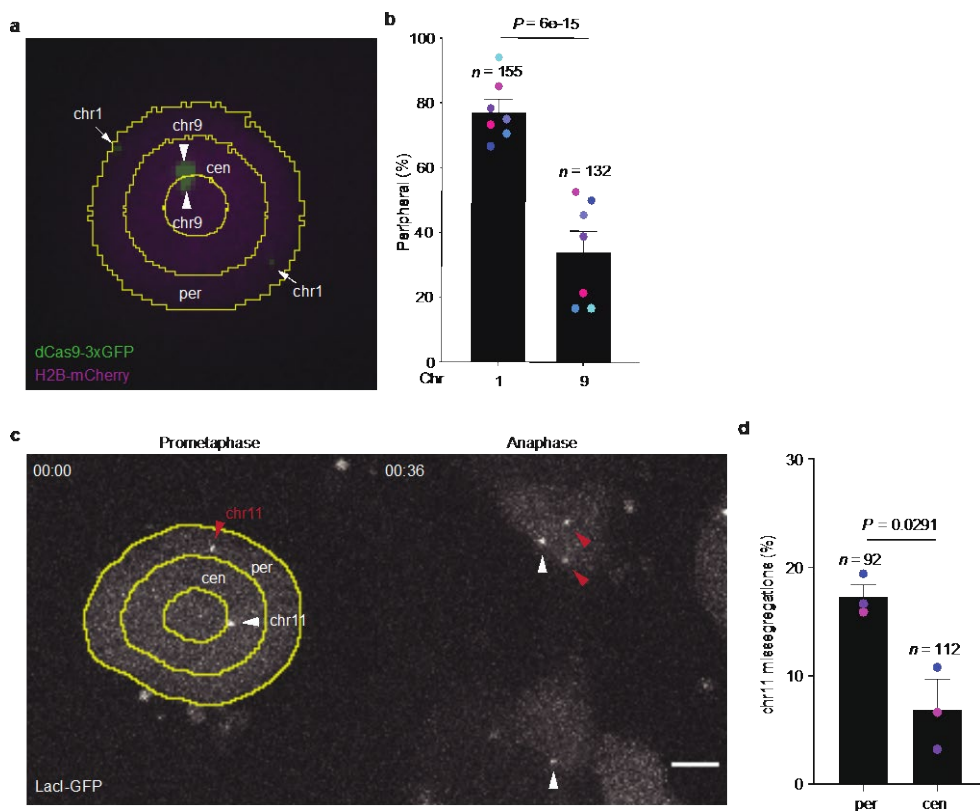
**Extended Data Fig. 6: Chromosomes behind the poles are more likely to missegregate.** a,b, Representative images (a) and quantification (b) of the distance from centromeric FISH probes to the center of the nucleus in BJ-hTERT cells (scale bar = 5  $\mu$ m, mean  $\pm$  s.d.,  $n > 70$ , 56, 68, 70 and 68 chromosomes, respectively). Data is pooled from two independent experiments. c,d,e, Distance of

centromeric FISH probes to the center of the nucleus in three cancer cell lines (mean  $\pm$  s.d., two-tailed ratio t-test,  $n = 133, 112, 81$  and  $108$ ;  $n = 125, 161, 134$  and  $153$ ;  $n = 160, 151, 185, 160$  chromosomes, respectively). Three independent experiments were performed. **f.** Schematic depicting the strategy to follow kinetochores with a similar distance to the metaphase plate (yellow circles). **g,h,i,** Representative stills (**g**) and quantification (**h-i**) of time to alignment for matched kinetochores based on them having the same distance to the metaphase plate in RPE1-hTERT CENPA-GFP Centrin1-GFP cells (scale bar =  $5\ \mu\text{m}$ ). White circles mark the centrosomes. Experiment was performed 10 times (mean  $\pm$  s.d., unpaired t-test,  $n = 21$ ). **j,k,** As in **e-g**, but instead cells were treated with  $62.5\ \text{nM}$  Cpd-5 and missegregations were measured (scale bar =  $5\ \mu\text{m}$ ). Experiment was performed in triplicate (mean  $\pm$  s.e.m., Fisher's exact test).

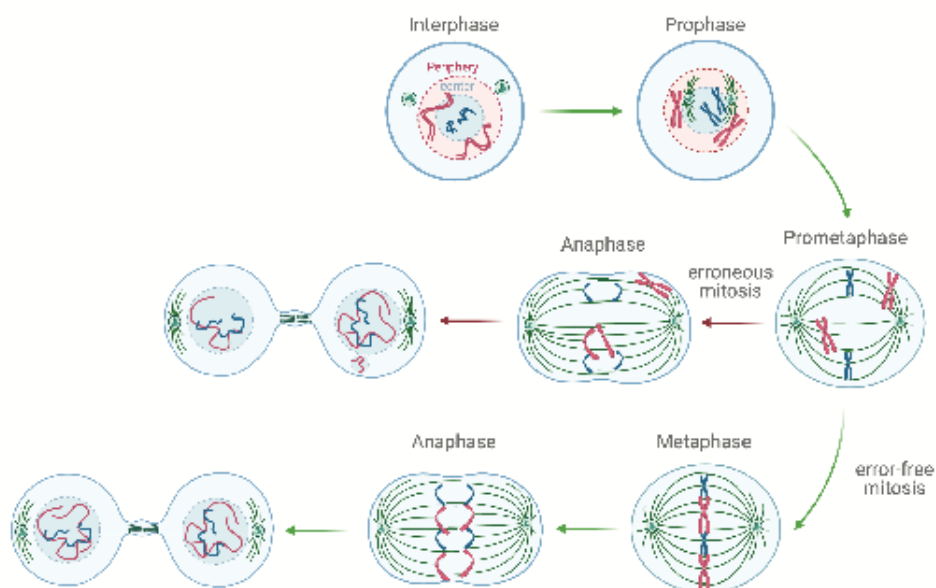


**Extended Data Fig. 7: Randomizing chromosome organization with monastrol decreases missegregation bias** **a.** Quantification of cell survival of RPE1-hTERT cells synchronized, treated for 4 h with monastrol, followed by a washout and shake-off. Experiment was performed three times (scale bar = 5  $\mu$ m, mean  $\pm$  s.e.m., two-tailed Fisher's exact test,  $n = 120$  daughter cells per condition). **b.** Representative scKaryo-seq results of RPE1-hTERT cells undergone a monastrol washout. **c.** Quantification of the change in the observed missegregation rate compared to expected (4.3%) for Cpd-

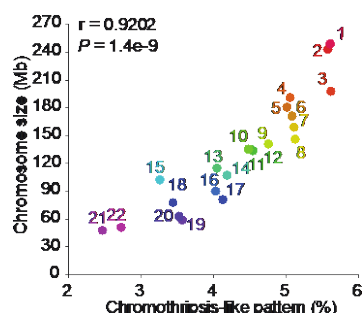
5 only treated RPE1-hTERT cells versus monastrol plus Cpd-5 treated ones (mean  $\pm$  s.e.m., two-tailed Fisher's exact test). **d.** Quantification of aneuploidy levels of HCT116 either treated with Cpd-5 only or a combination of monastrol and Cpd-5 as described before. Experiment was performed twice for the Cpd-5 treated cells and three times for the monastrol treated ones (mean  $\pm$  s.e.m.,  $n = 233$  and 180 aneuploid cells, respectively). **e.** As in c, but for HCT116 cells (mean  $\pm$  s.e.m., two-tailed Fisher's exact test).



**Extended Data Fig. 8: Chromosomes in the periphery of the nucleus missegregate more frequently independent of identity.** **a,b,** Representative still (**a**) and quantification (**b**) of the percentage of Cas9-tagged peripheral chromosomes just before mitosis onset (mean  $\pm$  s.e.m., two-tailed Fisher's exact test). Only chromosomes in the most outer ring were considered peripheral. **b,c,** Representative stills (**c**) and quantification (**d**) of chr11 missegregation rate of LacI-GFP-expressing HT1080 cells containing a LacO array in chr11 (scale bar = 5  $\mu$ m). Experiment was performed in triplicate (mean  $\pm$  s.e.m., two-tailed Fisher's exact test).



**Extended Data Fig. 9: Graphical representation of a cell going through an error-free mitosis (green arrows) or an erroneous one (red arrows).** Red chromosomes start out peripheral, while blue ones are more central.



**Extended Data Fig. 10: Chromothripsis-like patterns correlate with chromosome size.** Plot comparing chromosome size and chromothripsis-like patterns percentages per chromosome calculated from previously published data (two-tailed Pearson correlation coefficient).

## References

1. van Jaarsveld, R. H. & Kops, G. J. P. L. Difference Makers : Chromosomal Instability versus Aneuploidy in Cancer. *Trends in Cancer* **2**, 561–571 (2016).
2. Compton, D. A. Mechanisms of aneuploidy. *Curr. Opin. Cell Biol.* **23**, 109–113 (2011).
3. Zhang, C. Z. *et al.* Chromothripsis from DNA damage in micronuclei. *Nature*

- 522**, 179–184 (2015).
4. Ly, P. *et al.* Chromosome segregation errors generate a diverse spectrum of simple and complex genomic rearrangements. *Nat. Genet.* **51**, 705–715 (2019).
5. Shoshani, O. *et al.* Chromothripsis drives the evolution of gene amplification in cancer. *Nature* **591**, 137–141 (2021).
6. Davoli, T. *et al.* Cumulative haploinsufficiency and triplosensitivity drive aneuploidy patterns and shape the cancer genome. *Cell* **155**, 948–962 (2013).
7. Knouse, K. A., Davoli, T., Elledge, S. J. & Amon, A. Aneuploidy in cancer: Seq-ing answers to old questions. *Annu. Rev. Cancer Biol.* **1**, 335–354 (2017).
8. Bolhaqueiro, A. C. F. *et al.* Ongoing chromosomal instability and karyotype evolution in human colorectal cancer organoids. *Nat. Genet.* **51**, 824–834 (2019).
9. Cortés-Ciriano, I. *et al.* Comprehensive analysis of chromothripsis in 2,658 human cancers using whole-genome sequencing. *Nat. Genet.* **52**, 331–341 (2020).
10. McCoy, R. C. *et al.* Evidence of Selection against Complex Mitotic-Origin Aneuploidy during Preimplantation Development. *PLoS Genet.* **348**, 235–238 (2015).
11. Ben-David, U. & Amon, A. Context is everything: aneuploidy in cancer. *Nat. Rev. Genet.* **21**, 44–62 (2020).
12. Nagaoka, S. I., Hassold, T. J. & Hunt, P. A. Human aneuploidy: Mechanisms and new insights into an age-old problem. *Nat. Rev. Genet.* **13**, 493–504 (2012).
13. Vasudevan, A. *et al.* Aneuploidy as a promoter and suppressor of malignant growth. *Nat. Rev. Cancer* **21**, 89–103 (2021).
14. Bakhoun, S. F., Genovese, G. & Compton, D. A. Deviant Kinetochore Microtubule Dynamics Underlie Chromosomal Instability. *Curr. Biol.* **19**, 1937–1942 (2009).
15. Ertych, N. *et al.* Increased microtubule assembly rates influence chromosomal instability in colorectal cancer cells. *Nat. Cell Biol.* **16**, 779–791 (2014).
16. Solomon, D. A. *et al.* Mutational inactivation of STAG2 causes aneuploidy in human cancer. *Science*. **333**, 1039–1043 (2011).
17. Vázquez-Diez, C., Paim, L. M. G. & FitzHarris, G. Cell-Size-Independent Spindle Checkpoint Failure Underlies Chromosome Segregation Error in Mouse Embryos. *Curr. Biol.* **29**, 865–873 (2019).
18. Hatch, E. M., Fischer, A. H., Deerinck, T. J. & Hetzer, M. W. Catastrophic Nuclear Envelope Collapse in Cancer Cell Micronuclei. *Cell* **154**, 47–60



- (2013).
19. Muzny, D. M. *et al.* Comprehensive molecular characterization of human colon and rectal cancer. *Nature* **487**, 330–337 (2012).
  20. Duijf, P., Schultz, N. & Benezra, R. Cancer cells preferentially lose small chromosomes. *Int. J. Cancer* **132**, 1–20 (2013).
  21. Taylor, A. M. *et al.* Genomic and Functional Approaches to Understanding Cancer Aneuploidy. *Cancer Cell* **33**, 676–689 (2018).
  22. Turajlic, S. *et al.* Tracking Cancer Evolution Reveals Constrained Routes to Metastases: TRACERx Renal. *Cell* **173**, 581–594 (2018).
  23. Li, Y. *et al.* Patterns of somatic structural variation in human cancer genomes. *Nature* **578**, 112–121 (2020).
  24. Gruhn, J. R. *et al.* Chromosome errors in human eggs shape natural fertility over reproductive life span. *Science* **1469**, 1466–1469 (2019).
  25. Drpic, D. *et al.* Chromosome Segregation Is Biased by Kinetochore Size. *Curr. Biol.* **28**, 1344–1356 (2018).
  26. Worrall, J. T. *et al.* Non-random Mis-segregation of Human Chromosomes. *Cell Rep.* **23**, 3366–3380 (2018).
  27. Dumont, M. *et al.* Human chromosome-specific aneuploidy is influenced by DNA-dependent centromeric features. *EMBO J.* **39**, 1–21 (2020).
  28. Koch, A., Maia, A., Janssen, A. & Medema, R. H. Molecular basis underlying resistance to Mps1/TTK inhibitors. *Oncogene* **35**, 2518–2528 (2016).
  29. Bakhoun, S. F. & Compton, D. A. Chromosomal instability and cancer: a complex relationship with therapeutic potential. *J. Clin. Invest.* **122**, 1138–1143 (2012).
  30. Ditchfield, C. *et al.* Aurora B couples chromosome alignment with anaphase by targeting BubR1, Mad2, and Cenp-E to kinetochores. *J. Cell Biol.* **161**, 267–280 (2003).
  31. Hauf, S. *et al.* The small molecule Hesperadin reveals a role for Aurora B in correcting kinetochore-microtubule attachment and in maintaining the spindle assembly checkpoint. *J. Cell Biol.* **161**, 281–294 (2003).
  32. Dick, A. E. & Gerlich, D. W. Kinetic framework of spindle assembly checkpoint signalling. *Nat. Cell Biol.* **15**, 1370–1377 (2013).
  33. Avlasevich, S. L., Bryce, S. M., Cairns, S. E. & Dertinger, S. D. In vitro micronucleus scoring by flow cytometry: Differential staining of micronuclei versus apoptotic and necrotic chromatin enhances assay reliability. *Environ. Mol. Mutagen.* **47**, 56–66 (2006).
  34. Bochtler, Tilmann, Kartal-Kaess, Mutlu, Granzow, Martin, Hielscher, Thomas, R. Cosenza, Marco, Herold-Mende, Christel, Jauch, Anna, Krämer, A. Micronucleus formation in human cancer cells is biased by chromosome size. *Genes Chromosom. Cancer* **58**, 392–395 (2019).
  35. Bridger, J. M., Boyle, S., Kill, I. R. & Bickmore, W. A. Re-modelling of nuclear

- architecture in quiescent and senescent human fibroblasts. *Curr. Biol.* **10**, 149–152 (2000).
36. Croft, J. A. *et al.* Differences in the localization and morphology of chromosomes in the human nucleus. *J. Cell Biol.* **145**, 1119–1131 (1999).
  37. Bolzer, A. *et al.* Three-dimensional maps of all chromosomes in human male fibroblast nuclei and prometaphase rosettes. *PLoS Biol.* **3**, 0826–0842 (2005).
  38. Lenain, C. *et al.* Massive reshaping of genome-nuclear lamina interactions during oncogene-induced senescence. *Genome Res.* **27**, 1634–1644 (2017).
  39. Meuleman, W. *et al.* Constitutive nuclear lamina-genome interactions are highly conserved and associated with A/T-rich sequence. *Genome Res.* **23**, 270–280 (2013).
  40. Sobecki, M. *et al.* MadID, a Versatile Approach to Map Protein-DNA Interactions, Highlights Telomere-Nuclear Envelope Contact Sites in Human Cells. *Cell Rep.* **25**, 2891–2903 (2018).
  41. Chen, Y. *et al.* Mapping 3D genome organization relative to nuclear compartments using TSA-Seq as a cytological ruler. *J. Cell Biol.* **217**, 4025–4048 (2018).
  42. Kind, J. *et al.* Single-cell dynamics of genome-nuclear lamina interactions. *Cell* **153**, 178–192 (2013).
  43. Stanyte, R. *et al.* Dynamics of sister chromatid resolution during cell cycle progression. *J. Cell Biol.* **217**, 1985–2004 (2018).
  44. Finlan, L. E. *et al.* Recruitment to the nuclear periphery can alter expression of genes in human cells. *PLoS Genet.* **4**, 1–13 (2008).
  45. Barisic, M., Aguiar, P., Geley, S. & Maiato, H. Kinetochore motors drive congression of peripheral polar chromosomes by overcoming random arm-ejection forces. *Nat. Cell Biol.* **16**, 1249–1256 (2014).
  46. McCoy, R. C. Mosaicism in Preimplantation Human Embryos: When Chromosomal Abnormalities Are the Norm. *Trends Genet.* **33**, 448–463 (2017).
  47. Itoh, G. *et al.* Lateral attachment of kinetochores to microtubules is enriched in prometaphase rosette and facilitates chromosome alignment and bi-orientation establishment. *Sci. Rep.* **8**, 1–18 (2018).
  48. Daniela Cimini, Lisa A. Cameron, E. D. S. Anaphase Spindle Mechanics Prevent Mis-Segregation of Merotelically Oriented Chromosomes. *Curr. Biol.* **14**, 2149–2155– (2004).
  49. Vukušić, Kruno, Tolic, I. M. Polar Chromosomes — Challenges of a Risky Path. (2022).
  50. Parada, L. A., Mcqueen, P. G. & Misteli, T. Tissue-specific spatial organization of genomes. *Genome Biol.* **5**, 1–9 (2004).
  51. Hadders M.A. *et al.* Untangling the contribution of Haspin and Bub1 to Aurora

- B function during mitosis. *J. Cell Biol.* **219**, 1-20 (2020)
52. Sato, T. *et al.* Long-term expansion of epithelial organoids from human colon, adenoma, adenocarcinoma, and Barrett's epithelium. *Gastroenterology* **141**, 1762–1772 (2011).
  53. Truong, M.A. *et al.* A motor-based approach to induce chromosome-specific mis-segregations in human cells. *BioRxiv*, *preprint* (2022).
  54. Bolhaqueiro, A. C. F. *et al.* Ongoing chromosomal instability and karyotype evolution in human colorectal cancer organoids. *Nat. Genet.* **51**, 824–834 (2019).
  55. Buđa, R., Vukušić, K. & Tolić, I. M. Dissection and characterization of microtubule bundles in the mitotic spindle using femtosecond laser ablation. *Methods Cell Biol.* **139**, 81–101 (2017).
  56. Vukušić, K., Ponjavić, I., Buđa, R., Risteski, P. & Tolić, I. M. Microtubule-sliding modules based on kinesins EG5 and PRC1-dependent KIF4A drive human spindle elongation. *Dev. Cell* **56**, 1253–1267 (2021).
  57. Avlasevich, S. L., Bryce, S. M., Cairns, S. E. & Dertinger, S. D. In vitro micronucleus scoring by flow cytometry: Differential staining of micronuclei versus apoptotic and necrotic chromatin enhances assay reliability. *Environ. Mol. Mutagen.* **47**, 56–66 (2006).
  58. de Luca, K. L. & Kind, J. Single-Cell DamID to Capture Contacts Between DNA and the Nuclear Lamina in Individual Mammalian Cells. in *Capturing Chromosome Conformation: Methods and Protocols* 159–172 (Springer US, 2021).
  59. Kind, J. *et al.* Genome-wide Maps of Nuclear Lamina Interactions in Single Human Cells. *Cell* **163**, 134–147 (2015).



# Chapter 4

## **LossTag: an aneuploidy selection tool to study the consequences of whole chromosome losses**

Sjoerd J. Klaasen<sup>1,2</sup> & Geert J.P.L. Kops<sup>1,2</sup>

### **Affiliations**

<sup>1</sup>Hubrecht Institute - KNAW (Royal Netherlands Academy of Arts and Sciences) and University Medical Centre Utrecht, Utrecht, the Netherlands.

<sup>2</sup>Oncode Institute, Utrecht, the Netherlands

**In preparation**

**Aneuploidy is caused by chromosome segregation errors during cell divisions and is prevalent in cancer. Aneuploidy leads to a general stress response induced by changes in expression of hundreds of genes at once. Cancers from the same tissue origin have similar aneuploidy patterns. The reason for this is unclear. Certain copy number combinations may have selective benefit in a given tissue, or the order of losses and gains is somehow restricted depending on which copy number alterations arise first. In order to investigate this, we developed a tool to enrich for specific monosomies (LossTag). Using live-cell imaging, flow cytometry and bulk and single-cell DNA sequencing we confirmed the tool heavily enriches for aneuploid cells and losses of specific chromosomes when chromosomal instability is induced in non-transformed RPE1-hTERT cells. Strikingly, cells quickly reacquired a second copy of the monosomic chromosome, possibly due non-disjunction events in mitosis. When following aneuploidy landscapes over time, we found that, in general, aneuploidy is heavily selected against, but that certain copy number changes eventually emerged in the population. RNA-sequencing on clonal LossTag cell lines enriched for particular monosomies revealed monosomy-specific differentially expressed genes within a few days after aneuploidy induction. In conclusion, we developed a tool to enrich for specific chromosome monosomies, allowing us to study the complex consequences of recurrent aneuploidy patterns.**

One of the most common genetic abnormalities in cancer is aneuploidy<sup>1</sup>. It is defined as cells having a genomic state with abnormal chromosome numbers due to gains or losses of chromosomes and usually arises from mis-segregating chromosomes during mitosis. Copy number changes alter gene dosages and therefore expression<sup>2-4</sup>. In many cases, this results in a decrease in cell proliferation<sup>2,3,5-7</sup> through a general stress response: ribosomal genes are present on almost every chromosome and haploinsufficiency of only one of them leads to issues with translation<sup>2</sup>. Concomitantly, trisomies cause hypo-osmotic stress, proteotoxic stress and genetic instability<sup>4,8-10</sup>. It is much less clear if cells respond differently to copy number changes of specific chromosomes and if so, how.

Hints for chromosome-specific copy number aberration effects come from observations that copy number aberrations have a high degree of similarity within cancer types<sup>11,12</sup>. For example in colorectal cancer, tumors frequently gain chromosome 7, 8, 13 and 20, but lose chromosome 18<sup>13</sup>. It is unclear what causes such aneuploidy patterns. Tumor type-specific oncogenes or tumor suppressors are often present on chromosomes that are gained or lost, respectively<sup>14,15</sup>, suggesting that cells can benefit from aneuploidy by increasing expression of oncogenes or losing tumor suppressors. Another reason why recurrent aneuploidy patterns may exist is that only a combination of certain copy number changes is beneficial. For example, colorectal cancer organoids first lose chromosome 18 before they lose chromosome 4, suggesting loss of chromosome 18 is required for the loss of 4<sup>16</sup>. To make it easier to shape aneuploidies in order to study their consequences, we developed a tool to select for the loss of specific chromosomes. Using this tool, we investigate which combinations of copy number changes are compatible and how cells respond differently to specific chromosome losses.

## Results

### LossTag increases survival of chromosomally unstable cells

The ability to select for specific chromosome loss events will enable: 1) general enrichment for cells with aneuploid karyotypes, and 2. Specific enrichment for cells with the same monosomic chromosome. To this end, we developed the LossTag (Fig. 1a). In short, LossTag utilizes *tBID*<sup>17</sup>, a mitochondrial membrane-targeted death ligand<sup>18</sup>, under the control of a TetO sequence. Treating cells with doxycycline will induce expression of *tBID* and thus apoptosis in cells carrying the integrated LossTag. Cells which have lost the LossTag chromosome will survive. The LossTag construct also contains a red fluorescent protein (RFP), which in cells will be constitutively expressed. This will allow for microscopy or flow cytometry-based quantification or selection of cells that have lost the LossTag chromosome. The LossTag was randomly integrated into the genome of non-transformed, near-diploid RPE1-hTERT cells using a lentivirus with a ~0.3 MOI followed by the generation of clonal cell lines (Fig. 1b). Each clonal cell line should in theory have one LossTag construct inserted into a yet to be identified chromosome. Indeed, when we treated

three clonal cell lines with doxycycline, cells started dying 48 min after the addition of doxycycline (Fig. 1c). In two lines, all measured cells went into apoptosis 120 min after doxycycline treatment, although we could still detect a minute number of survivors. Inducing chromosomal instability by treating cells overnight with 62.5 nM Cpd-5<sup>19</sup>, a small molecule inhibitor of the mitotic kinase Mps1<sup>20</sup>, significantly increased the percentage of surviving cells to 3-7% following the addition of doxycycline (Fig. 1c). We also witnessed 2.7% of cells losing RFP after being treated for 3 days with Cpd-5. Taken together, LossTag induces massive and abrupt cell death, which can be rescued in some cells by the induction of chromosomal instability.

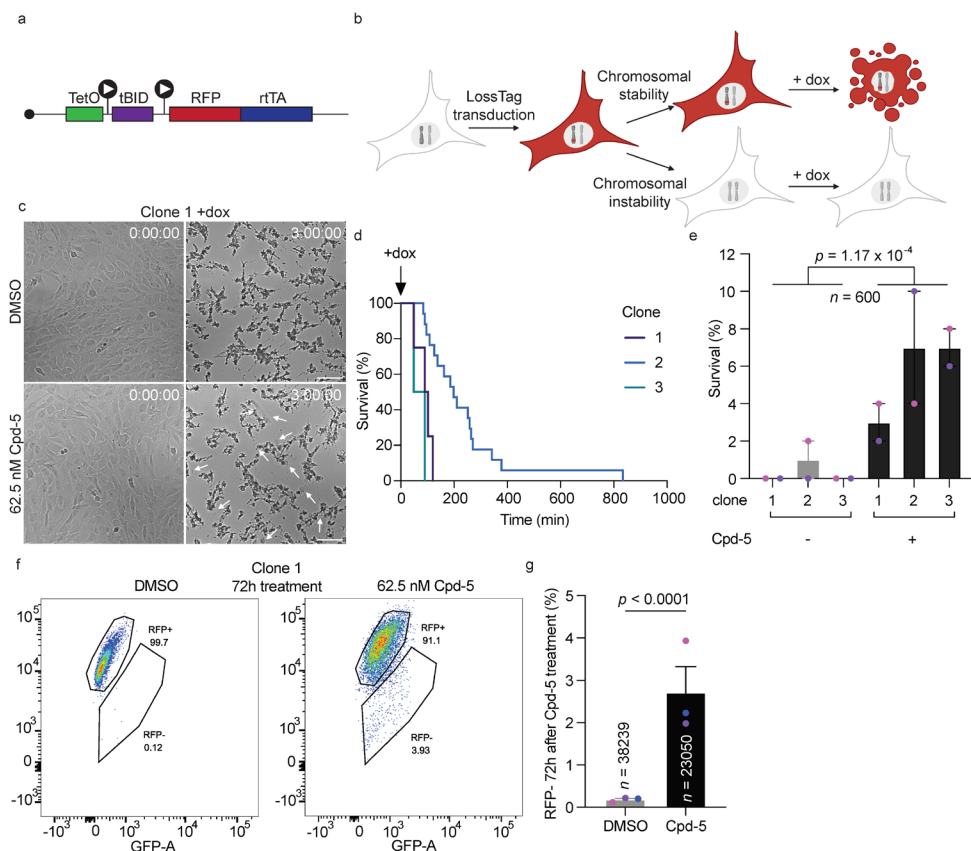


**Figure 1: Chromosomal instability decreases LossTag-dependent cell death.** **a.** Overview of the LossTag construct. **b.** Principle of the LossTag system. Cells which have lost the construct (red-tagged chromosome) will survive doxycycline treatment. **c,d,e,** Representative live-cell images (**c**) and quantification of survival (**d-e**) of RPE1-hTERT LossTag clones treated with DMSO or Cpd-5 followed by 100



doxycycline. White arrows in the images indicate survivors (scale bar = 100  $\mu$ m). Experiment was performed twice (mean  $\pm$  s.e.m., two-tailed Fisher's exact test). **f,g**, Representative flow cytometry graphs (**f**) and quantification (**g**) of cells treated for 3 days with DMSO or 62.5 nM Cpd-5. Clones 1, 2 and 3 have been combined to create the three replicates (mean  $\pm$  s.e.m., two-tailed Fisher's exact test).

### **LossTag enriches for the loss of a specific chromosome**

To identify the chromosome in which the LossTag had integrated in the surviving chromosomally unstable cells, we employed single-cell whole genome sequencing (scKaryo-seq)<sup>21</sup> on two clones both treated for 8h with Cpd-5 with and without doxycycline (Fig. 2a). This revealed that the vast majority of cells that survived doxycycline treatment had lost chromosome 1 (clone 1) or chromosome 11 (clone 2) (Fig. 2a-c). Bulk Karyo-seq<sup>21</sup> also allowed us to identify the chromosome in which the LossTag was integrated, but at a fraction of the cost (Fig. 2d). Surprisingly, the scKaryo-seq data revealed that some cells were still diploid for the chromosome presumably carrying the LossTag. We envision two possibilities: either these rare cells had undergone loss of heterozygosity for the LossTag, or somehow *tBID* was insufficiently expressed after doxycycline treatment. The latter seems unlikely, as cell survival without inducing CIN is far below 1% (Fig. 1e). We further note that cells are frequently nullisomic for the lossTag chromosome, meaning both parental chromosomes have mis-segregated. Such non-disjunction event can also cause loss of heterozygosity. Besides more losses of specific chromosomes, we also witnessed a substantial overall increase of aneuploidy upon doxycycline treatment (from 3.4 to 7.3 events) (Fig. 2b). We hypothesize that this is due to indirect enrichment for cells that have undergone segregation errors in addition to loss of the LossTag chromosome. We conclude that the LossTag significantly enriches for cells with specific chromosome losses as well as general aneuploidy.

### **Aneuploid cells are rapidly outcompeted by diploid and mildly aneuploid cells**

Since selection for loss of LossTag enriched for aneuploid cells in general and for cells with specific monosomies in particular, this allowed us to ask the following questions: 1. How does a monosomy of a specific chromosome shape recurrent

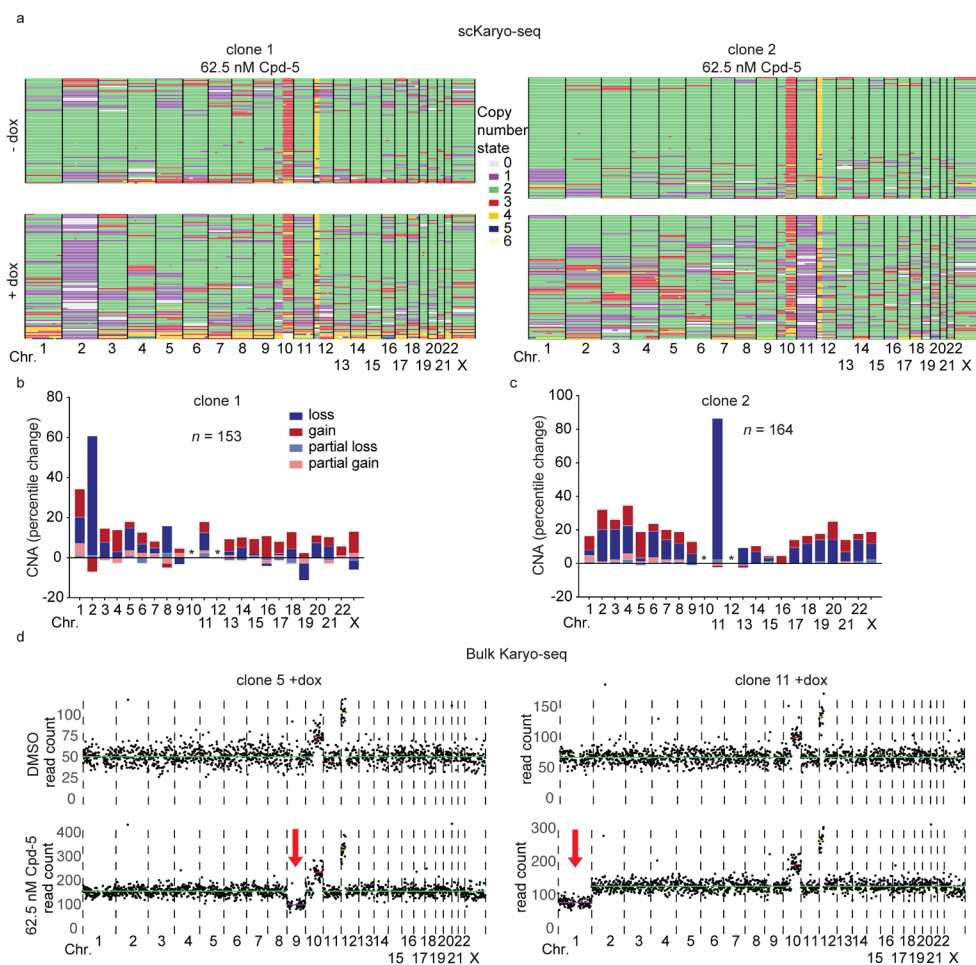


**Figure 2: LossTag enriches for global aneuploidies and specific chromosome losses.** **a.** scKaryo-seq data of clones 1 and 2 treated for 8h with 62.5 nM Cpd-5 followed by 24h of doxycycline. Each column is a chromosome and each line is a cell. Colors indicate copy number states. Experiment was performed once for the two clones. **b.c.** Quantification of the percentile increase of aneuploidy in dox-treated compared to no dox-treated cells using the scKaryo-seq data from a). Colors represent the type of copy number variation. **d.** Bulk Karyo-seq of clones 5 and 11 treated for 16h with DMSO or Cpd-5 followed by a 24h of doxycycline. Graphs display the chromosome number on the x-axis and the read count on the y-axis. The dots represent genomic bins which the Aneufinder software uses to determine copy number states with (see colored lines). Experiment was performed once for every clone.

aneuploidy patterns? 2. Are the non-random aneuploidy landscapes we see in **Chapter 3** still present after long-term culture and if not, how quickly does it

disappear? 3. How do aneuploidy landscapes change regardless of the LossTag chromosome (e.g. aneuploidy per cell, gains versus losses, structural versus whole chromosomes)? To answer these questions, we treated three different *TP53* knockout LossTag clones (from now on referred to as Chr1<sup>LossTag</sup>, Chr9<sup>LossTag</sup> or Chr19<sup>LossTag</sup>) with Cpd-5 overnight followed by doxycycline for 3 days. We chose these clones because they have the LossTag in chromosomes that represent a wide array of features, for example in size, location and gene density. Cells were cultured for up to 4 weeks and were harvested at 8h (or 0 weeks), 1 and 4 weeks after doxycycline addition for scKaryo-seq processing. Sequencing issues unfortunately prevented us from using the 0 week timepoint of the three selected clones, and we therefore resorted to other clones for this time point only. This should not affect the results, because the aneuploidy patterns (apart from the LossTag chromosome) at 0 weeks following Cpd5 are similar for all clones (Extended Data Fig. 1a-b). As expected, the large majority of LossTag chromosomes were lost at least once in every cell at 0 weeks (Fig. 3b, Extended Data Fig. 1a-b). Interestingly however, the majority of cells became disomic for the LossTag chromosome and diploid over time, precluding us from determining the effect of specific monosomies on shaping recurrent aneuploidy patterns (Fig. 3b-c). Chromosome 1, 9 or 19 monosomies were still common at week 1 in the three different clones, and only chromosome 1 displayed substantial partial gains/losses, but this was limited to one replicate. After 4 weeks, partial gains/losses represented the vast majority of chromosome 1 CNAs.

To determine if the non-random aneuploidy patterns as a result of non-random segregation errors uncovered in chapter 3 persisted after long-term culture, we quantified the amount of whole chromosome aneuploidies of the different time-points and plotted them against each other. As expected, the aneuploidy landscape at 0 weeks followed the chromosome location-dependent segregation error bias as shown in chapter 3, and this persisted up to week 1 (Fig. 3d). After 4 weeks however, aneuploidy frequencies no longer correlated with week 0 aneuploidy frequencies (Fig. 3e). We thus conclude that in the context of our experiment the non-random aneuploidy patterns disappear between 1-4 weeks.

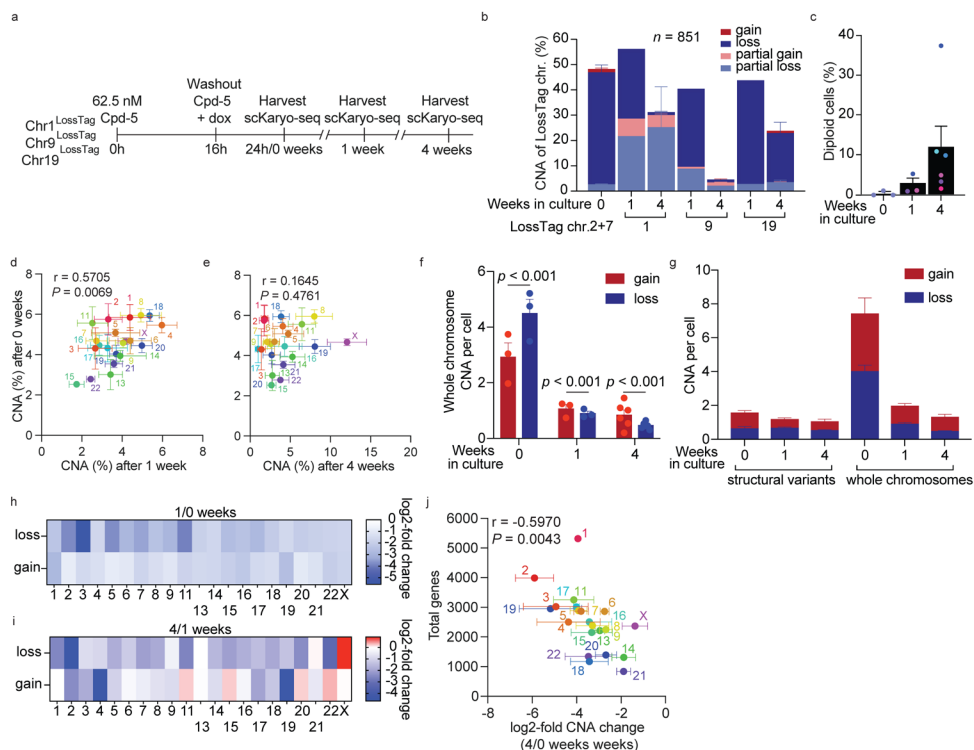


**Figure 3: Selection dictates aneuploidy patterns.** **a.** Illustration of the workflow used in this figure. **b.** LossTag chromosome copy number aberrations (CNA) 0, 1 or 4 weeks after culture. Colors depict if chromosomes have been gained (red), lost (blue), partially gained (light red) or partially lost (light blue) (mean  $\pm$  s.e.m.). Experiment was performed in duplicate for week 0 and 4, and once for week 1. **c.** Percentage of diploid cells in the population 0, 1 and 4 weeks after Cpd-5 treatment (mean  $\pm$  s.e.m.). **d,e,** Plots showing the correlation between the aneuploidy percentages 0 weeks and 1 week (**d**) or 4 weeks (**e**) after Cpd-5 treatment (mean  $\pm$  s.e.m., Pearson correlation coefficient). **f.** Number of whole chromosome gains (red) or losses (blue) after 0, 1 or 4 weeks of culture (mean  $\pm$  s.e.m., two-tailed Fisher's exact test). **g.** Number of structural or whole chromosome copy number aberrations 0, 1 or 4 weeks after culture. **h,i,** Heatmaps of the log<sub>2</sub>-fold change in whole chromosome gains and losses over time for every chromosome. **j.** Plot comparing the log<sub>2</sub>-fold change in CNA and the total number of genes per chromosome (mean  $\pm$  s.e.m., Pearson correlation coefficient).

To investigate general trends of aneuploidy evolution in our culture experiment, we quantified the amount of overall aneuploidy, structural and whole chromosome aberrations, gains and losses of every chromosome over time. At 0 weeks, cells had an average of around 9 structural and whole copy number variations with more whole chromosome losses than gains (4.5 versus 2.9 events per cell) (Fig. 3e).

Whole chromosome aneuploidies disappeared a week after Cpd-5 treatment to 2 event per cell (Fig. 3f-g). A slight bias for chromosome gains could be observed after 4 weeks, showing that, in general, chromosome gains are better tolerated than chromosome losses. Structural variations were less common than whole chromosome aneuploidies at week 0 (1.6 versus 7.4 events per cell), but became more prominent over time resulting in only a minor difference 4 weeks (1 versus 1.3 events). This implies that cells are less tolerant to whole chromosome than structural aneuploidies. Surprisingly, when comparing losses and gains of individual chromosomes between 0 weeks and 4 weeks or 1 week and 4 weeks, chromosome 4 and 19 were the only ones for which losses were better tolerated than gains (Fig. 3h-i). We next looked at chromosome-specific changes over time. The fold-change in aneuploidy between 0 and 4 weeks anti-correlated with the number of genes on a chromosome, suggesting that tolerance to CNAs of a given chromosome diminishes with its gene content (Fig. 3j). Although the overall trend was for cells to become less aneuploid over time, some cells with specific aneuploidies emerged. For example, gains of chromosomes 16, 20 or X and losses of chromosome 10 or X became more prominent at week 4 in Chr9<sup>LossTag</sup> cells, while gains of chromosome 3 and 6 became prominent in Chr1<sup>LossTag</sup> cells (Extended Data Fig. 1a-b). Copy number changes did not, however show a high similarity between replicates. In summary, we conclude that aneuploidies are rapidly selected against: severely aneuploid cells are quickly lost from the population, and cells with whole chromosome losses are more rapidly lost than cells with structural variations or cells that have undergone loss of heterozygosity.

### Immediate response to chromosome loss differs per chromosome

In order to investigate how cells respond to loss of specific chromosomes, we treated Chr1<sup>LossTag</sup>, Chr9<sup>LossTag</sup> and Chr19<sup>LossTag</sup> cells with 31.25 nM Cpd-5 for 16 h followed by 32 h of doxycycline to select for chromosome losses (Fig. 4a). We then performed bulk RNA-seq on surviving cells. To account for clone-specific expression differences, we also treated cells with Cpd-5 only (no doxycycline). As expected, differential expression analysis between doxycycline untreated and treated clones demonstrated a near 2-fold reduction in expression of genes on the LossTag

chromosome (Fig. 4b). Next, we removed all genes located on chromosome 1, 9 and 19 from the analysis to correct for the direct effect of gene dosage on gene expression levels and performed differential expression analyses between the three different clones. This revealed that when the LossTag was not activated (no doxycycline addition) clones did not have differentially expressed genes, indicating the clones have very similar expression profiles (Fig. 4c). By contrast, the three clones treated with doxycycline had on average 6.5% of genes differentially expressed. Interestingly, none of the differentially expressed genes were shared between all three clones (Fig. 4d). Reactome pathway analyses<sup>22</sup> showed that chromosome 9 loss led to a significant decrease in expression of genes related to protein translation and ribosome biogenesis (for example peptide chain elongation, translation elongation and rRNA processing in the nucleus) (Fig. 4e-f), while chromosome 19 loss significantly decreased expression of genes involved in mitosis (for example resolution of sister chromatid cohesion, amplification of signal from the kinetochores and mitotic spindle checkpoint) (Fig. 4g). Taken together, the initial gene expression response to aneuploidy is dependent on which chromosome is aberrant.

## Discussion

Recent work showed cells respond similarly to any type of copy number abnormality<sup>2-4,8-10</sup>, but the presence of recurrent aneuploidy patterns in cancer suggests a chromosome-specific effect also exists. In order to study differences in consequences between distinct copy number changes, we developed and characterized the LossTag tool. Using this tool, we found striking changes in gene expression depending on the chromosome that was lost, suggesting cells respond differently to a loss of one chromosome compared to another. We hypothesize these effects are 1. A direct consequence of a reduction in expression of gene regulators subsequently altering expression of other genes. 2. A more indirect effect where a decrease in expression of a few genes induces certain stresses leading to a specific or general stress response. 3. A result of reduced expression of many genes leading to an aneuploidy stress response of which the severity depends on the number of genes on that particular chromosome. Pathway analyses revealed chromosome 9

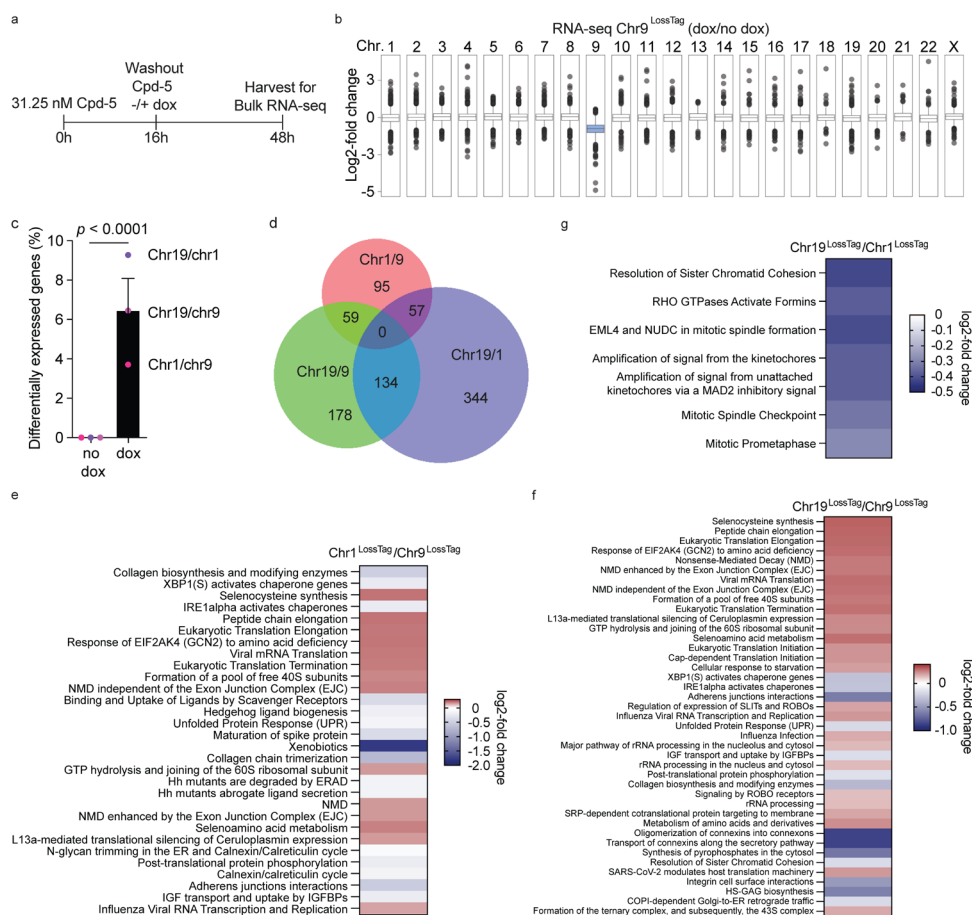


**Figure 4: Cellular responses to aneuploidy change depending on the affected chromosome. a.** Illustration of the workflow used in this figure. **b.** Chromosome-specific differential expression analysis of clone 5. Experiment was performed in triplicate. **c.** Percentage of differentially expressed genes between clones (mean  $\pm$  s.e.m., two-tailed Fisher's exact test). Each comparison was performed in triplicate. **d.** Venn diagram of the number of differentially expressed genes after doxycycline addition shared between comparisons. BioVenn.nl was used to generate this figure. **e,f,g.** Differential Reactome pathway analysis of doxycycline-treated clones.

loss resulted in a significant decrease in expression of genes related to translation compared to the two other clones. Interestingly, translation has been suggested to decrease because of aneuploidy due to haploinsufficiency of ribosomal proteins or by activation of a general stress response<sup>2,5,23</sup>. Unexpectedly though, chromosome

9 has the lowest number of genes encoding for proteins involved in translation and total number of genes of the three chromosomes. We also found a lower expression of mitotic genes when chromosome 19 was lost compared to chromosome 1, which is perhaps caused by a difference in the proportion of mitotic cells between the two cell populations. We hypothesize a chromosome 1 loss induces a mitotic arrest or chromosome 19 loss cells cycle slower.

Since the LossTag chromosome was quickly regained, probably due to loss-of-heterozygosity, we were unable to check whether copy number combinations giving a proliferative advantage in the background of loss of a specific chromosome exist. Instead, we used the scKaryo-seq data to follow the copy number states of all chromosomes in single-cells and made multiple observations: 1. A population of cells quickly purges their most aneuploid cells. 2. Cells are less tolerant to chromosome losses than to chromosome gains. 3. Structural variations are better tolerated than whole chromosome copy number variations. 4. Copy number variations of chromosomes with less genes are better tolerated than chromosomes with many genes. These observations are in line with previous findings in which cell fitness decreases as a function of increasing level and number of gene dosage changes<sup>4,5,24</sup>. This is because certain aneuploidy-induced stresses, such as proteotoxic and hypo-osmotic stress<sup>4,10</sup>, are caused by overexpression of hundreds of genes at the same time. Increasing this number will increase the amount of stress and therefore its anti-proliferative effects. Interestingly, we find that there are exceptions to this rule. Firstly, for chromosome 4 and 19 losses are better tolerated than gains. This is probably due to genes on these particular chromosomes having more deleterious effects when they are gained compared to when they are lost (which would be the case for negative regulators of essential genes). Secondly, cells with specific copy number aberrations eventually grow out. These chromosomes most likely contain specific genes important for proliferation in this particular context. It would be interesting to figure out which genes are responsible for this increased proliferation.



The LossTag construct integrates into a chromosome, allowing for efficient selection of its loss. We envision this tool can be of use when one would want to manipulate the karyotype of non-cancerous and cancerous cells to study the consequences of aneuploidy. For example, LossTag methodology can be used to revert a trisomy in a cancer cell line back to a disomy to examine if cancer cells still requires the trisomy for survival and if certain trisomic cells are more vulnerable to particular drugs than disomic counterparts. Our tool also selects for aneuploid cells in general, making it an interesting option for generating purely aneuploid populations of cells. One caveat of our approach is that we induce mis-segregations of multiple chromosomes during one cell division. This increases the likelihood of both homologs' mis-segregating, which in 50% of cases leads to loss-of-heterozygosity. Lowering the dose of Cpd-5 or using other small molecules or genetic tools to induce low levels of CIN should circumvent this issue and thus lead to a purely aneuploid population. The previously described issue of loss-of-heterozygosity could however also be used to our advantage in case one would want to generate a cell line with loss-of-heterozygosity for a specific chromosome. Another limitation of our tool is that it only selects for chromosome losses. Other tools will need to be developed in order to also be able to select for chromosome gains. We can imagine the use of Brainbow2.1, a Cre//ox-based system which stochastically expresses one of four fluorescent proteins<sup>25</sup>. A cell with two copies of this transgene because of a chromosome gain will have a 75% likelihood to express two colors instead of one. This system could also be used with four different antibiotic resistance genes instead of fluorescent proteins.

## Methods

### Cell culture

RPE1-hTERT cells were cultured in DMEM/F12, GlutaMAX supplement (Gibco) supplemented with 9% Tet-free foetal bovine serum (Sigma-Aldrich) and 1% penicillin/streptomycin (Sigma-Aldrich). To generate RPE1-hTERT LossTag cells, cells were transduced with the LossTag construct followed by single-cell sorting of tagRFP-positive cells into a 96 well plate. tagRFP-negative cells were also sorted as a negative control for the RNA sequencing experiment. 18 RFP-positive and 3 RFP-negative clones grew out and were frozen down. In order to study the evolution of

the karyotypes, TP53 was knocked out using a lentiviral LentiCRISPR v2 construct (Addgene #52961) with a guide (5' CGGTTTCATGCCGCCCATGC 3') against TP53. Cells were cultured for at least two weeks in the presence of Nutlin-3a (Sigma-Aldrich) to select for TP53-deficient cells. H2B-mNeon was introduced to the cells as described before<sup>21</sup>.

### **Plasmids**

The LossTag construct was generated by Gibson assembly using the backbone of a BmtI and BamHI digested pCW9-STAG2 plasmid and a tBID PCR product from the pSFFV-neo Bid human plasmid (Addgene #8766). The pCW9-STAG2 plasmid originates from the pCW9-Cas9 plasmid (Addgene #50661). tagRFP was also inserted by Gibson assembly.

### **Live-cell imaging**

To determine the survival of LossTag cells after doxycycline treatment, we plated cells at a 40% confluency in a 24 well plate and treated them with DMSO or 62.5 nM Cpd-5 (gift from René Medema) overnight. Right before imaging, cells were treated with 2 µg/ml doxycycline (Sigma-Aldrich). For imaging, we used a Nikon Ti-E motorized microscope equipped with a Zyla 4.2Mpx sCMOS camera (Andor) and 10 × 0.45 NA dry objective lens (Nikon). Cells were imaged with brightfield every 6 min for 18h. Analysis was performed using Fiji.

### **Flow cytometry**

To quantify RFP loss after induction of chromosomal instability, cells were plated at 10% confluency in a 6 well plate and treated with DMSO or 62.5 nM Cpd-5 for 3 days. Single-cell suspensions were then analyzed on a BD LSR Fortessa X-20 (BD Biosciences). Analysis was performed using FlowJo v10.

### **Bulk Karyo-seq**

To see if the LossTag selected for specific chromosome losses, cells in a 12 well plate at a 40% confluency were treated for 16h with DMSO or 62.5 nM Cpd-5 followed by a 24h doxycycline treatment. Cell debris was washed away and cells

were pelleted using centrifugation. After the addition of 10  $\mu$ l MQ, the library prep and analysis was performed as described before<sup>21</sup>.

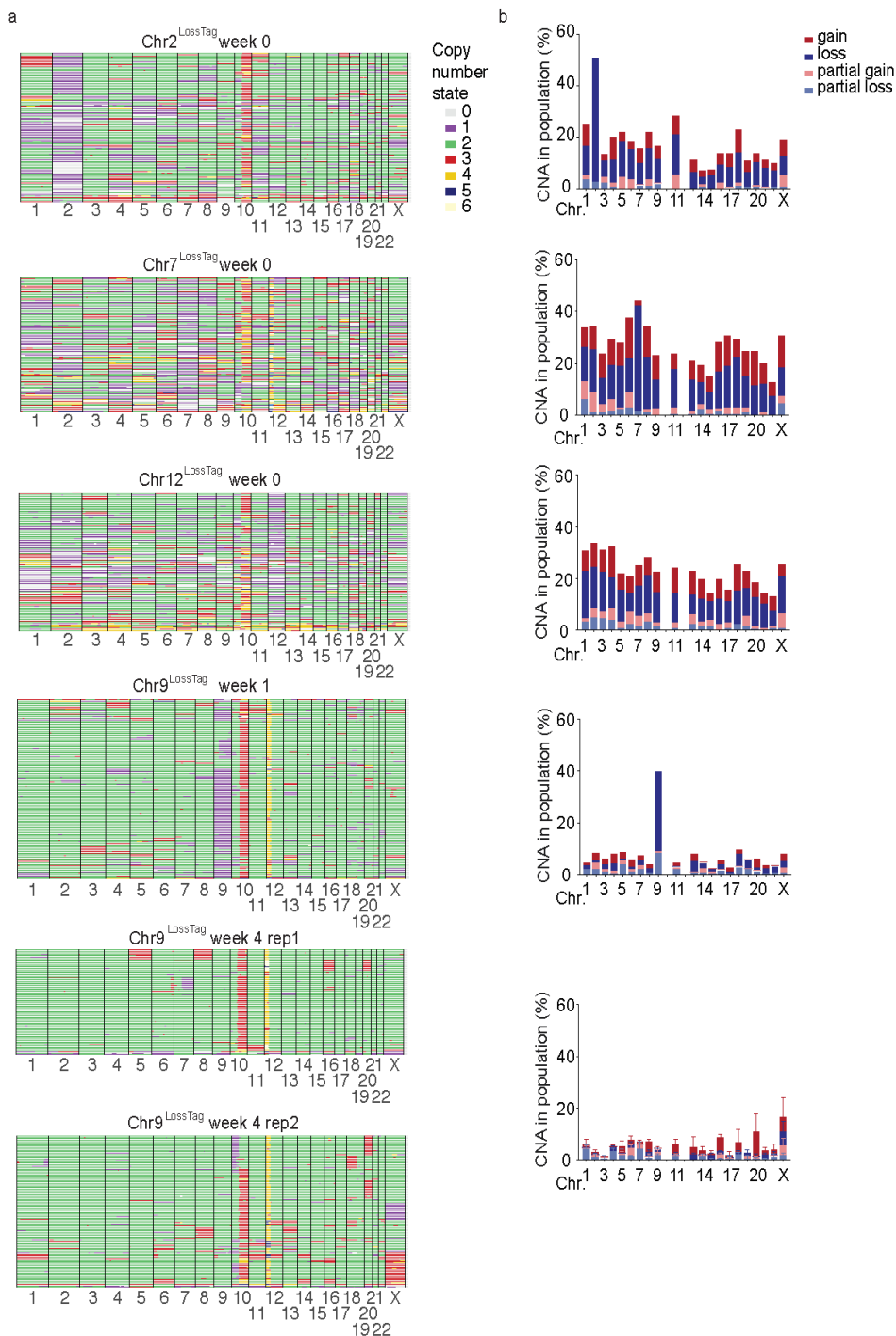
### **scKaryo-seq**

scKaryo-seq and analysis was performed as described previously<sup>21</sup> on cells at 20% confluency in a 10 cm plate treated for 8h with 62.5 nM Cpd-5 followed by 24h of doxycycline. Quality control was performed using a custom script (TWvR/AneufinderFileFilter on github) which filters for the minimum total read count (>15,000), the maximum spikiness (<0.25) and the minimum Bhattacharyya (>0.65). Copy numbers were counted automatically using AneuFinder. Copy number variations below 15 Mb in size and the already aneuploid chromosomes 10 and 12 were excluded from the analysis.

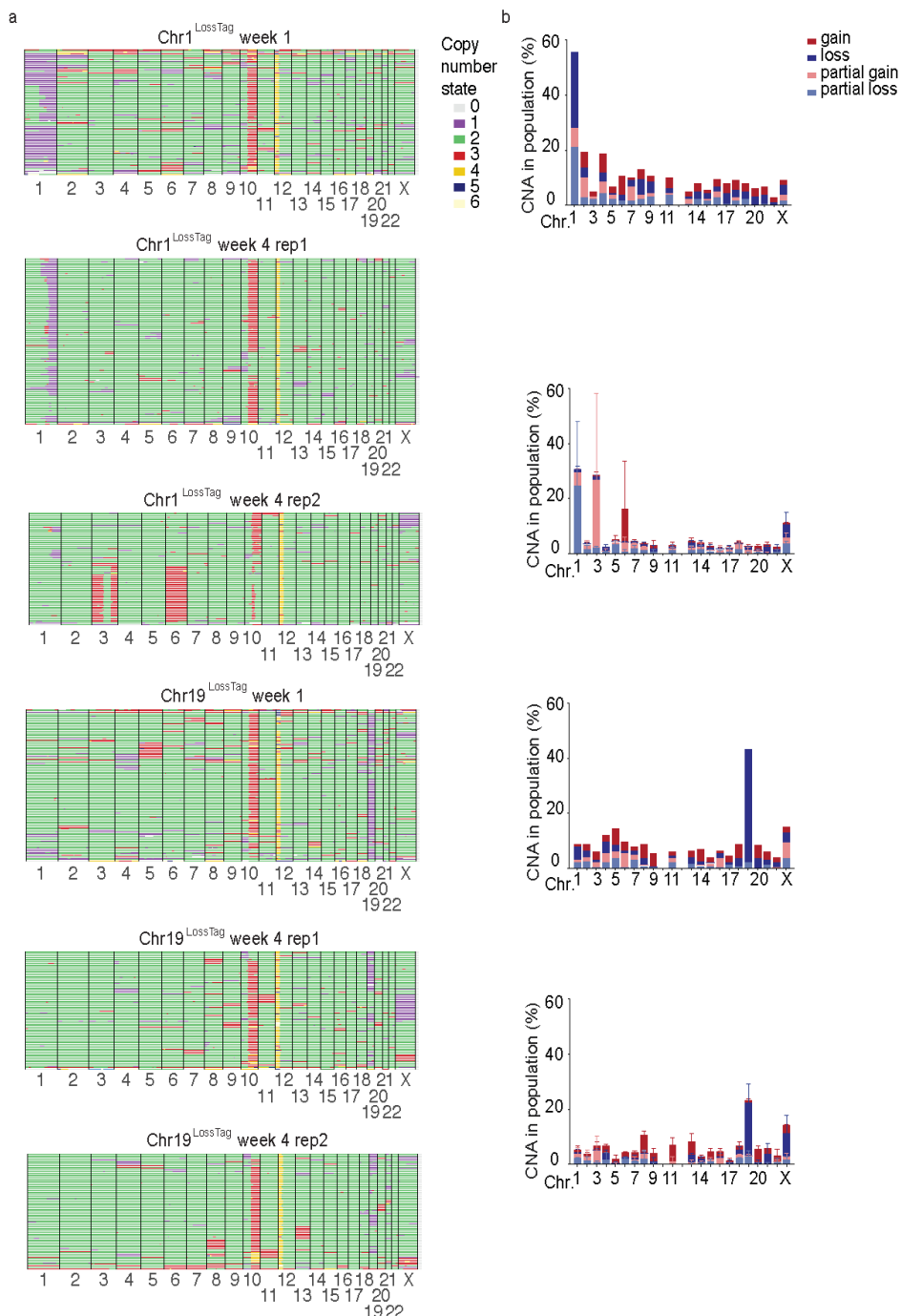
The evolutionary experiment was performed by plating cells in 40% in a 10 cm plate, treating them for 16h with 62.5 nM Cpd-5, followed by a 72h treatment of doxycycline. Cells were frozen down 8h after doxycycline addition, 1 week or 4 weeks for scKaryo-seq.

### **RNA-sequencing**

Cells were plated at 40% confluency in a 15 cm plate and treated for 16h with 31.25 nM Cpd-5. The Cpd-5 was washed away and cells were treated without or with doxycycline. Cells were harvested 48h after the start of the Cpd-5 treatment and snap-frozen at -20 °C. RNA was subsequently harvested using the Quick-RNA MiniPrep kit (Zymo Research) and library preparation was performed using the Nextflex Poly(A) beads and Nextflex Rapid Directional mRNA-seq Kit (Perkin-Elmer) according to the manufacturers' instructions. 24 of the libraries were sequenced on an Illumina NextSeq2000 at 2x50bp (400 million reads). Raw data was processed using the RNA-seq pipeline of the USEQ (<https://github.com/UMCU/Genetics/RNAseq-NF/>). We subsequently used raw read counts for the Camera algorithm on reactome.org for differential expression and pathway analyses.



CONTINUING ON NEXT PAGE



**Extended Data Figure 1: Copy number states of LossTag clones over time. a,b, scKaryo-seq plots (a) and quantifications (b) of CNAs in the population of LossTag clones.**

## References

1. Duijf, P., Schultz, N. & Benezra, R. Cancer cells preferentially lose small chromosomes. *Int. J. Cancer* **132**, 1–20 (2013).
2. Chunduri, N. K. *et al.* Systems approaches identify the consequences of monosomy in somatic human cells. *Nat. Commun.* **12**, 1–17 (2021).
3. Stinge, S. *et al.* Global analysis of genome, transcriptome and proteome reveals the response to aneuploidy in human cells. *Mol. Syst. Biol.* **8**, 1–12 (2012).
4. Torres, E. M. *et al.* Effects of aneuploidy on cellular physiology and cell division in haploid yeast. *Science* **317**, 916–924 (2007).
5. Hintzen, D. C. *et al.* The impact of monosomies, trisomies and segmental aneuploidies on chromosomal stability. *PLoS One* **17**, 1–27 (2022).
6. Williams, B. R. *et al.* Aneuploidy Affects Proliferation and Spontaneous Immortalization in Mammalian Cells. *Science* **322**, 703–710 (2008).
7. Thompson, S. L. & Compton, D. A. Proliferation of aneuploid human cells is limited by a p53-dependent mechanism. **188**, 369–381 (2010).
8. Sheltzer, J. M. *et al.* Aneuploidy drives genomic instability in yeast. *Science* **333**, 1026–1030 (2011).
9. Passerini, V. *et al.* The presence of extra chromosomes leads to genomic instability. *Nat. Commun.* **7**, 1–12 (2016).
10. Tsai, H. J. *et al.* Hypo-osmotic-like stress underlies general cellular defects of aneuploidy. *Nature* **570**, 117–121 (2019).
11. Zack, T. I. *et al.* Pan-cancer patterns of somatic copy-number alteration. *Nat. Genet.* **45**, 1134–1140 (2013).
12. Hoadley, K. A. *et al.* Cell-of-Origin Patterns Dominate the Molecular Classification of 10,000 Tumors from 33 Types of Cancer. *Cell* **173**, 291–304 (2018).
13. Muzny, D. M. *et al.* Comprehensive molecular characterization of human colon and rectal cancer. *Nature* **487**, 330–337 (2012).
14. Davoli, T. *et al.* Cumulative haploinsufficiency and triplosensitivity drive aneuploidy patterns and shape the cancer genome. *Cell* **155**, 948–962 (2013).
15. Sack, L. M. *et al.* Profound Tissue Specificity in Proliferation Control Underlies Cancer Drivers and Aneuploidy Patterns. *Cell* **173**, 499–514 (2018).
16. Kester, L. *et al.* Integration of multiple lineage measurements from the same cell reconstructs parallel tumor evolution. *Cell Genomics* **2**, 100096 (2022).
17. Wang, K., Yin, X. M., Chao, D. T., Millman, C. L. & Korsmeyer, S. J. BID: A novel BH3 domain-only death agonist. *Genes Dev.* **10**, 2859–2869 (1996).
18. Zinkel, S. S., Yin, X. M. & Gross, A. Rejuvenating Bi(d)ology. *Oncogene* **32**, 3213–3219 (2013).

19. Caldarelli, M. *et al.* Pyrazolo-quinazolines. Patent WO 2009156315 A1
20. Pachis, S. T. & Kops, G. J. P. L. Leader of the SAC: Molecular mechanisms of Mps1/TTK regulation in mitosis. *Open Biol.* **8**, 1–10 (2018).
21. Klaasen, S. J. *et al.* Nuclear chromosome locations dictate segregation error frequencies. *Nature* **607**, 604–609 (2022).
22. Gillespie, M. *et al.* The reactome pathway knowledgebase 2022. *Nucleic Acids Res.* **50**, 687–692 (2022).
23. Terhorst, A. *et al.* The environmental stress response causes ribosome loss in aneuploid yeast cells. *Proc. Natl. Acad. Sci.* **117**, 17031–17040 (2020).
24. Sheltzer, J. M. & Amon, A. The Aneuploidy Paradox: Costs and Benefits of an Incorrect Karyotype. *Trends Genet.* **27**, 446–453 (2011).
25. Livet, J. *et al.* Transgenic strategies for combinatorial expression of fluorescent proteins in the nervous system. *Nature* **450**, 56–62 (2007).





# Chapter 5

## High incidence of chromosome mosaicism in inner cell mass and trophectoderm of human blastocysts

E.A. Chavli<sup>1\*</sup>, S.J. Klaasen<sup>4,5\*</sup>, D. van Opstal<sup>2</sup>, G.J.P.L. Kops<sup>4,5, #</sup>, E.B. Baart<sup>1,3, #</sup>

*<sup>1</sup>Division of Reproductive Endocrinology and Infertility, Department of Obstetrics and Gynecology, Erasmus MC, University Medical Center Rotterdam, The Netherlands*

*<sup>2</sup>Department of Clinical Genetics, Erasmus MC, University Medical Center Rotterdam, The Netherlands*

*<sup>3</sup>Department of Developmental Biology, Erasmus MC, University Medical Center Rotterdam, The Netherlands*

*<sup>4</sup>Hubrecht Institute-KNAW (Royal Academy of Arts and Sciences) and University Medical Centre Utrecht, Utrecht, the Netherlands*

*<sup>5</sup>Oncode Institute, Utrecht, the Netherlands*

*\* These authors contributed equally*

*# Joint senior and corresponding authors*

**In preparation**

**Most human zygotes from *in-vitro* fertilization (IVF) do not develop to term. This is primarily due to the frequent occurrence of uniform or mosaic chromosomal aberrations in preimplantation embryos. In an attempt to improve ongoing pregnancy rates, it is common practice for IVF clinics to take a biopsy of a few cells of the trophectoderm (TE) to predict the aneuploidy status of the whole embryo (also known as preimplantation genetic testing for aneuploidy (PGT-A)). It is unclear if PGT-A can properly recognize chromosomal mosaicism and if the TE biopsy is predictive of the karyotype of the inner cell mass (ICM). The frequency of mosaicism is also unclear, because generally analyses are performed only for a few chromosomes, a few cells per embryo and/or using bulk-sequencing methods. Here, we separated the TE and ICM of 55 good quality day 5 human embryos and successfully performed single-cell whole genome DNA sequencing on 1057 cells. This revealed that 87% of embryos contained aneuploid cells and 82% displayed chromosomal mosaicism. Aneuploid cells were observed in the TE as frequently as in the ICM, but cells with complex aneuploidies were more frequent in the TE. Furthermore, *in-silico* bulk-sequencing of the TE showed that PGT-A would not detect 53% of mosaic embryos due to low levels of mosaicism or reciprocal copy number changes. In conclusion, our work shows that mosaicism is widespread in human blastocysts, and that current methods of PGT-A are prone to false-negative outcomes.**

Aneuploidy, a deviation from the normal chromosome copy number, is common in human embryos<sup>1–4</sup>. Chromosomes can be gained or lost as a whole or as segments. In general, aneuploidy is detrimental to the fitness of embryonic cells and therefore is one of the major causes for miscarriages. Chromosomal abnormalities in preimplantation embryos can be the result of two processes: chromosomes can mis-segregate in meiotic divisions during gametogenesis, or during mitotic divisions after fertilization. Meiotic errors give rise to embryos in which all cells will have the same chromosomal abnormality. On the other hand, mitotic errors will lead to chromosomal mosaicism, where only a proportion of cells have a certain abnormality depending on when the mis-segregation event occurred during embryogenesis.

Chromosomal mosaicism may affect up to 91% of cleavage stage embryos<sup>1,2,5–11</sup>. The incidence of both uniform aneuploidy and mosaicism appears to decline as embryo development progresses towards the blastocyst stage<sup>12,13</sup>. This is likely due to selective loss of aneuploid embryos or cells<sup>12,14</sup>. Recent studies of blastocyst biopsies using next-generation sequencing (NGS) approaches revealed a range of mosaicism between 14% and 80%, indicating that a significant proportion of blastocysts contains abnormal cells<sup>4,15–23</sup>. Furthermore, the use of NGS has revealed the presence of segmental abnormalities that range between 2.4% and 15.6% at the blastocyst stage<sup>24–26</sup>.

NGS on a biopsied sample of several cells is thought to be the most sensitive technique to identify chromosomal abnormalities, both numerical and segmental. However, since NGS is performed on bulk DNA, it can only assess net average chromosome gains or losses. This makes it difficult to identify mosaicism when only a small percentage of cells may have a chromosomal abnormality, and it makes distinguishing true mosaicism from technical artefact problematic. As a result, the incidence of chromosomal mosaicism at the blastocyst stage remains a hotly debated issue<sup>27–29</sup>. Although laborious single-cell methods such as FISH can be used to investigate chromosomal mosaicism, comprehensive chromosome screening on a single-cell level for all cells in dozens of embryos requires sequencing-based single-cell methods<sup>30,31</sup>. Two such methods have been used on human embryos, but either with error-prone methods based on single-cell RNA-sequencing or using only a limited number of cells per embryo<sup>30,32</sup>. Comprehensive single-cell chromosome analysis could also reveal important information regarding underlying mechanisms. For instance, it is hypothesized that aneuploid cells in the two embryonic lineages, trophoctoderm (TE) and inner cell mass (ICM), behave differently<sup>33</sup>, leading to retainment and/or enrichment of aneuploid cells in the TE but not the ICM.

To investigate the copy number state for all chromosomes in many cells, we here apply single-cell whole genome sequencing (scKaryo-seq)<sup>34</sup> on individual human blastocysts. The two embryonic lineages of the blastocysts, ICM and TE, were

analyzed separately in order to investigate whether there is an enrichment of chromosomally abnormal cells in one of the lineages. The single cell data also allowed us to distinguish meiotic from mitotic errors and the developmental timing of these events.

## **Results**

### **scKaryo-seq allows for accurate chromosome copy number calling in embryo cells**

Although our scKaryo-seq approach accurately calls copy numbers from flow-sorted samples<sup>34,35</sup>, we wished to ensure that this would also be the case if single cells were deposited in a 384 well plate manually. We therefore first performed scKaryo-seq on manually sorted cells from freeze-thawed cell lines obtained from cultures of amniotic fluid or chorionic villi with known numerical chromosomal abnormalities (45,X, 47,XX,+21, 47,XX,+18, 47,XY,+13) and segmental chromosomal abnormalities of different lengths (a gain of 48Mb (46,XX,der(15)t(1;15)(q32.1;p11)), a gain of 24.5Mb (46,XY,der(9)t(4;9)(q33;p24)) and a loss of 4.2Mb (46,XY,der(13;20)(p10;q10))). Known abnormalities were called in 97-100% of cells, depending on the cell line. On average, 8% of cells had an unexpected extra chromosomal abnormality that was detected only once (Table 1). This could be a technical artefact or biological reality, meaning that some cells may have mis-segregated chromosomes during culture. We thus consider the 8% deviation from expected to be conservative. We conclude that our embryo-customized scKaryo-seq approach allows us to accurately call chromosome copy numbers and segmental chromosomal abnormalities.

### **Most human blastocyst-stage embryos are aneuploid**

For the purposes of this study, we used good quality frozen morula stage embryos of unknown chromosomal content that were donated for research. Fifty-five embryos reached the full blastocyst stage. Embryos were biopsied and disaggregated, and single cells were distributed in 384 well plates with the aim to have all cells of an embryo sequenced (Fig. 1a). The plate was subsequently subjected to the scKaryo-seq protocol. A successful sequencing result of at least 1 cell of each lineage was

obtained from 41 embryos. For 11 embryos only cells from the TE ( $n = 9$ ) or ICM ( $n = 2$ ) were successfully sequenced, and for three embryos TE and ICM were not separated. The mean percentage of successfully analyzed cells per embryo was 42%.

**Table 1: scKaryo-seq copy number calling of cultured amniotic fluid and chorionic villi cells with a known karyotype.**

Karyotype	Karyotyped cells	Cells with known abnormality	Cells with known abnormality + additional abnormalities	Cells with false negative result	Efficiency	Specificity
45,X	81	71	10	0	100%	88%
47,XX,+21	94	87	6	1	99%	93%
47,XX,+18	62	60	2	0	100%	97%
47,XY,+13	34	31	3	0	100%	91%
46,XX,der(15)t(1;15)(q32.1;p11)	21	21	0	0	100%	100%
46,XY,der(9)t(4;9)(q33;p24)	23	20	3	0	100%	87%
46,XY,der(13;20)(p10;q10)	61	55	4	2	97%	90%

Chromosomally abnormal cells were detected in 87% ( $n=48/55$ ) of the analyzed embryos, while 13% (7/55) consisted of only normal cells (Fig. 1b-c, supplemental figure 1). The average number of analyzed cells in fully diploid embryos was significantly lower than the average number analyzed in partially or fully aneuploid embryos (6.6 versus 21.8 cells) (Fig. 1d). The classification into fully diploid embryos may therefore be the result of a sampling error, making it likely that the percentage of fully diploid embryos in our dataset is over-estimated. In 33% of embryos (18/55) only abnormal cells were observed. Half (54%) of the embryos ( $n=30/55$ ) contained

both normal and abnormal cells. Substantial variability was observed in the proportion of abnormal cells, where 22 out of 30 embryos contained more normal than abnormal cells (Fig. 1e). Given these data, we conclude that in the vast majority of human embryos aneuploid cells are present.

### **Mitotic errors are a larger source of aneuploidy than meiotic errors**

Aneuploidy arises due to meiotic segregation errors during gametogenesis or due to mitotic errors during post-fertilization cleavage divisions. In order to estimate the frequency of both types of errors, we quantified the occurrences of uniform aneuploidies (present in all cells: evidence for a meiotic segregation error) and the occurrences of sub-clonal aneuploidies (defined by at least two cells with a different karyotype within an embryo: evidence for a mitotic segregation error). Chromosomal mosaicism was observed in 94% (46/49) of embryos indicating post-zygotic chromosome segregation errors (Fig. 1f). 63% (31/49) of aneuploid embryos contained both normal and abnormal cells.

37% (18/49) of embryos were fully abnormal. Meiotic errors were observed in 83% (15/18) of those embryos. Some cells also contained non-uniform abnormalities that most probably were of mitotic origin, showing that aneuploidies of both meiotic and mitotic origins co-existed in the same embryo. The remaining three embryos were mosaic for the sex chromosomes, contained polyploid cells and cells with different abnormalities that arose postzygotically. In conclusion, although meiotic segregation errors are not uncommon, the aneuploidies we observed mostly originated from segregation errors during mitosis.

### **TE contains a similar proportion of aneuploid cells but of more complex karyotypes than ICM**

Previous reports suggested aneuploid cells are more prevalent in the TE compared to the ICM, because aneuploid cells are either pushed towards the TE or because aneuploidies are actively eliminated from the ICM<sup>33,36</sup>. This has implications for preimplantation genetic testing of aneuploidy (PGT-A), because multiple cells are frequently biopsied and sequenced in bulk only from the TE to infer the aneuploidy

status of the whole embryo. To see if the TE indeed contains more aneuploid cells than the ICM, we quantified the number of aneuploid cells in the TE versus the ICM and found that the proportion was comparable (Fig. 2a). We next quantified the

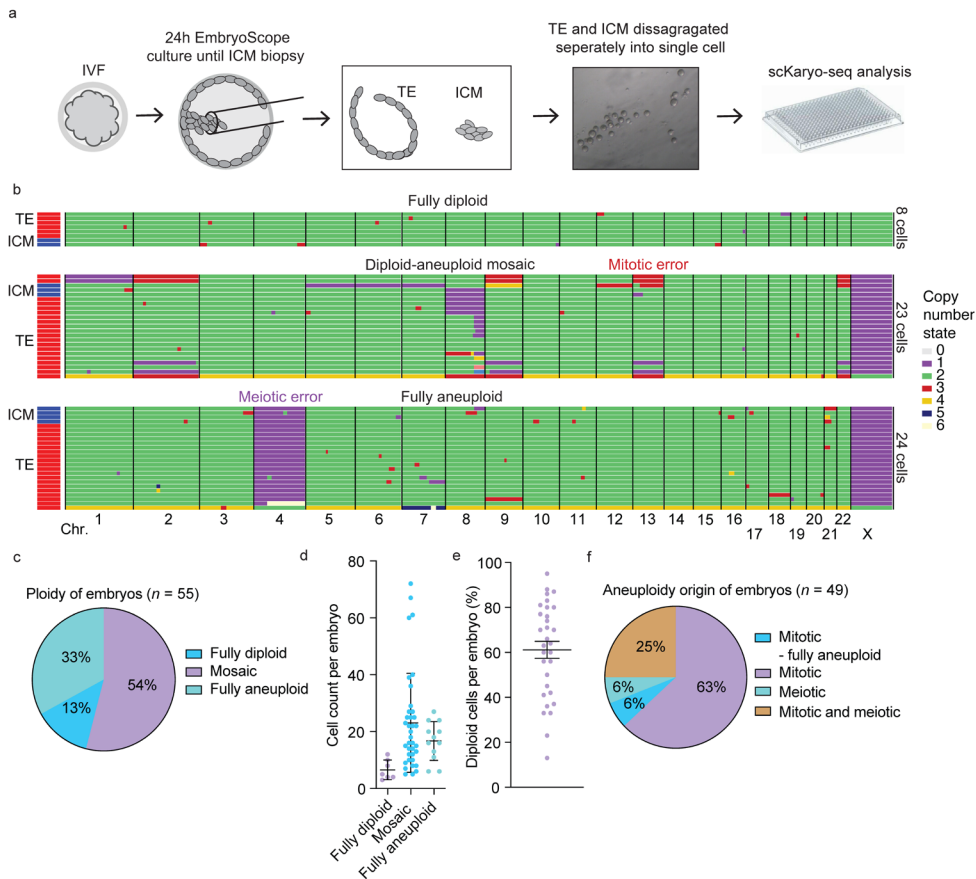


**Figure 1: Aneuploidy is pervasive in human embryos.** **a.** Schematic depicting the procedure by which embryo cells were prepared for scKaryo-seq. **b.** Examples of scKaryo-seq of three embryos, which were either fully diploid (top), mosaic aneuploid (middle) or fully aneuploid (bottom). Every row represents a single cell and every column is a different chromosome. The colors portray copy number states. Colors on the left depict if cells came from the TE (red) or ICM (blue). **c.** Pie chart of the percentage of aneuploid and diploid embryos. **d.** Number of successfully sequenced cells per embryo split based on their karyotype (mean  $\pm$  s.e.m.,  $n = 7$ ,  $n = 36$   $n = 12$ , respectively). **e.** Percentage of diploid cells per embryo of mosaic embryos only (mean  $\pm$  s.e.m.). **f.** Pie chart of the percentage of embryos which are fully mosaic aneuploid due to mitotic errors (light blue,  $n = 3$ ), mosaic aneuploid due to mitotic errors (lilac,  $n = 30$ ), fully aneuploid due to a meiotic error (green,  $n = 3$ ) or have meiotic and mitotic errors (brown,  $n = 12$ ).

number of complex aneuploidies of all cells together in both lineages and found that these were much more common in the TE than the ICM (Fig. 2b). Next, we checked if the TE is a good predictor of aneuploidy in the ICM. All 12 fully aneuploid TE samples were also fully aneuploid in the ICM (see red dots in Fig. 2a), while 5 of 6 fully diploid TE were fully diploid in the ICM (see green dots in Fig. 2a). The discrepancy was probably due to a low number of successfully sequenced cells in this particular embryo ( $n = 2$  and  $n = 4$  for TE and ICM, respectively), keeping open the possibility that the TE may in fact have been mosaic if more cells were sequenced. Mosaic TE samples less frequently properly predicted the presence of aneuploid cells in corresponding ICM; 52% (12/23) of TE mosaic samples were mosaic in the ICM as well, while another 17% (4/23) of TE mosaic samples were fully aneuploid in the ICM. 31% (7/23) of TE mosaic samples were fully diploid in the ICM. This discrepancy may however reflect a sampling issue, as more TE cells per embryo were successfully sequenced than ICM cells (Fig. 2c). In conclusion, TE cells have more copy number aberrations per cell and the karyotype of the TE may be a sub-par predictor of the aneuploidy status of the ICM.

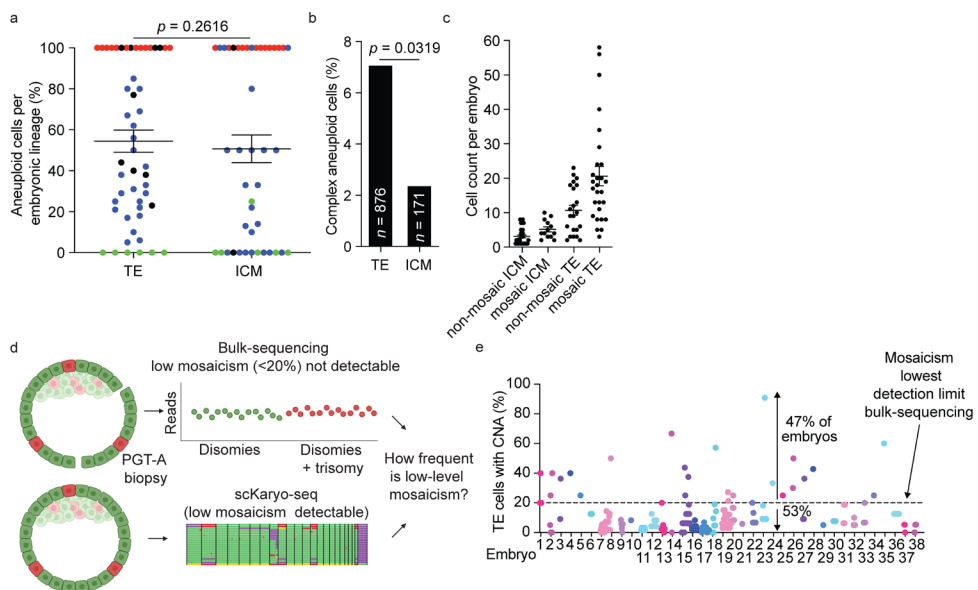


**Figure 2: High occurrence of low-level mosaicism in TE.** **a.** Percentage of aneuploid cells in TE versus ICM per embryo (mean  $\pm$  s.e.m., two-tailed Fisher's exact test,  $n = 812$  (left)  $n = 160$  cells (right)). **b.** Mean percentage of complex aneuploid cells in TE versus ICM. Complex cells have more than 4 copy number



aberrations. **c.** Cell count per embryo of a fully diploid or aneuploid ICM (left), mosaic ICM (second to left), fully diploid or aneuploid TE (third to left) and mosaic TE (right) (mean  $\pm$  s.e.m.). **d.** Schematic depicting experimental approach to determine how frequently bulk-sequencing underestimates mosaicism. **e.** *In-silico* bulk-sequencing of TE cells containing a certain copy number change. Horizontal line at 20% mark detection limit of bulk-sequencing.

### ***In-silico* bulk-sequencing underestimates TE mosaicism**

PGT-A is routinely performed on a biopsy of 5-10 cells, using bulk-DNA sequencing<sup>37</sup>. Copy number aberrations present in only one or a few cells or reciprocal events will therefore go undetected. Consequently, we wondered how often bulk-sequencing may not be able to identify mosaicism. To answer this question, we performed '*in-silico* bulk-sequencing' based on our single-cell data: we quantified the percentage of cells per TE with a copy number change of the same chromosome and corrected for reciprocal events. We then quantified the number of mosaic embryos in which specific copy number aberrations were present in at least 20% of TE cells, as a cut-off of what PGT-A methods are expected to detect (Fig 2d)<sup>14</sup>. Surprisingly, our analysis predicted that only around 11% (24/226) of mosaic copy number changes will be picked up by bulk-sequencing, and that only 47% (17/36) of mosaic embryos will be recognized as such (Fig. 2e). Taken together, we found that the majority of copy number changes are rare or reciprocal, which means they are likely to go undetected by bulk-sequencing approaches.

### **Chromosome losses are more common than gains**

Trisomies constitute the majority of constitutional aneuploidies compatible with live births, implying that chromosomal gains are better tolerated in an embryo than losses. We therefore compared the number of whole or segmental chromosome gains versus losses. To our surprise, chromosome losses were more common than chromosome gains when abnormalities originated from mitotic segregation errors, whether they were numerical or segmental (Fig. 3a). Segmental abnormalities were more abundant than numerical ones. Furthermore, we observed no segmental aneuploidies from a meiotic origin (0/16 meiotic aneuploidies) (Fig. 3b). Taken together, although chromosome gains are more prevalent in live births, they are less prevalent than chromosome losses in blastocysts.

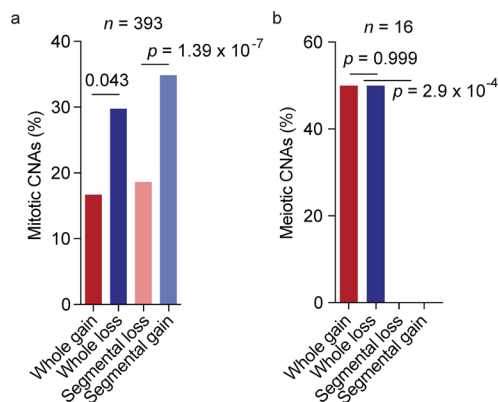


**Figure 3: Types of chromosome aberrations of mitotic or meiotic origin.** **a.** Mean percentage of numerical or segmental copy number aberrations of mitotic origin (Two-tailed Fisher's exact test). **b.** Mean percentage of numerical or segmental copy number aberrations of meiotic origin (Two-tailed Fisher's exact test). Copy number changes of meiotic origin were counted per embryo and not as in **a**) per copy number change.

### Chromosome-specific differences in aneuploidy frequencies

Next, we wanted to examine whether there are chromosome-specific differences in aneuploidy frequencies. This may indicate whether certain chromosomes are either more prone to mis-segregate or are more compatible with development than others. We compiled aneuploidies if they originated from the same mis-segregation event and split them based on mis-segregation origin (Fig. 4a). This revealed copy number variation can occur for all chromosomes in blastocysts. The frequency of being involved in an abnormality was comparable for most chromosomes. Chromosome 9, 12 and 21 were the exception as they were more (9, 21) or less (12) frequently affected. Meiotic errors seemed to impact chromosome 22 (and 4?) relatively frequently. There were also chromosome-specific differences in mitotic whole and segmental gains and losses (Fig. 4b). Numerical abnormalities anti-correlated significantly with the number of genes per chromosome (Fig. 4c), as predicted if proteotoxic stress from unbalanced protein production impacts cell fitness<sup>38,39</sup>. Together, our data show that although all chromosomes can be involved in CNA, some chromosomes are more likely to be involved in human embryos.

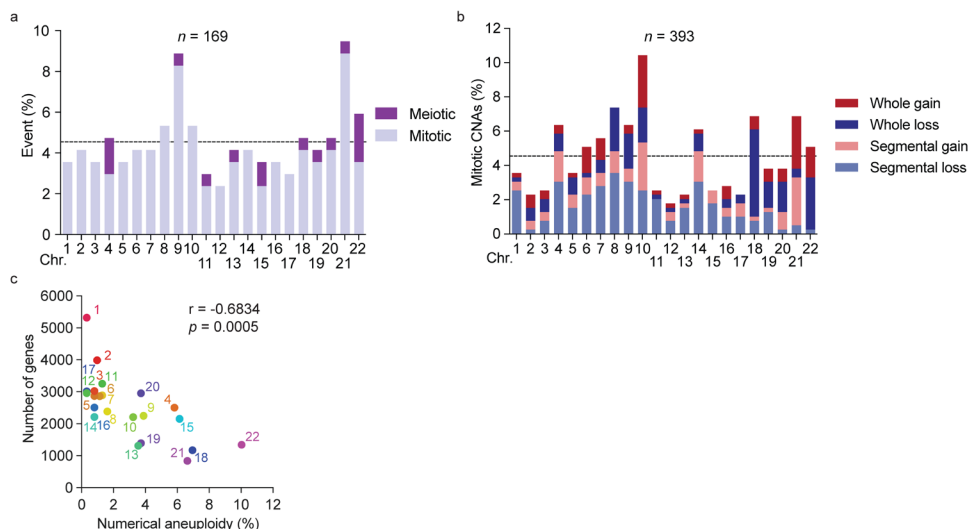


**Figure 4: Chromosome-specific aneuploidy differences.** **a.** Graph shows the mean percentage of aneuploidy per chromosome based on the origin of the mis-segregation event (meiotic or mitotic). Horizontal line depicts expected chance to find an aneuploidy ( $1/22=4.54\%$ ). **b.** Mean percentage of total mitotic aneuploidies. Colors represent type of change (numerical or segmental gain/loss). **c.** Graph comparing the mean percentage of total numerical aneuploidies and the number of genes per chromosome (Pearson's correlation coefficient).

### Chromosome mis-segregations occur both before and after cell lineage specification

The first few embryonic divisions are rather error-prone<sup>1,2,5–11</sup>. To estimate if mis-segregations mostly originate before or after embryonic lineage specification, we examined common and unique aneuploidies in TE and ICM. In 51% (18/35) of embryos cells from both embryonic lineages had at least one chromosome abnormality in common indicating that the mitotic error took place before cell lineage specification (Fig. 5a-b). This type of abnormality represented 22% (19/87) of all mitotic abnormalities we counted. The remaining 49% (16/35) of embryos did not have common abnormalities in the two lineages and, together with the unique abnormalities in the other embryos, make up for 78% (68/87) of all mitotic abnormalities. It should be noted that, since we were not able to sequence every cell of the embryos, our analysis is likely incomplete.

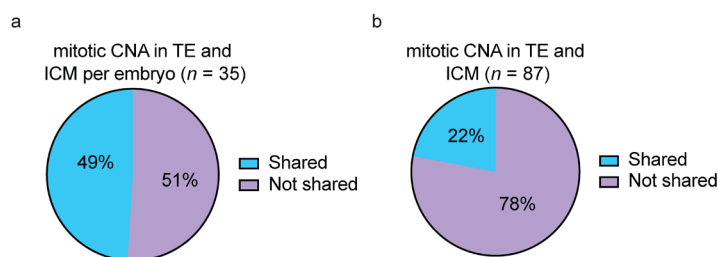


**Figure 5: Chromosome segregation errors occur before and after lineage specification. a.** Percentage of embryos that share a CNA in the TE and ICM (light blue) or do not share (lilac). **b.** Percentage of CNAs that can be found in both lineages (light blue) or not (lilac).

## Discussion

In this study, we investigated the chromosomal constitution of good quality blastocysts on a single-cell level. We observed a high incidence of chromosomal abnormalities, affecting 87% of blastocysts. The majority of these embryos (94%) displayed chromosomal mosaicism (68%) or had meiotic errors (32%). Only 13% of embryos were fully diploid, which is probably an over-estimation since fewer cells in these embryos were successfully sequenced. Future research should aim to improve the success rate of isolating and sequencing single cells from embryos in order to get an even better understanding of its aneuploidy levels. For that same reason, other studies investigating chromosomal abnormalities on single cells of individual embryos are scarce<sup>27</sup>. Previously, using FISH to investigate the chromosomal composition of individual cells in blastocysts, others showed 45-81% of mosaicism after analysis of a limited number of chromosomes<sup>1,13,40</sup>. This was corroborated by a study using a novel method based on chromosome dosage-induced changes in gene expression after reanalysis of single-cell RNA sequencing data (74% of embryos are mosaic)<sup>30</sup>. Moreover, single-cell DNA sequencing in blastocysts that had previously undergone PGT-A revealed 66% of mosaicism<sup>32</sup>. However, because these studies used either a limited number of cells per embryo, assessed a limited number of chromosomes, or used insufficiently validated copy-number calling methods, the conclusion that mosaicism was prevalent in human embryos was questioned. Our validated comprehensive chromosome screening

now lends strong support to these previously reported high incidences of chromosomal abnormalities in human blastocysts.

Our *in-silico* bulk-sequencing analysis showed that the majority (89%) of mosaic copy number aberrations in the TE will not be detected by next-generation bulk-sequencing methods. Since embryos are mosaic for multiple different abnormalities, this means that in the end 63% of mosaic TE biopsies will not be recognized as such. Bulk-sequencing of TE biopsies report a level of mosaicism of 2-19%<sup>27</sup>, suggesting that the level of mosaicism is indeed vastly underestimated in PGT-A. How this underestimation affects implantation rates and successful pregnancy outcomes is unknown. Mosaic embryos have a reduced implantation rate compared to diploid embryos, but they can still result in successful pregnancy outcomes<sup>41</sup>. Furthermore, adding a low percentage (25%) of diploid mouse blastomeres to fully aneuploid ones partially rescued embryo viability, while combining them 1/1 fully restores viability<sup>33</sup>. Low levels of aneuploidy are therefore probably well tolerated in the embryo. However, it is important to note that even diploid embryos after PGT-A do not show 100% implantation rate. Future studies combining PGT-A and single-cell sequencing techniques will reveal how relevant low levels of mosaic aneuploidy is for successful pregnancy outcomes.

We show that chromosome losses were significantly more frequent than gains. An analysis on a large dataset from TE biopsies analyzed with SNParray also found more numerical losses than gains<sup>12</sup>. It is unclear what causes this difference. One possibility is that mis-segregating chromosomes end up in micronuclei, which are common during human embryogenesis<sup>42</sup>. The nuclear membrane of micronuclei can rupture, leading to DNA underreplication and chromosome shattering and consequently loss of parts or whole chromosomes<sup>43,44</sup>. Another possibility is that chromosomes are unequally distributed in multiple cells by multipolar divisions, a process frequently observed in IVF embryos<sup>45-47</sup>. This will lead to a net loss of chromosomes. Finally, chromosome gains may have a proliferative disadvantage over losses. This would be surprising, because chromosomal gains are generally better tolerated than losses (also see **Chapter 4**) and later in pregnancy only gains

are observed (with the exception of monosomy X). Chromosome losses are however frequently observed in polyploid cells<sup>48</sup>, so perhaps the preference for losses stems from these cells. A change in gene dosage, which is what leads to most of the decrease in fitness in aneuploid cells, is more severe when chromosomes are lost. In line with this, we observed a significant association between the number of genes per chromosome and the CNA frequency in blastocysts.

Studies on multicellular TE biopsies have reported a range of segmental abnormalities between 2.4% and 31%<sup>24–26,49</sup>. We observed a higher incidence of segmental abnormalities of mitotic origin (62% of embryos). The limited number of cells with a common affected segment demonstrates their mitotic origin as previously described<sup>26</sup>. The high incidence of segmental abnormalities in our cohort of embryos could indicate that the segmental abnormalities observed in later developmental stages are likely to have originated during the preimplantation period<sup>50,51</sup>.

Why segmental aneuploidies are only of mitotic and not meiotic origin is unclear. We hypothesize that this discrepancy is either explained by the mechanism by which chromosomes mis-segregate or by a selection process. For example, meiotic segregation errors are often the result of crossover maturation failure or loss of cohesin<sup>52–54</sup>, which perhaps mostly leads to mis-segregations of whole chromosomes. On the other hand, DNA replication stress causes mitotic mis-segregations, increasing the chances of segmental abnormalities<sup>55</sup>. Furthermore, segmental aneuploidies could also be tolerated less efficiently when they originate from a meiotic error. A segmental aneuploidy likely is the result of a double-strand break on at least one end of the DNA during its creation, raising the possibility this triggers a developmental arrest in zygotes versus later-stage embryos.

In conclusion, we show that mosaicism is observed in almost all day 5 human blastocysts. In the clinic, this means PGT-A will misidentify around half of mosaic embryos as diploid. It is currently unclear what this means for successful pregnancy outcomes and aneuploidy live births after IVF. Future research should aim at elucidating the consequences of (low-level) mosaicism.

## **Methods**

### **Ethical approval**

Surplus cryopreserved human preimplantation embryos of unknown chromosomal constitution were donated with written consent from patients that underwent an IVF treatment at the Erasmus MC, University Medical Center Rotterdam. The use of these embryos for this study was approved by the Dutch Central Committee on Research Involving Human Subjects (CCMO, NL 38053.000.111) and the local institutional ethics committee.

### **Embryo warming and culture**

Ovarian stimulation, oocyte retrieval, IVF procedures, assessment of embryo morphology and cryopreservation were performed as described<sup>56</sup>. The supernumerary good-quality embryos that were donated to research were cryopreserved at the morula stage between 2013 and 2015. These embryos were thawed and cultured in the EmbryoScope™ time-lapse incubator (Vitrolife, Göteborg, Sweden) until the blastocyst stage as previously described<sup>4</sup>. The blastocysts were morphologically evaluated according to the ESHRE consensus scoring system<sup>57</sup>. Only embryos that managed to reach the full blastocyst stage and had enough TE cells to form at least a loose epithelium were used (Grade 3BB and higher).

### **Disaggregation of ICM and TE cells of human IVF embryos at the blastocyst stage**

Before embryo disaggregation, the ICM was dissociated from the TE. The aspiration of the ICM was achieved as previously described with the assistance of a biopsy pipette (type MBB-FP-SM-30, Cooper Surgical, Trumbull, CT, USA), a holding pipette (type MPH-MED-30, Cooper Surgical) and an OCTAX laser system (Vitrolife)<sup>4</sup>. After the collection of the ICM, the TE was removed from the zona pellucida with the use of the OCTAX laser system. For the disaggregation of the cells, the ICM and TE were placed in separate droplets of accutase for 10 min on 37°C. Remaining clusters of cells were disaggregated mechanically with the assistance of the biopsy pipette. The single cells of ICM and TE were placed

manually with a 170  $\mu\text{m}$  stripper tip (Cooper surgical) in a 384 well plate filled with oil at room temperature<sup>34</sup>. The 384 well plate was placed on ice between transfers. Before storage at -20 °C, the plate was centrifuged at 2000g for 1 min.

### **scKaryo-seq**

scKaryo-seq was performed as described previously with a few modifications<sup>34</sup>. To every 1  $\mu\text{l}$  of PBS in a 384 well plate, we added 200 nl of lysis buffer (6x Cutsmart (New England Biolabs) and 1.8  $\mu\text{g}$  Proteinase K (Fisher Scientific)). This was incubated for 2 h at 55 °C and heat inactivated for 10 min at 80 °C. Genomic DNA was digested using 100 nl of digestion mix (1x CutSmart and 0.1 U of NlaIII (New England Biolabs)) at 37 °C for 2 h and 80 °C for 20 min. 100 nl of 500 nM NlaIII-specific adapters were dispensed in each well followed by 400  $\mu\text{l}$  of an adapter ligation mix (1x ligase buffer (New England Biolabs), 3.33 mM ATP (New England Biolabs) and 4000 U of T4 DNA ligase (New England Biolabs)). The rest of the protocol was performed as described previously<sup>34</sup>.

### **Quality control and interpretation of scKaryo-seq results**

Copy number analysis and quality control was performed with AneuFinder software<sup>58</sup>. scKaryo-seq of lymphocytes from healthy donors and BJ-hTERT cells were used as a diploid reference to determine variable bin sizes. Copy numbers were called using the edivisive algorithm. Cells were included in the analysis if they had a minimum total read count of 15,000, a maximum spikiness score of 0.25 and a minimum Bhattacharyya score of 0.65. Copy number aberrations in cells that did not pass quality control were included when the abnormality was present in a cell which passed quality control and when copy number calling looked decent. Chromosomal abnormalities that were present only once within an embryo were considered true only when the cell had passed the quality control. An embryo was considered mosaic when at least two cells with a different karyotype were present. Furthermore, according to the proportion of abnormal cells in which a specific chromosome was involved, we made a distinction between meiotic and mitotic errors. A chromosomal abnormality observed in every cell within an embryo was considered the result of a meiotic error, whereas the origin of an abnormality



observed in part of the cells was considered mitotic. Cells with more than four chromosomal abnormalities were considered complex. *In-silico* bulk-sequencing was performed manually by determining the percentage of cells having a certain copy number aberration. We corrected for reciprocal copy number changes by not including them when they were present.

## References

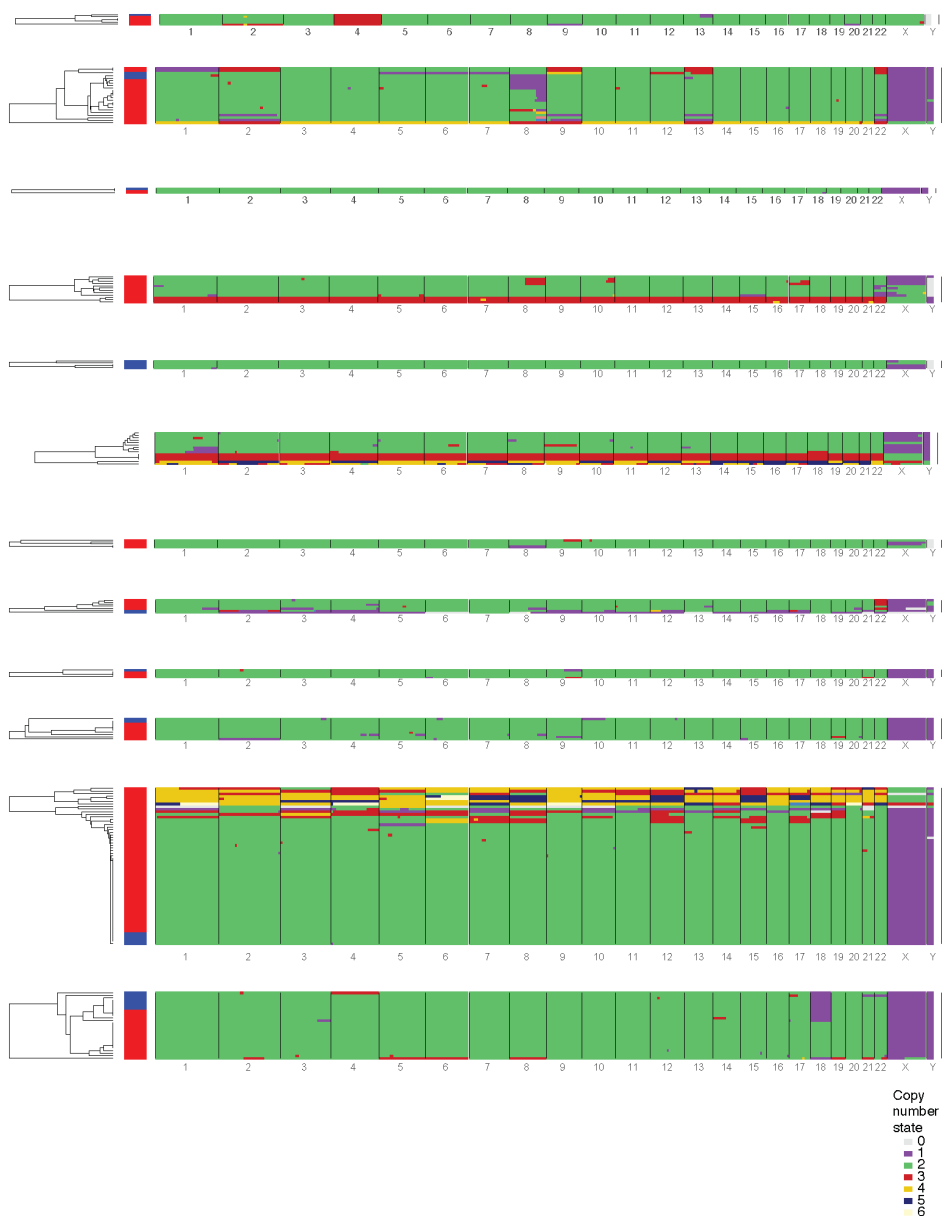
1. Baart, E. B. *et al.* Preimplantation genetic screening reveals a high incidence of aneuploidy and mosaicism in embryos from young women undergoing IVF. *Hum. Reprod.* **21**, 223–233 (2006).
2. Vanneste, E. *et al.* Chromosome instability is common in human cleavage-stage embryos. *Nat. Med.* **15**, 577–583 (2009).
3. Fragouli, E. *et al.* The origin and impact of embryonic aneuploidy. *Hum. Genet.* **132**, 1001–1013 (2013).
4. Chavli, E. *et al.* Chromosomal mosaicism in human blastocysts: a cytogenetic comparison of trophectoderm and inner cell mass after next-generation sequencing. *Reprod. Biomed. Online* **00**, 1–11 (2022).
5. Baart, E. B., Van Opstal, D., Los, F. J., Fauser, B. C. J. M. & Martini, E. Fluorescence in situ hybridization analysis of two blastomeres from day 3 frozen-thawed embryos followed by analysis of the remaining embryo on day 5. *Hum. Reprod.* **19**, 685–693 (2004).
6. Bielanska, M., Tan, S. L. & Ao, A. Chromosomal mosaicism throughout human preimplantation development in vitro: Incidence, type, and relevance to embryo outcome. *Hum. Reprod.* **17**, 413–419 (2002).
7. Chow, J. F. C. *et al.* Array comparative genomic hybridization analyses of all blastomeres of a cohort of embryos from young IVF patients revealed significant contribution of mitotic errors to embryo mosaicism at the cleavage stage. *Reprod. Biol. Endocrinol.* **12**, 1–10 (2014).
8. Mantzouratou, A. *et al.* Variable aneuploidy mechanisms in embryos from couples with poor reproductive histories undergoing preimplantation genetic screening. *Hum. Reprod.* **22**, 1844–1853 (2007).
9. Mertzaniidou, A., Spits, C., Nguyen, H. T., Van De Velde, H. & Sermon, K. Evolution of aneuploidy up to Day 4 of human preimplantation development. *Hum. Reprod.* **28**, 1716–1724 (2013).
10. Voullaire, L., Slater, H., Williamson, R. & Wilton, L. Chromosome analysis of blastomeres from human embryos by using comparative genomic hybridization. *Hum. Genet.* **106**, 210–217 (2000).
11. Wells, D. & Delhanty, J. D. A. Comprehensive chromosomal analysis of human preimplantation embryos using whole genome amplification and

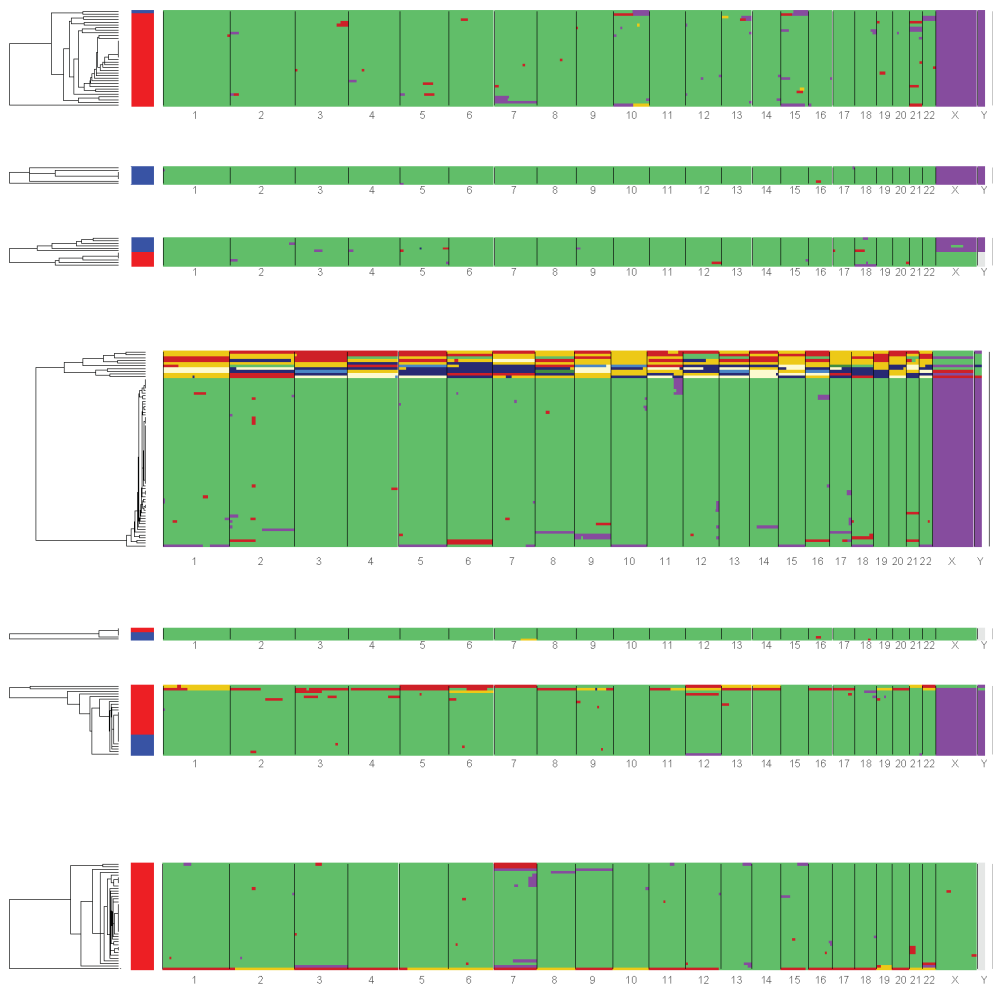
- single cell comparative genomic hybridization. *Mol. Hum. Reprod.* **6**, 1055–1062 (2000).
12. McCoy, R. C. *et al.* Evidence of Selection against Complex Mitotic-Origin Aneuploidy during Preimplantation Development. *PLoS Genet.* **11**, 1–31 (2015).
  13. Santos, M. A. *et al.* The fate of the mosaic embryo: Chromosomal constitution and development of Day 4, 5 and 8 human embryos. *Hum. Reprod.* **25**, 1916–1926 (2010).
  14. Fragouli, E., Munne, S. & Wells, D. The cytogenetic constitution of human blastocysts: Insights from comprehensive chromosome screening strategies. *Hum. Reprod. Update* **25**, 15–33 (2019).
  15. Chuang, T. H. *et al.* Concordance between different trophectoderm biopsy sites and the inner cell mass of chromosomal composition measured with a next-generation sequencing platform. *Mol. Hum. Reprod.* **24**, 593–601 (2018).
  16. Huang, J., Yan, L., Lu, S., Zhao, N. & Qiao, J. Re-analysis of aneuploidy blastocysts with an inner cell mass and different regional trophectoderm cells. *J. Assist. Reprod. Genet.* **34**, 487–493 (2017).
  17. Lawrenz, B. *et al.* The clinicians' dilemma with mosaicism - an insight from inner cell mass biopsies. *Hum. Reprod.* **34**, 998–1010 (2019).
  18. Lin, P. Y. *et al.* Clinical outcomes of single mosaic embryo transfer: High-level or low-level mosaic embryo, does it matter? *J. Clin. Med.* **9**, 1–11 (2020).
  19. Orvieto, R. Preimplantation genetic screening- the required RCT that has not yet been carried out. *Reprod. Biol. Endocrinol.* **14**, 14–17 (2016).
  20. Popovic, M. *et al.* Chromosomal mosaicism in human blastocysts: The ultimate challenge of preimplantation genetic testing? *Hum. Reprod.* **33**, 1–13 (2018).
  21. Sachdev, N. M., McCulloh, D. H., Kramer, Y., Keefe, D. & Grifo, J. A. The Reproducibility of Trophectoderm Biopsies in Euploid, Aneuploid, and Mosaic Embryos Using Independently Verified Next-Generation Sequencing (NGS): A Pilot Study. *J. Assist. Reprod. Genet.* **37**, 559–571 (2020).
  22. Tšuiiko, O. *et al.* Karyotype of the blastocoel fluid demonstrates low concordance with both trophectoderm and inner cell mass. *Fertil. Steril.* **109**, 1127–1134 (2018).
  23. Victor, A. R. *et al.* One hundred mosaic embryos transferred prospectively in a single clinic: exploring when and why they result in healthy pregnancies. *Fertil. Steril.* **111**, 280–293 (2019).
  24. Babariya, D., Fragouli, E., Alfarawati, S., Spath, K. & Wells, D. The incidence and origin of segmental aneuploidy in human oocytes and

- preimplantation embryos. *Hum. Reprod.* **32**, 2549–2560 (2017).
25. Escribà, M. J., Vendrell, X. & Peinado, V. Segmental aneuploidy in human blastocysts: a qualitative and quantitative overview. *Reprod. Biol. Endocrinol.* **17**, 1–15 (2019).
  26. Girardi, L. *et al.* Incidence, Origin, and Predictive Model for the Detection and Clinical Management of Segmental Aneuploidies in Human Embryos. *Am. J. Hum. Genet.* **106**, 525–534 (2020).
  27. Popovic, M., Dhaenens, L., Boel, A., Menten, B. & Heindryckx, B. Chromosomal mosaicism in human blastocysts: The ultimate diagnostic dilemma. *Hum. Reprod. Update* **26**, 313–334 (2020).
  28. Capalbo, A. *et al.* Abnormally fertilized oocytes can result in healthy live births: improved genetic technologies for preimplantation genetic testing can be used to rescue viable embryos in in vitro fertilization cycles. *Fertil. Steril.* **108**, 1007–1015 (2017).
  29. Marin, D., Xu, J. & Treff, N. R. Preimplantation genetic testing for aneuploidy: A review of published blastocyst reanalysis concordance data. *Prenat. Diagn.* **41**, 545–553 (2020).
  30. Starostik, M. R., Sosina, O. A. & McCoy, R. C. Single-cell analysis of human embryos reveals diverse patterns of aneuploidy and mosaicism. *Genome Res.* **30**, 814–826 (2020).
  31. Vera-Rodriguez, M., Chavez, S. L., Rubio, C., Reijo Pera, R. A. & Simon, C. Prediction model for aneuploidy in early human embryo development revealed by single-cell analysis. *Nat. Commun.* **6**, (2015).
  32. Ren, Y. *et al.* Regional and developmental characteristics of human embryo mosaicism revealed by single cell sequencing. *PLoS Genet.* **18**, 1–15 (2022).
  33. Bolton, H. *et al.* Mouse model of chromosome mosaicism reveals lineage-specific depletion of aneuploid cells and normal developmental potential. *Nat. Commun.* **7**, 1–12 (2016).
  34. Klaasen, S. J. *et al.* Nuclear chromosome locations dictate segregation error frequencies. *Nature* **607**, 604–609 (2022).
  35. Bolhaqueiro, A. C. F. *et al.* Ongoing chromosomal instability and karyotype evolution in human colorectal cancer organoids. *Nat. Genet.* **51**, 824–834 (2019).
  36. Mantikou, E., Wong, K. M., Repping, S. & Mastenbroek, S. Molecular origin of mitotic aneuploidies in preimplantation embryos. *Biochim. Biophys. Acta - Mol. Basis Dis.* **1822**, 1921–1930 (2012).
  37. Takahashi, S., Johnston, J. & Patrizio, P. Lessons from the premature adoption of preimplantation embryo testing. *Genet. Med.* **21**, 1038–1040 (2019).
  38. Torres, E. M. *et al.* Effects of aneuploidy on cellular physiology and cell

- division in haploid yeast. *Science* **317**, 916–924 (2007).
39. Williams, B. R. *et al.* Aneuploidy Affects Proliferation and Spontaneous Immortalization in Mammalian Cells. *Science* **322**, 703–710 (2008).
  40. Baart, E. B. *et al.* FISH analysis of 15 chromosomes in human day 4 and 5 preimplantation embryos: the added value of extended aneuploidy detection. *Prenat. Diagn.* **27**, 55–63 (2007).
  41. Vázquez-Diez, C. & Fitzharris, G. Causes and consequences of chromosome segregation error in preimplantation embryos. *Reproduction* **155**, 63–76 (2018).
  42. Kort, D. H. *et al.* Human embryos commonly form abnormal nuclei during development: A mechanism of DNA damage, embryonic aneuploidy, and developmental arrest. *Hum. Reprod.* **31**, 312–323 (2016).
  43. Crasta, K. *et al.* DNA breaks and chromosome pulverization from errors in mitosis. *Nature* **482**, 53–58 (2012).
  44. Zhang, C. Z. *et al.* Chromothripsis from DNA damage in micronuclei. *Nature* **522**, 179–184 (2015).
  45. Ottolini, C. S. *et al.* Tripolar mitosis and partitioning of the genome arrests human preimplantation development in vitro. *Sci. Rep.* **7**, 1–10 (2017).
  46. Zhan, Q., Ye, Z., Clarke, R., Rosenwaks, Z. & Zaninovic, N. Direct unequal cleavages: Embryo developmental competence, genetic constitution and clinical outcome. *PLoS One* **11**, 1–19 (2016).
  47. Chatzimeletiou, K., Morrison, E. E., Prapas, N., Prapas, Y. & Handyside, A. H. Spindle abnormalities in normally developing and arrested human preimplantation embryos in vitro identified by confocal laser scanning microscopy. *Hum. Reprod.* **20**, 672–682 (2005).
  48. Laughney, A. M., Elizalde, S., Genovese, G. & Bakhoum, S. F. Dynamics of Tumor Heterogeneity Derived from Clonal Karyotypic Evolution. *Cell Rep.* **12**, 809–820 (2015).
  49. Kubicek, D. *et al.* Incidence and origin of meiotic whole and segmental chromosomal aneuploidies detected by karyomapping. *Reprod. Biomed. Online* **38**, 330–339 (2019).
  50. Srebniak, M. I. *et al.* Frequency of submicroscopic chromosomal aberrations in pregnancies without increased risk for structural chromosomal aberrations: systematic review and meta-analysis. *Ultrasound Obstet. Gynecol.* **51**, 445–452 (2018).
  51. Benn, P. & Grati, F. R. Genome-wide non-invasive prenatal screening for all cytogenetically visible imbalances. *Ultrasound Obstet. Gynecol.* **51**, 429–433 (2018).
  52. Wang, S. *et al.* Inefficient Crossover Maturation Underlies Elevated Aneuploidy in Human Female Meiosis. *Cell* **168**, 977–989 (2017).
  53. Gruhn, J. R. *et al.* Chromosome errors in human eggs shape natural fertility

- over reproductive life span. *Science* **365**, 1466–1469 (2019).
54. Webster, A. & Schuh, M. Mechanisms of Aneuploidy in Human Eggs. *Trends Cell Biol.* **27**, 55–68 (2017).
  55. Palmerola, K. L. *et al.* Replication stress impairs chromosome segregation and preimplantation development in human embryos. *Cell* **185**, 2988–3007 (2022).
  56. Hohmann, F. P., Macklon, N. S. & Fauser, B. C. J. M. A randomized comparison of two ovarian stimulation protocols with gonadotropin-releasing hormone (GnRH) antagonist cotreatment for in Vitro fertilization commencing recombinant follicle-stimulating hormone on cycle day 2 or 5 with the standard long GnRH a. *J. Clin. Endocrinol. Metab.* **88**, 166–173 (2003).
  57. Embryology, A. S. in R. M. and E. S. I. G. of. The Istanbul consensus workshop on embryo assessment: Proceedings of an expert meeting. *Hum. Reprod.* **26**, 1270–1283 (2011).
  58. Bakker, B. *et al.* Single-cell sequencing reveals karyotype heterogeneity in murine and human malignancies. *Genome Biol.* **17**, 115 (2016).

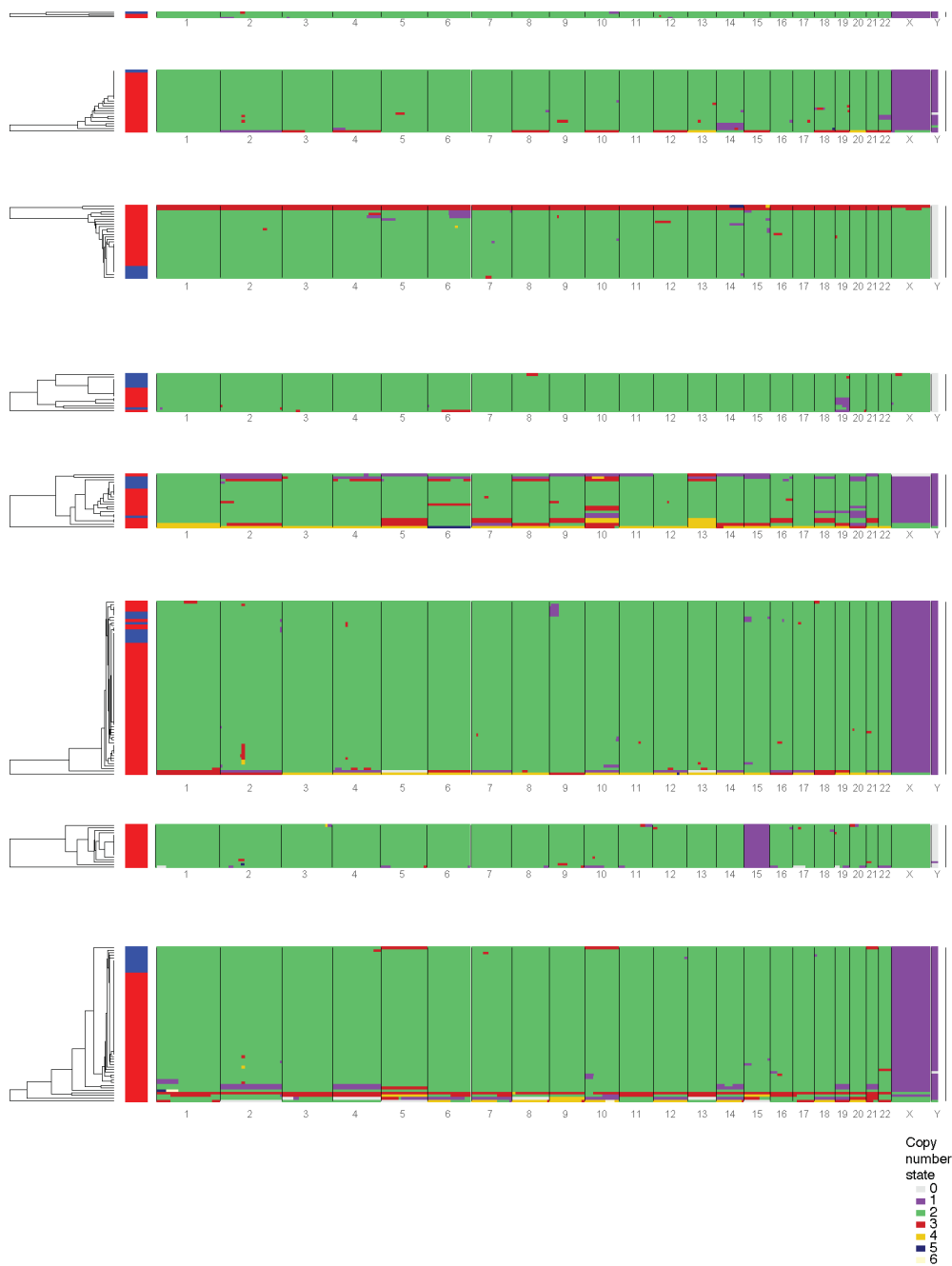




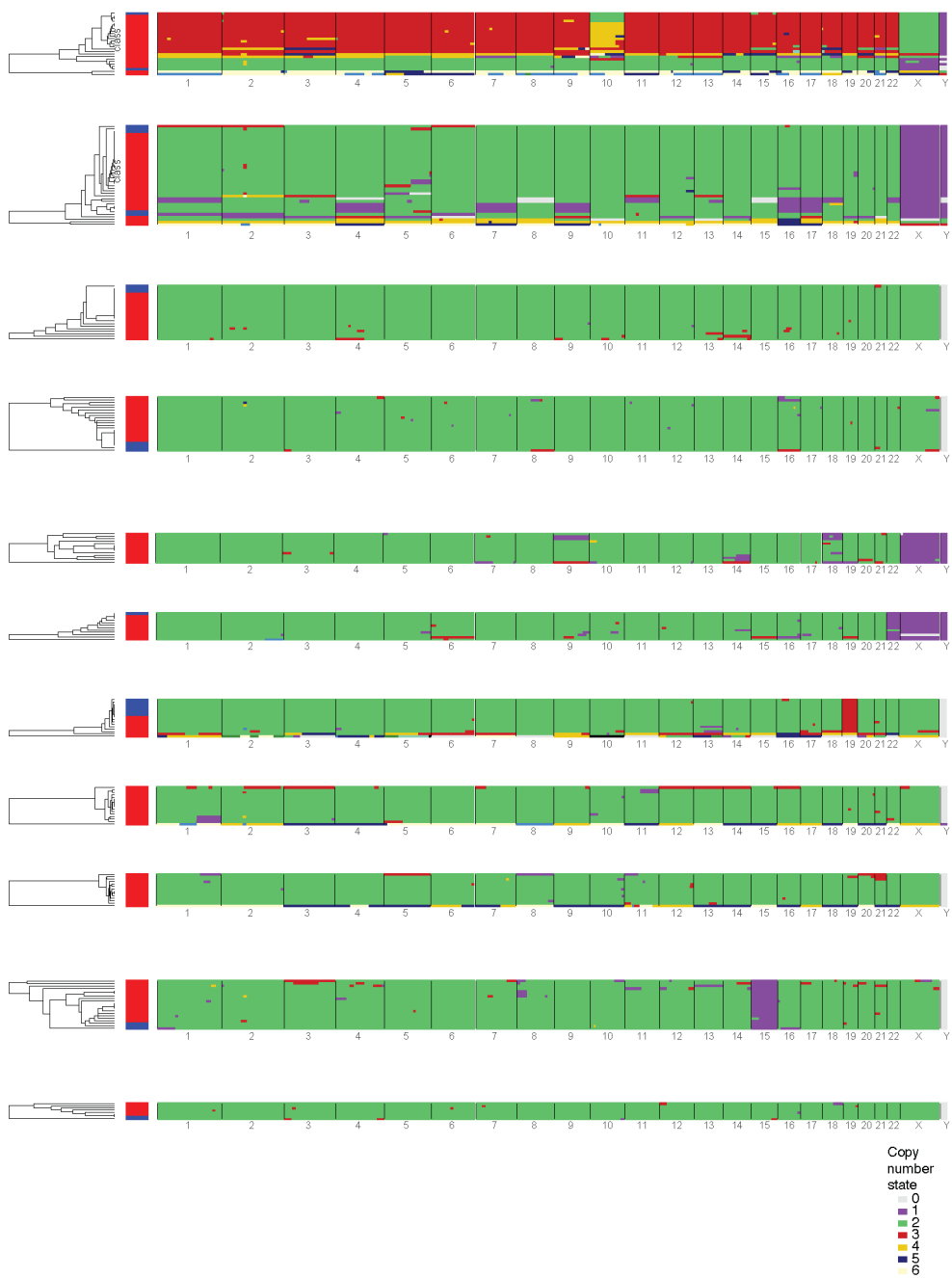
5

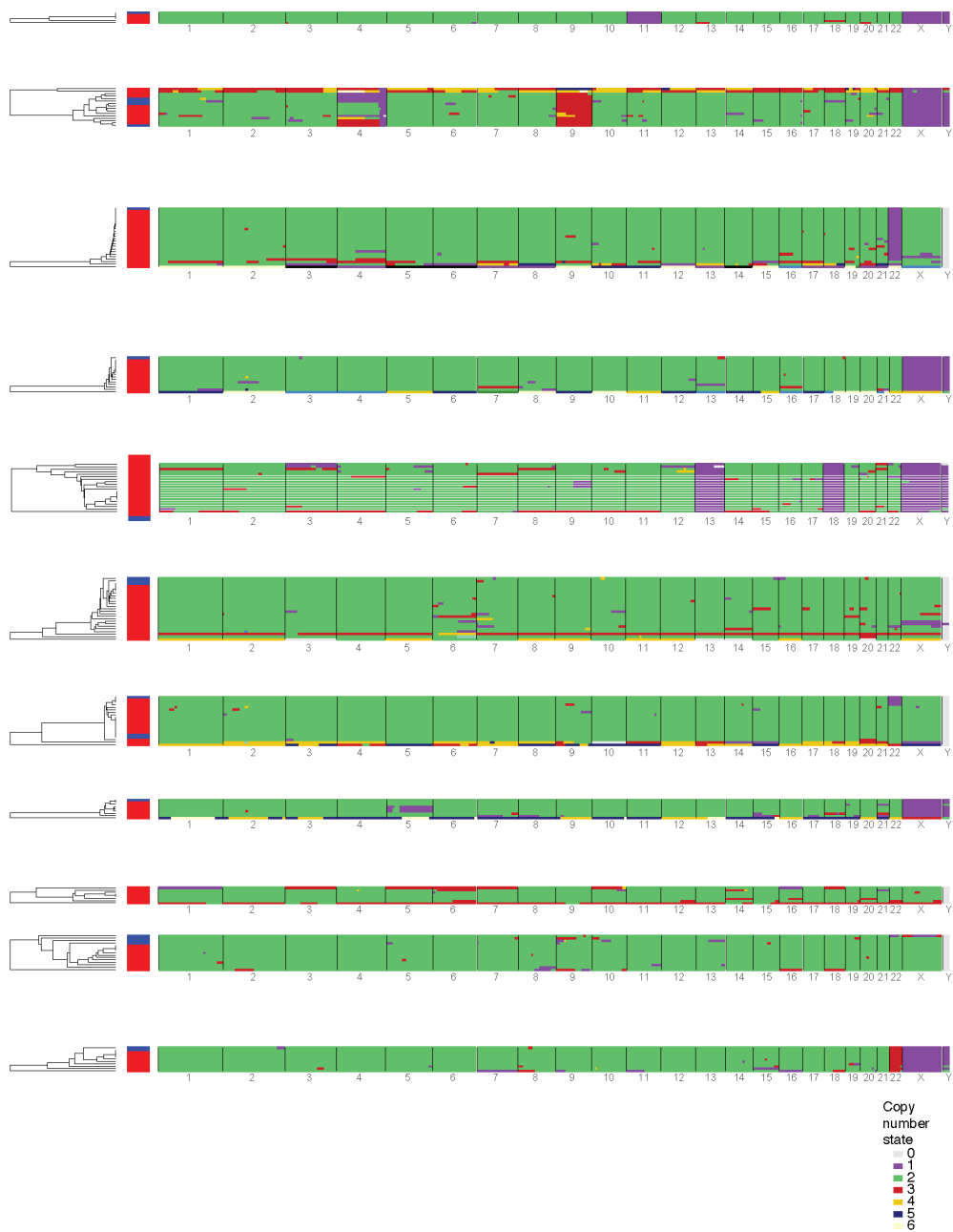
Copy  
number  
state

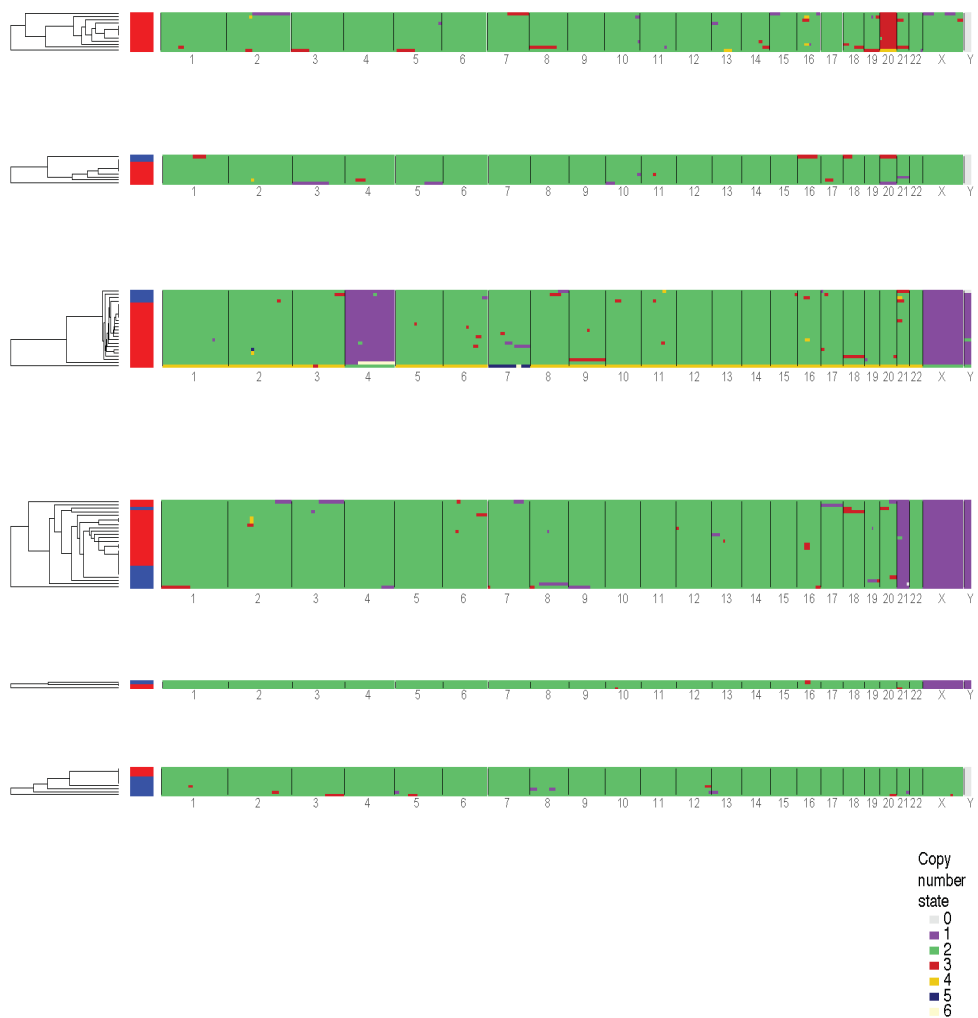
- 0
- 1
- 2
- 3
- 4
- 5
- 6











5

**Supplementary figure 1: all scKaryo-seq plots of the 55 embryos.** Colors on the left show origin of cells (TE in red and ICM in blue).



# Chapter 6

## Discussion

Sjoerd J. Klaasen<sup>1,2</sup>

<sup>1</sup> Hubrecht Institute – KNAW (Royal Netherlands Academy of Arts and Sciences) and University Medical Centre Utrecht, Utrecht, the Netherlands.

<sup>2</sup> Oncode Institute, Utrecht, the Netherlands

## Thesis summary

Aneuploidy is a hallmark of cancer and one of the main causes of miscarriages in humans<sup>1,2</sup>. Recent technical developments in the field of genomics allows one to count the number of chromosomes in a single cell at high-throughput<sup>3</sup>. Using our recently developed single-cell karyotype-sequencing (scKaryo-seq) technique, we tried to answer three long-standing questions in the field of aneuploidy: 1. Are certain chromosomes more likely to mis-segregate compared to others and if so, how? 2. How do cells respond differently to specific whole chromosome copy number changes? 3. How common is aneuploidy in human embryos? In this thesis, we first introduced the process of mitosis and the causes and consequences of when it goes wrong (**Chapter 1**). We then reviewed the prevalence, causes and consequences of non-random segregation errors (**Chapter 2**). In **Chapter 3**, we found that multiple different mitotic perturbations in various human cell lines led to the non-random mis-segregation of chromosomes. By following the behavior of single chromosomes during mitosis or by altering their location in the nucleus, we determined that peripherally located chromosomes, which are usually relatively large in size, are more likely to undergo segregation errors than centrally located ones. We also find that this happens in several chromosomally unstable cancer cell lines. We hypothesize that peripherally located chromosomes and in particular those ending up behind the spindle poles in mitosis are at higher risk to mis-segregate, because they experience more challenges in acquiring bi-oriented microtubule connections. In **Chapter 4**, we characterize the LossTag tool. This tool can be used to enrich for cells with specific monosomies, which allowed us to study the evolution of karyotypes of single cells over time and identify monosomy-specific responses. In **Chapter 5**, we use scKaryo-seq on 5 day old human embryos to show that chromosomal mosaicism is especially prevalent. Not only is it frequent, but we reason it is also commonly missed during bulk-sequencing because aneuploid cells are often present at low levels. In the current **Chapter 6**, I discuss our findings in the light of other literature and suggest potential research avenues. I propose explanations of why polar chromosomes so frequently mis-segregate compared to non-polar chromosomes, discuss the presence of mis-segregation biases in cancer cells and explore its consequences. Next, I suggest a potential use for the LossTag

tool to help explain recurrent aneuploidy patterns. I conclude this section by debating the consequences of our findings in embryos on preimplantation genetic testing of aneuploidy and argue how in the future different single-cell sequencing approaches can help us better understand the pervasiveness of aneuploidy in healthy tissue.

### **Cause of location-dependent differences in bi-orientation speeds and segregation error frequencies**

In **Chapter 3**, we reveal that chromosomes located behind the spindle poles at mitosis onset take longer to arrive at the metaphase plate and thus perhaps take longer to bi-orient than chromosomes in between the poles. This difference maybe increases mis-segregation frequencies of polar chromosomes when mitotic processes are inhibited as well as in cancer cells, such as the U2OS cell line we analyzed. We reasoned this effect on polar chromosomes is caused by them being unfavorably positioned for accomplishing biorientation compared to central chromosomes<sup>4</sup>.

Central chromosomes rapidly become bi-oriented by making end-on attachments to opposite poles, while polar chromosomes will only be captured by microtubules from a single pole, often via lateral attachments, thereafter requiring various steps to achieve biorientation and congression on the metaphase plate. Clearly, polar chromosomes face more challenges in becoming bi-oriented than central chromosomes, raising the question if any one processes is responsible for their inefficient biorientation prior to missegregation. I envision three possibilities: Firstly, since central chromosomes rapidly make amphitelic attachments, perhaps polar chromosomes are more likely to make erroneous ones, which take time to correct. Electron microscopy studies in PtK1 cells suggest polar chromosomes frequently make monotelic attachments<sup>6,7</sup>. Increasing the number of polar chromosomes by first treating human cells with monastrol followed by a release from nocodazole revealed the same is true for syntelic attachments<sup>8</sup>. It was reasoned centrosomes only search the peripheral space closest to them, because they are unable to penetrate the dense microtubule networks already present on the other side. Consequently, polar chromosomes are only captured by one pole and possibly with

microtubule connections to both sister kinetochores. Secondly, polar chromosomes depend on motor proteins: first require the activity of the motor protein dynein to be brought to a centrosome, where CENP-E takes over and congresses the chromosome towards the equatorial plate<sup>5</sup>. This increases the chance the unattached kinetochore is captured by the opposite pole. The lateral attachment is then converted to an end on one. Motor proteins can make chromosomes move up to 18  $\mu\text{m}/\text{min}$ , these movements last 5-15 seconds and occurs multiple times for the same chromosome<sup>9</sup>. Thirdly, polar chromosomes need to cross the centrosome onto the spindle body. Recent unpublished data (Iva Tolić, personal communication) suggests that pivoting of astral microtubules towards the spindle body allows chromosomes to cross over the centrosome, similar to another process already described in yeast<sup>10</sup>. Which of these processes contribute the most to the delayed bi-orientation of polar chromosomes is unknown. During the kinetochore tracking experiments described in **Chapter 3** we noticed polar chromosomes could be stuck for quite some time near the centrosome, suggesting the time to bi-orientation is mostly affected by difficulties traversing the centrosome. Furthermore, polar and central kinetochores with an equal distance to the equatorial plate have significantly different alignment times (**Chapter 3**), further supporting that the centrosome hinders bi-orientation. Properly quantifying the types of attachments and timing of polar chromosome congression will teach us more.

Another important question is what exactly causes the mis-segregation bias observed in **Chapter 3**. In the case of Mps1 inhibition, for example, various processes are disturbed. It could be that the SAC defect imposed by Mps1 inhibition causes non-random mis-segregation predominantly via the above described slowness in bi-orientation of polar chromosomes, but Mps1 is known to also affect other mitotic processes. For example, Mps1 is involved in error correction by increasing recruitment of Aurora B and in chromosome congression by recruiting CENP-E<sup>4,11</sup>. Partial abrogation of these processes could also potentiate the mis-segregation of polar chromosomes. In conclusion, the increase in bi-orientation timing and mis-segregations of polar chromosomes is probably caused by their reliance on the peripheral congression pathway<sup>4</sup>.



## Segregation error bias in cancer

In **Chapter 2** and **3** we discuss that different small molecules perturbing various mitotic processes all induce the same mis-segregation bias. Similarly, naturally-occurring CIN has been widely reported to be biased, such as in female meiosis and the first few mitotic division of the human embryo (**Chapter 2**). There is currently much less known about chromosome mis-segregation frequencies when cells mis-segregate chromosomes naturally in cancer cells. This probably is because one cannot differentiate between selection or a mis-segregation bias as a cause for copy number changes in single cancer cells. Instead, a few reports use sequencing (**Chapter 3**) or fluorescence in-situ hybridization (FISH) on micronuclei to infer the mis-segregation bias in a limited amount of cancer cell lines<sup>12,13</sup>. It is unclear how often micronuclear incorporation of chromosomes follow mis-segregation frequencies; **Chapter 3** shows a clear correlation between the two, while other reports suggests certain chromosomes also have a higher tendency to become incorporated in micronuclei because they are preferentially located further away from the anaphase packs<sup>14,15</sup>. A more direct approach using FISH on anaphase figures for five chromosomes in six cancer cell lines revealed that larger chromosomes mis-segregated more often than the smaller ones<sup>16</sup>. From these initial experiments, I find it likely that a mis-segregation bias is not only a common phenomenon when chromosomal instability is induced, but also when it occurs naturally. How common it really is in cancer, whether it differs between cancer types and which factors determine the bias remain to be identified. To answer these types of questions new tools need to be developed, because performing FISH on anaphase figures is too laborious and expensive. This is especially the case if segregation error frequencies of all chromosomes need to be determined and on cells with low levels of chromosomal instability. One could think of imaging approaches in which the identity of all chromosomes during an erroneous division can be visualized simultaneously live or in fixed samples, maybe with the use of dCas9-based unique fluorophore combinations for each chromosome. Another option would be to sort single cells in a plate, wait for the majority to have divided and use limiting dilution to separate the sisters into two new wells for sequencing (similar to the Look-seq approach<sup>17</sup>). Reciprocal copy number changes reveal the chromosome that had just mis-

segregated. One could also use single-cell methylation sequencing to pair sisters, because they have a unique reciprocal methylation signature<sup>18</sup>. At the same time, this technique allows for the determination of copy number states.

### **Consequences of segregation error bias on the evolution of aneuploidy**

In the previous section I discussed the (lack of) evidence for a mis-segregation bias in cancer and possible research avenues to more thoroughly characterize it. One still major outstanding question related to a mis-segregation bias is what its consequences are on cancer evolution. Firstly, it may be that recurrent aneuploidy patterns seen in cancer are in part shaped by a segregation error bias; cancer cells will often acquire CNAs of frequently mis-segregating chromosomes, after which these CNAs become more prominent in the population due to genetic drift. For this to happen there should not be any selective pressures, because otherwise certain aneuploidies will simply be outcompeted by others. I find it unlikely that the majority of CNAs are simply passengers and thus argue against the idea that a mis-segregation bias directly determines recurrent aneuploidy patterns. Unlike small-scale DNA alterations such as point mutations, of which passengers are rampant in the genome<sup>19,20</sup>, whole chromosome abnormalities have consistently been shown to impact cell fitness<sup>21–25</sup>. This should come to no surprise, because CNAs have the capacity to alter the expression of thousands of genes at the same time. Recurrent aneuploidy patterns are therefore probably shaped by either positive selection, where oncogene gain or tumor suppressor loss increases cell fitness, or negative selection, where different stresses caused by deregulation of expression of only a few or thousands of genes at the same time decreases cell fitness. However, I can imagine CNAs do not always impact cell fitness. For example, cells can become tolerant to aneuploidy through whole-genome duplication and mutating stress-sensing pathways, such as *TP53* and *BCL9L*<sup>2,26–28</sup>. Give these cells CNAs of small chromosomes or small parts of chromosomes and one may have a situation where aneuploidy is suddenly not detrimental nor beneficial. It would be interesting to test this by for example creating cells extremely tolerant to aneuploidy, introduce stable CNAs and compare their growth to a diploid control.

Secondly, a mis-segregation bias may alter the time it takes and the steps needed to reach a recurrent aneuploidy pattern. Aneuploidy likely increases the fitness of cancer cells, implicating a mis-segregation in said fitness. For example, head and neck cancers lose chromosome arm 9p in order to evade the immune system<sup>29</sup>. Cells in precancerous lesions frequently mis-segregating this chromosome will more quickly acquire a cell that has lost it and vice versa, leading to a faster or slower fixation of the aneuploidy. I envision the use of mathematical models, such as the one used by the Pavin lab<sup>30</sup>, to see how big this effect of non-random mis-segregations on the dynamics of CNAs would be. The model should allow for the characterization of aneuploidy evolution in a population of cells and should include proliferation advantages and disadvantages for specific chromosomes and non-random chromosome segregation error frequencies. These *in-silico* experiments could be complemented by karyotype evolution experiments similar to the one performed in **Chapter 4**. In it, cells are made to have different mis-segregation biases and are known to eventually acquire a beneficial aneuploidy. One could then look for a difference in the fixation time of this beneficial aneuploid state. Some of the difficulties will lie in finding manipulations that introduce the different segregation error biases and getting equal CIN levels.

### Using the LossTag to identify aneuploidy driver genes

Cancers from the same tissue have similar copy number aberrations (CNAs)<sup>27,31,32</sup>, implying that cancer cells somehow benefit from their altered karyotype. When looking at the genes present on the CNAs it quickly became clear that the gene dosage of oncogenes was frequently increased and that of tumor suppressors was decreased<sup>33</sup>. Aneuploidy can change the expression of any gene in the genome and has therefore been implicated in a multitude of advantageous effects, from therapy resistance<sup>34</sup> to genome evolution<sup>35</sup> and immune evasion<sup>29</sup>. Interestingly, many of the genes driving CNAs are not known, owing to challenges in identifying which of the hundreds of genes is or are responsible for selection of a certain CNA. We aimed to aid this endeavor by developing the LossTag (**Chapter 4**). The LossTag enriches for cells with a specific chromosome loss. How can it be used to determine aneuploidy drivers?

To first zoom in on potential drivers, I propose the following. Copy number variations are not always the size of whole chromosomes, as they are frequently the size of arms or smaller (focal) regions<sup>32</sup>. One could use these CNAs present in the same cancer type to zoom in on a smaller chromosomal region. Such an approach was for example used to identify a gene amplification-dependent drug resistance mechanism in cancer<sup>36</sup>. Another option would be to narrow down the list of candidate drivers by only considering cancer driver genes<sup>37</sup>, as their altered expression is (directly or indirectly) expected cause the CNAs at least in some cases<sup>33</sup>. Given that cancer driver genes are specific to tumor types and that oncogenes are frequently gained and tumor suppressors are frequently lost, only a handful of candidates will most likely be left. Once candidates have been found, a next major challenge is to establish causal links. Here, the LossTag can be of use. One could start with already aneuploid cancer cells and manipulate them so that they lose the aberrant chromosome. If the aberrant chromosome were to give a selective advantage *in vitro*, the cells are expected to over time reacquire their aneuploid karyotype. Introducing the candidate aneuploidy drivers one by one on a different chromosome and determine if the aneuploidy landscape over time changes from what is expected should reveal which gene is the actual driver. One such experiment was recently performed in a high CIN mouse model, where T-cell lymphomas frequently gained chromosome 15<sup>38</sup>. The authors realized the *Myc* oncogene was located on this chromosome, and introduced it on chromosome 6. This resulted in a significant increase of chromosome 6 gains.

Another option to confirm causal links between aneuploidy and its driver(s) would be to use cancer models known to acquire aneuploidies over time in culture, which are also recurrent in their respective tissue. For example, culturing colon organoids carrying engineered driver mutations in *APC*, *TP53*, *KRAS* and *SMAD4* leads to loss of chromosome 4, 18 or 8p over a period of time<sup>39</sup>. These aberrations are frequently observed in colorectal cancer as well<sup>39,40</sup>, suggesting the proliferative advantage they give cells *in vivo* are also present *in vitro*. This example also illustrates the importance of using the right cell-of-origin to model cancer type-specific

aneuploidies, because copy number variations between cancer types differ substantially. Organoids, which are stem-cell derived 3D cell lines, are extremely useful in this regard, because a wide variety of tissue types can now be grown with this technology<sup>41</sup>.

### Single-cell sequencing to assess the aneuploidy level in normal cells

**Chapter 3, 4 and 5** demonstrate that single-cell sequencing allows for accurate calling of copy numbers in single cells. This is especially important when only a few cells in a population have a specific CNA, such as in 5 day old embryos after *in-vitro* fertilization (**Chapter 5**). The high amount of chromosome mosaicism we and others<sup>42</sup> describe has an implication for the usefulness of preimplantation genetic testing of aneuploidy (PGT-A), which is a technique frequently used to exclude aneuploid embryos from implantation after *in-vitro* fertilization. It works by taking a biopsy of 5-10 cells from the trophectoderm followed by next-generation sequencing of the bulk sample<sup>43</sup>. Unsurprisingly, embryos with a whole chromosome abnormality present in all cells due to a meiotic error will efficiently be recognized as aneuploid<sup>44</sup>. Embryos with such uniform CNAs are unlikely to give rise to live births. 86% of uniform aneuploid embryos as determined by PGT-A miscarry<sup>45</sup>, illustrating PGT-A is good predictor of a bad outcome when aneuploidies are constitutional. For similar reasons, PGT-A also accurately calls fully diploid embryos as diploid<sup>46</sup>. Things become complicated when embryos are mosaic, because low level mosaicism is not visible in bulk sampling or because copy number changes are reciprocal. Using scKaryo-seq, we predict PGT-A inaccurately calls around half of embryos diploid when they are actually mosaic (**Chapter 5**). A second problem related to assessing mosaicism with PGT-A is that the copy number states in the biopsy are not always an accurate representation of what is left in the embryo due to sampling bias. Indeed, PGT-A estimates that 2-13% of embryos are mosaic<sup>46</sup>, which vastly underestimates the mosaicism measured by different single-cell sequencing approaches (**Chapter 5**)<sup>42,47</sup>. In conclusion, PGT-A is a poor predictor of mosaicism in embryos.

Nevertheless, one could argue that having the ability to accurately call mosaicism is not relevant at all, because mosaic embryos have the capacity to develop into fully

functional offspring<sup>48,49</sup>. Diploid cells still present in the embryo will grow faster than the aneuploid cells and will over time take over the whole embryo<sup>48,49</sup>. Therefore, excluding mosaic embryos from being implanted may even be problematic, because it decreases the number of available embryos which have a chance to generate viable offspring. However, PGT-A studies comparing diploid and mosaic embryos show there is a slight decrease in the implantation rate and increase in miscarriage rate of mosaic embryos<sup>46</sup>, suggesting there is some justification in not using mosaic embryos for implantation. Recent work suggests the level of mosaicism in an embryo is important for its viability. In mice, aneuploid and diploid cells were mixed together 1:1 showing the mosaic embryos were as viable as diploid embryos<sup>49</sup>. Only when the majority of cells were aneuploid (75%) did the viability decrease. This finding is corroborated by a study of 1000 human mosaic embryos where implantation and birth rates started declining when 50% mosaicism was reached<sup>50</sup>. As discussed before, PGT-A does not pick up low level mosaicism meaning embryos that are classified as diploid in the studies described in this section may actually be mosaic. Furthermore, reciprocal copy number changes decrease the perceived level of mosaicism in bulk samples. These considerations support the notion that it may be a better option to use single-cell instead of bulk sequencing to measure mosaicism levels in TE biopsies as it may increase implantation and successful pregnancy rates and decrease miscarriage rates even more. Taken together, the field is in much need of clearly defined guidelines on what to do with mosaic embryos.

One drawback of our approach in **Chapter 5** is that we are unable to sequence every cell from an embryo. This is due to difficulties associated with isolating single cells, but also because the library preparation is prone to failure due to the low amounts of input DNA. We therefore hypothesize the percentage of mosaic embryos (82% of embryos) to be higher. However, there is also a chance we overestimate the number of mosaic embryos. Single-cell sequencing allows one to measure hundreds of cells and tens of thousands of chromosome states. Having so many measurements increases the likelihood of false positives per embryo and therefore mosaicism. Indeed, we noticed it was not always easy to correctly identify copy number states, because the read count of some cells were more noisy than others. To get an even

more accurate estimate of mosaicism, improvements in isolation and sequencing of single cells must be made.

Besides quantifying aneuploidy in human embryos, recent sequencing efforts have also used single-cell sequencing approaches to identify that aneuploidy in tissue of healthy individuals, such as the in the skin, liver and brain of humans, is relatively rare (~3%)<sup>51</sup>. However, one report challenges this notion by arguing up to 40% of neuronal cells can be aneuploid<sup>52</sup>. Due to the limited number of studies using single-cell techniques to infer aneuploidy levels in healthy tissue, perhaps due to high costs, there are still many interesting open questions regarding this topic. For example, how common is aneuploidy really? What are the aneuploidy levels in many of the non-examined tissues and does it differ per cell type? Does aneuploidy change with age and if yes, by how much? These questions will be more easily answered with the advent of new and cheaper sequencing platforms, such as the one that was recently released by Ultima Genomics<sup>53</sup>. Another opportunity lies within the wide availability of single-cell RNA sequencing (scRNA-seq) data. scRNA-seq does not only permit the comparison of the transcriptome of one cell to another to for example identify new cell types, but also enables one to assign copy number states to individual cells. The expression of many genes' scales with their dosage, meaning that an increase of all genes from a particular chromosomes can be measured on the RNA level and used to discern copy numbers<sup>54</sup>. scRNA-seq has become the standard in the single-cell sequencing field and has been applied to a multitude of tissues, such as the lung, colon, small intestine, pancreas and enteric nervous system<sup>55–59</sup>. Many more tissues will be sequenced to compile the first human cell atlas<sup>60</sup>. One could leverage the enormous datasets generated by these types of studies to determine the level of aneuploidy in different individuals, tissues and cell types.

## References

1. Webster, A. & Schuh, M. Mechanisms of Aneuploidy in Human Eggs. *Trends Cell Biol.* **27**, 55–68 (2017).
2. Ben-David, U. & Amon, A. Context is everything: aneuploidy in cancer. *Nat. Rev. Genet.* **21**, 44–62 (2020).

3. Bakker, B., van den Bos, H., Lansdorp, P. M. & Foijer, F. How to count chromosomes in a cell: An overview of current and novel technologies. *BioEssays* **37**, 570–577 (2015).
4. Maiato, H., Gomes, A. M., Sousa, F. & Barisic, M. Mechanisms of chromosome congression during mitosis. *Biology (Basel)*. **6**, 1–56 (2017).
5. Barisic, M., Aguiar, P., Geley, S. & Maiato, H. Kinetochore motors drive congression of peripheral polar chromosomes by overcoming random arm-ejection forces. *Nat. Cell Biol.* **16**, 1249–1256 (2014).
6. Roos, U. P. Light and Electron Microscopy of Rat Kangaroo Cells in Mitosis II. Kinetochore Structure and Function. *Chromosoma* **41**, 195–220 (1973).
7. Roos, U.-P. Light and Electron Microscopy of Rat Kangaroo Cells in Mitosis III. Patterns of Chromosome Behavior during Prometaphase. *Chromosoma* **54**, 363–385 (1976).
8. Silkworth, W. T., Nardi, I. K., Paul, R., Mogilner, A. & Cimini, D. Timing of centrosome separation is important for accurate chromosome segregation. *Mol. Biol. Cell* **23**, 401–411 (2012).
9. Magidson, V. *et al.* The spatial arrangement of chromosomes during prometaphase facilitates spindle assembly. *Cell* **146**, 555–567 (2011).
10. Kalinina, I. *et al.* Pivoting of microtubules around the spindle pole accelerates kinetochore capture. *Nat. Cell Biol.* **15**, 82–87 (2013).
11. Jelluma, N. *et al.* Mps1 Phosphorylates Borealin to Control Aurora B Activity and Chromosome Alignment. 233–246 (2008). doi:10.1016/j.cell.2007.11.046
12. Klaasen, S. J. *et al.* Nuclear chromosome locations dictate segregation error frequencies. *Nature* **607**, 604–609 (2022).
13. Bochtler, T. *et al.* Micronucleus formation in human cancer cells is biased by chromosome size. *Genes Chromosom. Cancer* **58**, 392–395 (2019).
14. Catalán, J., Falck, G. C. M. & Norppa, H. The X chromosome frequently lags behind in female lymphocyte anaphase. *Am. J. Hum. Genet.* **66**, 687–691 (2000).
15. Falck, G. C., Catala, J. & Norppa, H. Nature of anaphase laggards and micronuclei in female cytokinesis-blocked lymphocytes. *Mutagenesis* **17**, 111–117 (2002).
16. Klein, A., Zang, K. D., Steudel, W. I. & Urbschat, S. Different mechanisms of mitotic instability in cancer cell lines. *Int. J. Oncol.* **29**, 1389–1396 (2006).
17. Zhang, C. Z. *et al.* Chromothripsis from DNA damage in micronuclei. *Nature* **522**, 179–184 (2015).
18. Mooijman, D., Dey, S. S., Boisset, J. C., Crosetto, N. & Van Oudenaarden, A. Single-cell 5hmC sequencing reveals chromosome-wide cell-to-cell variability and enables lineage reconstruction. *Nat. Biotechnol.* **34**, 852–856 (2016).



19. Kumar, S. *et al.* Passenger Mutations in More Than 2,500 Cancer Genomes: Overall Molecular Functional Impact and Consequences. *Cell* **180**, 915–927 (2020).
20. Williams, M. J., Werner, B., Barnes, C. P., Graham, T. A. & Sottoriva, A. Identification of neutral tumor evolution across cancer types. *Nat. Genet.* **48**, 238–244 (2016).
21. Torres, E. M. *et al.* Effects of aneuploidy on cellular physiology and cell division in haploid yeast. *Science* **317**, 916–924 (2007).
22. Chunduri, N. K. *et al.* Systems approaches identify the consequences of monosomy in somatic human cells. *Nat. Commun.* **12**, 1–17 (2021).
23. Stingle, S. *et al.* Global analysis of genome, transcriptome and proteome reveals the response to aneuploidy in human cells. *Mol. Syst. Biol.* **8**, 1–12 (2012).
24. Williams, B. R. *et al.* Aneuploidy Affects Proliferation and Spontaneous Immortalization in Mammalian Cells. *Science* **322**, 703–710 (2008).
25. Rutledge, S. D. *et al.* Selective advantage of trisomic human cells cultured in non-standard conditions. *Sci. Rep.* **6**, 1–12 (2016).
26. López-García, C. *et al.* BCL9L Dysfunction Impairs Caspase-2 Expression Permitting Aneuploidy Tolerance in Colorectal Cancer. *Cancer Cell* **31**, 79–93 (2017).
27. Taylor, A. M. *et al.* Genomic and Functional Approaches to Understanding Cancer Aneuploidy. *Cancer Cell* **33**, 676–689 (2018).
28. Gronroos, E. & López-García, C. Tolerance of chromosomal instability in cancer: Mechanisms and therapeutic opportunities. *Cancer Res.* **78**, 6529–6535 (2018).
29. William, W. N. *et al.* Immune evasion in HPV-head and neck precancer-cancer transition is driven by an aneuploid switch involving chromosome 9p loss. *Proc. Natl. Acad. Sci. U. S. A.* **118**, 1–12 (2021).
30. Ban, I., Tomasic, L., Trakala, M., Tolic, I. M. & Pavin, N. Proliferative advantage of specific aneuploid cells drives evolution of tumor karyotype. *bioRxiv* (2022).
31. Hoadley, K. A. *et al.* Cell-of-Origin Patterns Dominate the Molecular Classification of 10,000 Tumors from 33 Types of Cancer. *Cell* **173**, 291–304 (2018).
32. Beroukhi, R. *et al.* The landscape of somatic copy-number alteration across human cancers. *Nature* **463**, 899–905 (2010).
33. Davoli, T. *et al.* Cumulative haploinsufficiency and triplosensitivity drive aneuploidy patterns and shape the cancer genome. *Cell* **155**, 948–962 (2013).
34. Shoshani, O. *et al.* Chromothripsis drives the evolution of gene amplification in cancer. *Nature* **591**, 137–141 (2021).

35. Burrell, R. A. *et al.* Replication stress links structural and numerical cancer chromosomal instability. *Nature* **494**, 492–496 (2013).
36. Alt, F. W., Kellems, R. E., Bertino, J. R. & Schimke, R. T. Selective multiplication of dihydrofolate reductase genes in methotrexate-resistant variants of cultured murine cells. *J. Biol. Chem.* **253**, 1357–1370 (1978).
37. Martínez-Jiménez, F. *et al.* A compendium of mutational cancer driver genes. *Nat. Rev. Cancer* **20**, 555–572 (2020).
38. Trakala, M. *et al.* Clonal selection of stable aneuploidies in progenitor cells drives high-prevalence tumorigenesis. *Genes Dev.* **35**, 1079–1092 (2021).
39. Kester, L. *et al.* Integration of multiple lineage measurements from the same cell reconstructs parallel tumor evolution. *Cell Genomics* **2**, 100096 (2022).
40. Muzny, D. M. *et al.* Comprehensive molecular characterization of human colon and rectal cancer. *Nature* **487**, 330–337 (2012).
41. Clevers, H. Modeling Development and Disease with Organoids. *Cell* **165**, 1586–1597 (2016).
42. Starostik, M. R., Sosina, O. A. & McCoy, R. C. Single-cell analysis of human embryos reveals diverse patterns of aneuploidy and mosaicism. *Genome Res.* **30**, 814–826 (2020).
43. Takahashi, S., Johnston, J. & Patrizio, P. Lessons from the premature adoption of preimplantation embryo testing. *Genet. Med.* **21**, 1038–1040 (2019).
44. Marin, D., Xu, J. & Treff, N. R. Preimplantation genetic testing for aneuploidy: A review of published blastocyst reanalysis concordance data. *Prenat. Diagn.* **41**, 545–553 (2020).
45. Capalbo, A., Poli, M., Jalas, C., Forman, E. J. & Treff, N. R. On the reproductive capabilities of aneuploid human preimplantation embryos. *Am. J. Hum. Genet.* **109**, 1572–1581 (2022).
46. Popovic, M., Dhaenens, L., Boel, A., Menten, B. & Heindryckx, B. Chromosomal mosaicism in human blastocysts: The ultimate diagnostic dilemma. *Hum. Reprod. Update* **26**, 313–334 (2020).
47. Ren, Y. *et al.* Regional and developmental characteristics of human embryo mosaicism revealed by single cell sequencing. *PLoS Genet.* **18**, 1–15 (2022).
48. Vázquez-Diez, C. & Fitzharris, G. Causes and consequences of chromosome segregation error in preimplantation embryos. *Reproduction* **155**, 63–76 (2018).
49. Bolton, H. *et al.* Mouse model of chromosome mosaicism reveals lineage-specific depletion of aneuploid cells and normal developmental potential. *Nat. Commun.* **7**, 1–12 (2016).
50. Viotti, M. *et al.* Using outcome data from one thousand mosaic embryo transfers to formulate an embryo ranking system for clinical use. *Fertil. Steril.* **115**, 1212–1224 (2021).

51. Knouse, K. A., Wu, J., Whittaker, C. A. & Amon, A. Single cell sequencing reveals low levels of aneuploidy across mammalian tissues. *Proc. Natl. Acad. Sci.* **111**, 13409–13414 (2014).
52. McConnell, M. J. *et al.* Mosaic Copy Number Variation in Human Neurons. *Science* **342**, 632–637 (2013).
53. Almogy, G. *et al.* Cost-efficient whole genome-sequencing using novel mostly natural sequencing-by-synthesis chemistry and open fluidics platform. *bioRxiv* 1–8 (2022).
54. Delaney, J. R. Aneuploidy: An opportunity within single-cell RNA sequencing analysis. *Biocell* **45**, 1167–1170 (2021).
55. Travaglini, K. J. *et al.* A molecular cell atlas of the human lung from single-cell RNA sequencing. *Nature* **587**, 619–625 (2020).
56. Lee, H. O. *et al.* Lineage-dependent gene expression programs influence the immune landscape of colorectal cancer. *Nat. Genet.* **52**, 594–603 (2020).
57. Drokhlyansky, E. *et al.* The human and mouse enteric nervous system at single cell resolution. *Cell* **182**, 1606–1622 (2020).
58. Wang, Y. *et al.* Single-cell transcriptome analysis reveals differential nutrient absorption functions in human intestine. *J. Exp. Med.* **217**, (2020).
59. Enge, M. *et al.* Single-Cell Analysis of Human Pancreas Reveals Transcriptional Signatures of Aging and Somatic Mutation Patterns. *Cell* **171**, 321–330 (2017).
60. Regev, A. *et al.* The human cell atlas. *Elife* **6**, 1–30 (2017).



# Addendum

## Nederlandse samenvatting

Een mens bestaat uit een moeilijk voor te stellen hoeveelheid cellen. Deze cellen zijn ontstaan door celdelingen (mitose) die teruggaan naar het moment waarop we nog maar uit één cel bestonden, net na de bevruchting. Ook in volwassenen speelt mitose een belangrijke rol; cellen gaan constant verloren en deze moeten door nieuwe vervangen worden. Tijdens mitose is het de bedoeling dat het genetische materiaal (DNA), wat verpakt zit in chromosomen, eerlijk verdeeld wordt over twee nieuwe dochtercellen. In normale gezonde cellen gaat dit meestal goed, maar in bijvoorbeeld kankercellen en tijdens de eerste delingen na bevruchting zien we dat dit niet het geval is. Fouten in de segregatie van chromosomen (chromosomale instabiliteit) zorgt ervoor dat cellen aneuploïde worden, wat inhoudt dat er een afwijking in het aantal chromosomen in een cel aanwezig is. In plaats van 46 chromosomen zijn er bijvoorbeeld 47 chromosomen. Aneuploïdie is vaak aanwezig in kankercellen en embryo's. In kankercellen zorgt het in veel gevallen waarschijnlijk voor een overlevingsvoordeel, terwijl het bij embryo's verantwoordelijk is voor bijvoorbeeld Down's syndroom en een groot deel van de miskramen. Een andere consequentie van chromosomale instabiliteit is de formatie van micronuclei. Micronuclei ontstaan wanneer één of meerdere chromosomen fysiek gescheiden liggen van de hoofdnucleus en hun eigen kernen vormen. Micronuclei zorgen voor een immuunrespons en het DNA wat in een micronucleus zit muteert zeer snel.

Een bijzonder soort celdeling vindt plaats om geslachtscellen te genereren. Deze deling wordt meiose genoemd en zorgt ervoor dat er cellen ontstaan met de helft (23) van het 'normale' aantal chromosomen. Verassend genoeg missegregeren chromosomen vaak tijdens deze deling specifiek bij vrouwen. Deze delingen gaan naarmate vrouwen ouder worden zelfs nog vaker fout, wat een verklaring is voor de daling in fertiliteit wanneer men ouder wordt.

In dit proefschrift bestuderen we de oorzaken en gevolgen van aneuploidie.

In hoofdstuk 2 behandelen we bestaande literatuur over het fenomeen dat bepaalde chromosomen vaker missegregeren dan anderen. We focussen vooral op de oorzaken, zoals de grootte, locatie en andere eigenschappen van chromosomen en bediscussiëren de nog onbeschreven gevolgen.

In hoofdstuk 3 laten we zien dat bepaalde chromosomen vaker missegregeren en in micronuclei terecht komen dan anderen. We komen erachter dat chromosomen die vaak missegregeren in de periferie van de nucleus liggen. Deze chromosomen doen er gemiddeld langer over om zich voor te bereiden op het proces van segregatie, omdat ze afhankelijker zijn van verschillende mitotische processen. Dit zorgt er dan ook voor dat ze vaker in de problemen komen dan chromosomen die aan de binnenkant van de nucleus liggen.

In hoofdstuk 4 ontwikkelen we genetisch gereedschap om te selecteren voor cellen met een verlies van een specifiek chromosoom. We laten zien dat dit gereedschap, ook wel LossTag genoemd, gebruikt kan worden voor het bestuderen van de evolutie van aneuploidie en bekijken de verschillen tussen de respons van cellen wanneer ze één versus een ander chromosoom verliezen.

In hoofdstuk 5 meten we de aneuploidie in honderden individuele cellen van tientallen 5 dagen oude humane embryo's. We vinden dat een overgrote meerderheid van de embryo's aneuploid zijn en dat de fouten tijdens het delen van chromosomen vooral plaats vindt tijdens de mitotische delingen. Ook laten we zien dat het prenataal genetisch testen van aneuploidie, wat vaak wordt gedaan na *in-vitro* fertilisatie, in veel gevallen aneuploidie niet kan oppikken.

In hoofdstuk 6 bediscussiëren we verschillende onderwerpen die te maken hebben met de hiervoor beschreven hoofdstukken. Zo zoeken we naar mogelijke verklaringen over waarom chromosomen in de periferie vaker missegregeren, doen we suggesties voor vervolgonderzoek naar de missegregatiefrequentie van individuele chromosomen in kankercellen en bekijken we de gevolgen van

verschillen in missegregatiefrequenties. Vervolgens beschrijven we manieren om LossTag te gebruiken en om de mate van aneuploidie te meten in normale cellen.

### ***Curriculum vitae***

Sjoerd Jurian Klaasen was born in Oegstgeest (the Netherlands) on the 5<sup>th</sup> of January 1993. Between 2005 and 2011 Sjoerd studied at the Rijnlands Lyceum in Oegstgeest. He then moved to Amsterdam in 2011 to study Biomedical Sciences at the University of Amsterdam. In 2014, he started his Master's at the same university and performed two internships. The first one was for 9 months at the Netherlands Cancer Institute under supervision of Tim Harmsen in the group of Hein te Riele. Here, he worked on the introduction of predefined substitutions with the help of Cas9 and discovered that DNA mismatch repair aids in this process. Sjoerd subsequently did a 6 months internship at Janssen Vaccines and Prevention where he helped generate an influenza vaccine meant to elicit an immune response against the stem domain of hemagglutinin. In December of 2016, he started his PhD in the group of Geert Kops. The work shown in this thesis is a culmination of more than 5 years of work under his supervision.



## List of publications

A. C. F. Bolhaqueiro, B. Ponsioen, B. Bakker, **S. J. Klaasen**, E. Kucukkose, R. H. van Jaarsveld, J. Vivié, I. Verlaan-Klink, N. Hami, D. C. J. Spierings, N. Sasaki, D. Dutta, S. F. Boj, R. G. J. Vries, P. M. Lansdorp, M. van de Wetering, A. van Oudenaarden, H. Clevers, O. Kranenburg, F. Foijer, H. J. G. Snippert, G. J. P. L. Kops, Ongoing chromosomal instability and karyotype evolution in human colorectal cancer organoids. *Nat. Genet.* 51, 824–834 (2019).

M. Dumont, R. Gamba, P. Gestraud, **S. Klaasen**, J. T. Worrall, S. G. De Vries, V. Boudreau, C. Salinas-Luypaert, P. S. Maddox, S. M. Lens, G. J. Kops, S. E. McClelland, K. H. Miga, D. Fachinetti, Human chromosome-specific aneuploidy is influenced by DNA-dependent centromeric features. *EMBO J.* 39, 1–21 (2020).

W. H. M. Hoevenaar, A. Janssen, A. I. Quirindongo, H. Ma, **S. J. Klaasen**, A. Teixeira, B. Van Gerwen, N. Lansu, F. H. M. Morsink, G. J. A. Offerhaus, R. H. Medema, G. J. P. L. Kops, N. Jelluma, Degree and site of chromosomal instability define its oncogenic potential. *Nat. Commun.* 11, 1–11 (2020).

**S. J. Klaasen**, M. A. Truong, R. H. Jaarsveld, I. Koprivec, V. Štimac, S. G. De Vries, P. Risteski, S. Kodba, K. Vukušić, J. Kind, I. M. Tolić, S. M. A. Lens, G. J. P. L. Kops, Nuclear chromosome locations dictate segregation error frequencies. *Nature.* 607, 604–609 (2022).

J. Wu, A. Larreategui-Aparicio, M. L. A. Lambers, D. L. Bodor, **S. J. Klaasen**, E. Tollenaar, M. de Ruijter-Villani, G. J. P. L. Kops. Microtubule nucleation from the fibrous corona by LIC1-pericentrin promotes chromosome congression (2022). *In review.*

**S. J. Klaasen**, G. J. P. L. Kops. Chromosome inequality: causes and consequences of non-random segregation errors in mitosis and meiosis, *Cells.* 11, 3564 (2022).

E. A. Chavli, **S. J. Klaasen**, D. van Opstal, G. J. P. L. Kops, E. B. Baart. High incidence of numerical and segmental chromosome mosaicism in inner cell mass and trophectoderm (2022). *Manuscript in preparation.*

## Acknowledgements

Het is inmiddels bijna zes jaar geleden dat ik als broekie het Hubrecht binnenliep om aan mijn PhD te beginnen. Zoals waarschijnlijk velen voor mij had ik geen flauw benul hoe het zich zou gaan ontfoutwen. Alhoewel het af en toe met vallen en opstaan was kan ik gelukkig op dit moment met trots zeggen dat het een zeer geslaagd experiment is gebleken. De meest belangrijke reden hiervoor zijn de mensen die ik gaandeweg heb ontmoet. Niet alleen op wetenschappelijk vlak hebben zij ervoor gezorgd dat ik mij heb kunnen ontwikkelen, maar velen beschouw ik ondertussen ook als vrienden. Via deze weg wil ik jullie allemaal één voor één bedanken!

**Geert**, wat ben jij een baas. Ik heb alleen maar lof voor de manier waarop jij je lab beheert. Je weet mensen te motiveren zonder ze af te kraken en hebt mij zo vrij mogelijk mijn werk laten doen. Iets wat ik achteraf gezien precies nodig had. Ook was je bijna altijd beschikbaar om dingen te bediscussiëren en kreeg ik stukken tekst bijna meteen weer retour met veel commentaar. Dit was waarschijnlijk niet makkelijk met al je andere verantwoordelijkheden. Ik kan alleen maar hopen dat ik in de toekomst net zo goed zal worden als jij. Super bedankt voor alles!

Ik wil ook graag mijn PhD commissieleden (**Alexander van Oudenaarden en Susanne Lens**) als ook mijn leescommissie (**Bas van Steensel, Marta De Ruijter-Villani, René Medema en Jeroen Bakkers**) bedanken voor de tijd die ze in mij hebben gestoken. Ik kan niet wachten om met jullie in discussie te gaan.

Labgenootjes. Ook al is het op het moment dat ik dit schrijf nog maar een paar weken geleden dat ik mijn laatste officiële dag had op het Hubrecht, denk ik met veel weemoed terug aan de goede oude tijd. Mede doordat de meesten van ons ongeveer even oud zijn en we allemaal in hetzelfde ingewikkelde schuitje zitten, heb ik het gevoel dat we meer als studenten met elkaar omgingen dan collega's. **Carlito**, although you definitely do not fit the previous description of being of similar age, I fondly think back of our time in the lab. Your knowledge and patience is unparalleled, which meant I could barrage you with an unparalleled number of questions and

ideas. I also like to think we had a special bond, because I was one of few you seemed comfortable with poking fun at. If you do not mind, I will keep giving you random calls. Not to teach me about science, but about life. **Jingie Chao**, ik hou van jou. You have a skill to come up with the most random unexpected funny jokes. I also enjoyed our somewhat philosophical science discussions. Keep those positive vibes! **Thomasso**, wie had gedacht dat we weer samen zouden werken na onze korte periode samen in de Te Riele groep. Toen al schroomde je niet om duidelijkheid te scheppen met je heldere vragen. Knap hoe je ontzettend goed werk hebt verricht met de AneuFinder analyse tools, waarmee ik veel mee ben geholpen. Ik weet zeker dat je project in jouw handen op vier pootjes terecht zal komen. Succes! **Tetraemine**, although it did not start out like that you have found your inner Dutchie of “subtle” and direct teasing, similarly to Carlito. Good luck with everything! **Natasja**, al het beste toegewenst met de kleine, je nieuwe osso en je project! **Joāns Fernands Marqs**, I am proud to give the torch of PhD eldest to you. I believe you were my PhD buddy the longest, meaning we shared many great things; projects, similar research topics, the gym, social events, holidays, games and last but not least some great parties and festivals. You are incredibly kind, were always up for listening to my random ideas and it was great to have you around, so see you soon! **Maaïke** (niet mijn bloedverwant), ik zou het vorige stukje van Joāna bijna één op één kunnen kopiëren. Je bent lekker no-nonsense, weet wat je wilt en slimmer dan je denkt ;). Ik denk vooral terug aan de vele en lange Witcher III sessies waardoor ik me snel thuis voelde in Utrecht. Bedankt! **Simona**, you are great at retelling some of my more unflattering stories (“I don’t trust like that”), which is mostly due to your great sense of humor, expressive language and addictive laughter. We will keep in touch! **Lorena**, I already thanked many people, but somehow you are the first of my roombuddies. Since you were only a 90 degrees turn away we had many great discussions about your and my projects, but also life. Your easygoingness made the office that much better. You are a bright scientist with great ideas, so no worries! **Ale**, another talented young scientist ready to replace the old science behemoths. It was inspiring to witness someone take control of their projects like you did. I wish I was like that when I started. Still curious how your homemade pizza tastes... **Ainhua**, I had great fun with you at some of our meet-ups. Hopefully we will finally

be able to go to fiesta macumba soon... **Anneloes**, ik heb jou alleen tijdens je sollicitatie mogen ervaren, maar ik ben ervan overtuigd dat we met jou een andere grote te pakken hebben. Go get 'em! **Pimmetje**, de spreekwoordelijke oom die ik nooit heb gehad. Als ik iemand ga missen ben jij het wel. Bedankt voor je positieve energie en je hilarische verhalen. Wel blijven gymmen hè, kast? Het ga je goed. **NicoOoooOoooOooooOtinamide**, als er één zin is die jou goed omschrijft in het lab is het wel "mwa, maakt niet uit". Wat we ook deden je bleef altijd relaxed, wat fijn was om mee samen te werken. Volgende keer kopen we wel pruimen in de appie, ja? **Bassie**, broeder van een andere moeder. Met jou kon ik, net zoals eigenlijk iedereen, altijd een lekker praatje maken. Gym ze, kerel! **Eloïse**, je was een top kantoorgenoot. Succes in Utrecht, op het Hubrecht en overal daarbuiten! **Anko**, stille kracht op het Hubrecht. Bedankt voor al het werk dat je steekt in het overeind houden van al onze experimenten!

Ex-labgenootjes, de meeste van jullie zijn al weer jaren weg, maar daarom niet minder in mijn geheugen! **Nannette**, poortwachter van wetenschappelijke degelijkheid in het lab. Ik ben meer van het 'quick en dirty', dus om iemand zoals jij in het lab te hebben om mij af en toe even goed wakker te schudden kwam als een geschenk uit de hemel. Succes met je nieuwe baan! **Bas**, de vader die ik wel heb gehad. Je kon me altijd advies geven op de gevraagde maar soms ook ongevraagde vragen des levens. Dankzij jou ben ik inmiddels een meesterinvesteerder, verslaafd aan de Xbox en mag ik mij inmiddels bijna PhD noemen ;). Als de kleine minder tijd kost kan ik jou leren hoe Apex werkt? **Ana**, at the start, although my research topic was maybe not really similar to anyone else's work, I naturally gravitated towards discussing things with you the most. I guess it just somehow clicked, perhaps due to your expressive and open nature. All the best in the third best city of the world (after Amsterdam and Utrecht of course). **Banana**, wat ben jij een lieverdje. Ik werd met open armen ontvangen, waardoor ik me meteen meer op mijn plek voelde. Bedankt voor al je warmte en vrolijkheid! **Timo**, de microscopieman. Als ik aan jou denk denk ik vaak aan je enorm ingewikkelde pathways, waarbij jij weer een nieuwe schakel hypothetiseerde, om je nieuwe vinding te verklaren. Jouw "carrièreswitch" was voor mij om een of andere reden een verrassing, maar na één seconde erover

nagedacht te hebben de meest logische keuze. Hopelijk zijn er genoeg Nikon microscopen op mijn volgende werkplek zodat ik je ook daar plotseling voorbij zie komen. **Kim**, I appreciated your kindness towards others, wittiness and enthusiasm for, but not limited to, boardgames. I hope you will enjoy living in the Netherlands as much as I do! **Ajit**, jij maakte een wereld van verschil toen ik als guppie het lab binnenkwam. Aardig, behulpzaam, begripvol. Dankjewel voor de goede tijd!

Ook alle Hubrechters in andere groepen bedankt voor de onvergeetbare tijd. We hebben samengewerkt en zo veel leuke dingen gedaan; van vrijmibo's tot "winter"-feesten, LabStapDagen en Mallorca en Ardennen-trips. Bedankt voor alles **Silke, Samy, Ramada, Kim, Gaby, Erik, Yike, Sjoerd, Judith** en alle anderen! **Bram**, sfeermaker van het MLII, Scandinaviëconnaisseur en mede Heldeep Radio liefhebber. Het is dat je in het verre Kanaleneiland woont, anders was ik elke dag lang geweest. Kom je binnenkort weer in Utrecht wonen? Kunnen we een keertje met de racefiets racen. **Max**, we enjoy many of the same things; music, gaming, racket sports and brewing/drinking, which meant we got along quite well. I'm sure we will drink many more experimental concoctions while solving another crazy baba puzzle. Please don't try to kill me again though like that time when we were driving through the mountains of Israel. **Herr Müller**, you are probably the second most talented racket player from Switzerland and a pleasure to be around. Our fermentation barrel has been gathering dust for a while now though, care to brew another cold one? **Stijntje**, omdat je zo open bent maakte niet uit waar ik je voor uitnodigde, als je tijd had ging je mee. Ik waardeer je kennis over allerhande zaken en de daaropvolgende discussies. Vooral omdat je vaak een net even andere mening had dan ik. Zie je hopelijk snel! **Deepak**, I miss your addictive laughter and positive attitude. I have fond memories of our many Friday afternoon escapades. See you around! **Stefan** en **Reinier**, ik heb vele uren met jullie doorgebracht en mede doordat ik toevallig met beide van jullie één hobby gemeen had, was dat geen straf. Stefan, bedankt voor al je gymadvies. Groei ze en gooi die schijven door het dak! Bedankt voor al jullie hulp! Mijn dank gaat ook uit aan het ondersteunend personeel. Van alle kanten hoor je dat het allemaal perfect geregeld is en daar zijn jullie mede verantwoordelijk voor.

Alle mensen met wie ik heb samengewerkt, bedankt! **My Anh**, thank you for the great collaboration! We really did something special. I enjoyed randomly popping by in the Stratenum to have a small chat about science and general things. Good luck finishing up your PhD. Ook alle anderen in het **Lens** lab bedankt voor de fijne samenwerking! Thank you to all the people in the **Tolić** and **Pavin** lab. We had fun scientific meetings together and also a successful collaboration. **Eefje** en **Esther**, langzaam maar zeker hebben we er uiteindelijk een mooie paper uitgesleept. Bedankt voor de leuke samenwerking!

En dan alle andere mensen om mij heen. **Tim**, bedankt voor de enorm leuke tijd op het NKI tijdens mijn eerste wetenschappelijke stage. Ik moest altijd erg lachen om je grappen en eigenaardigheden. Succes met alles! Huisgenootjes van het oude Kalkmarkt **Paul, Joris, Hugo, Elmar, Roland, David**. Bedankt voor de fantastische tijd! Ik heb zeker een pagina of twee nodig om alle leuke dingen die we samen hebben gedaan op te schrijven, dus dat doe ik niet. Ik heb niet voor niets 10 jaar op hetzelfde stekkie gewoond. Nieuwe huisgenootjes **Simon, Sofia, Chris** en **Imogen**. I enjoy living with you guys, because it is so relaxed and mellow. I also blew off some much needed steam in the evening thanks to the many Apex training sessions from Simon ;). Fløp C4 **Chung, Mike, Steph, David** and **Jeroen** it was a privilege to be adopted by such a talented bunch of rowers. Thanks for all the great times and holidays! **Steven, Marco, Ronald, Elmar, Paul** and **Ewout** wij gaan inmiddels wel heeeuuul ver terug. Alle pauzes was het KOENen geblazen en de vakanties waren uiteraard legendarisch. Op naar meer goede tijden! **Kas**, mede-motormuis. Onze paden kruisten zich op merkwaardige wijze, maar ik ben blij dat we lekker samen kunnen scheuren. Want zeg nou zelf, twee is altijd beter dan één. Hopelijk gaan we nog een keer een dikke trip maken naar een nader te bepalen gebergte. **Boris**, jij was er bij vanaf het allereerste begin en wat ben jij een chille gozer. Lekker samen knutselen aan autootjes en vele avonden een beetje rondhangen. Succes met alles! **Voorwaartsmakkers**, thank you for being the way you are! I felt welcome from the start and I enjoy playing football with you guys, even when we lose. Now let's win that cup for a change.

**Mam, pap<sup>1</sup>**, het is me gelukt! Bedankt voor alle kansen die jullie mij gegeven hebben. Ik heb me altijd vrij gevoeld in mijn keuzes en zonder jullie steun vanaf het begin was het er zeker niet van gekomen. **Maike**, mijn favoriete zusje. Ik ben blij dat we zo goed met elkaar op kunnen schieten. Helaas woon je nu ontzettend ver weg, maar wees niet bezorgd. Ik kom zeker terug in de mooiste stad van het land. **Jannes**, Wie is er een goede jongen, ja jij bent een goede jongen! Braaf! **Lau**, you were only there at the end, but have witnessed many of the ups-and-downs a PhD brings. Gosh, it feels like I already know you for years! You are one of the kindest people I know and your support and me being able to use your place to crash/work whenever I felt like was immensely important. I think I found the lid to the proverbial pot. Mucho gusto!

## References

1. Bogerd, J. C., Tijhuis, A. G. & Klaasen, J. J. A. Electromagnetic excitation of a thin wire: a traveling-wave approach. IEEE Trans. Antennas Propag. 46, 282–285 (1997).

